Distribution Agreement

In presenting this thesis or dissertation as a partial fulfillment of the requirements for an advanced degree from Emory University, I hereby grant to Emory University and its agents the non-exclusive license to archive, make accessible, and display my thesis or dissertation in whole or in part in all forms of media, now or hereafter known, including display on the world wide web. I understand that I may select some access restrictions as part of the online submission of this thesis or dissertation. I retain all ownership rights to the copyright of the thesis or dissertation. I also retain the right to use in future works (such as articles or books) all or parts of this thesis or dissertation.

Signature:

_____ _____

Wesley Daniel Robertson Date

Probing the Dynamical Basis of Radical Catalysis in a B_{12} Dependent Enzyme and Development of a Cobalamin/Protein Compressed Photosynthesis Device

By

Wesley Daniel Robertson
Doctor of Philosophy

Physics

_____
Prof. Kurt Warncke
Advisor

_____
Prof. Laura Finzi
Committee Member

_____
Prof. Tim Lian
Committee Member

_____
Prof. Ivan Rasnik
Committee Member

_____
Prof. Eric R. Weeks
Committee Member

Accepted:

_____

Lisa A. Tedesco, Ph. D.
Dean of the James T. Laney School of Graduate Studies

_____
Date

Probing the Dynamical Basis of Radical Catalysis in a B_{12} Dependent Enzyme and Development of a Cobalamin/Protein Compressed Photosynthesis Device

By

Wesley Daniel Robertson

B.S., University of Tennessee, Knoxville 2001

M.S., University of Tennessee, Knoxville 2003

Advisor: Kurt Warncke, Ph. D.

An abstract of
A dissertation submitted to the Faculty of the
James T. Laney School of Graduate Studies of Emory University
in partial fulfillment of the requirements for the degree of
Doctor of Philosophy

2010

Abstract

Probing the Dynamical Basis of Radical Catalysis in a B_{12} Dependent Enzyme and Development of a Cobalamin/Protein Compressed Photosynthesis Device

By Wesley Daniel Robertson

The contribution of chemical and protein coordinates, and the influence of substrate binding, to the formation and stabilization of the cob(II)alamin-5'-deoxyadenosyl radical pair were studied in the adenosylcobalamin (AdoCbl)-dependent enzyme, ethanolamine ammonia-lyase (EAL) from *Salmonella typhimurium.* The photoproduct dynamics on the 10^{-7} – 10^{-1} s time scale were monitored following pulsed-laser photolysis with a home designed and constructed ultraviolet(UV)/visible transient absorption spectrometer. Pulsed-laser photolysis of AdoCbl in EAL leads to a quantum yield at 10^{-7} s for cob(II)alamin which is 3-fold less than for AdoCbl in aqueous solution at 295 K, indicating that the protein binding site suppresses photoproduct radical pair formation. The quantum yield was further reduced by half following the binding of the substrate analog, (*S*)-1-amino-2-propanol, suggesting that it does not induce changes in the protein that are characteristic of true substrates. Therefore, a catalytically competent ternary complex, with negligible turnover on the photolysis/probe time scale, was created by using a fluid dimethylsulfoxide/water cryosolvent system at 230 - 240 K. The static UV/visible absorption spectra of holo-EAL and ternary complex are comparable, indicating that the binding of substrate does not weaken the cofactor cobalt-carbon (Co-C) bond by significantly distorting AdoCbl structure. The quantum yield of the cob(II)alamin-substrate radical pair is < 0.01. The results indicate that substrate binding to holo-EAL does not "switch" the protein to a new static structural state, which stabilizes the cob(II)alamin-5'-deoxyadenosyl radical pair photoproduct. Therefore, protein dynamics plays a critical role in native cleavage of the Co-C bond and radical pair separation. The EutB subunit of the EAL enzyme was selected as a template for the design of an artificial photosynthetic unit for the reduction of carbon dioxide (CO_2) and toxic halo-organic compounds. Cobalamin (Cbl) or cobinamide (Cbi) in solution and bound to EutB were chemically or photo reduced to the Co^{I} state. Interaction of the compounds with CO_2 and halo organics was monitored by using UV/visible spectroscopy. The results suggest CO_2 binding to the Co^{I} centers, and light-driven pathways for haloalkane reduction.

Probing the Dynamical Basis of Radical Catalysis in a B_{12} Dependent Enzyme and Development of a Cobalamin/Protein Compressed Photosynthesis Device

By

Wesley Daniel Robertson

B.S., University of Tennessee, Knoxville 2001

M.S., University of Tennessee, Knoxville 2003

Advisor: Kurt Warncke, Ph. D.

A dissertation submitted to the Faculty of
the James T. Laney School of Graduate Studies of Emory University
in partial fulfillment of the requirements for the degree of
Doctor of Philosophy

2010

Acknowledgements

I would first like to thank my gonzo advisor Kurt for all of his support, encouragement and guidance. His influence and friendship have been invaluable and made me a better scientist. I am eternally obliged. We also had some good times.

I would like to thank my family and friends for all their support along the way. A special thank you to Chuck and Lala, you guys are the best and I couldn't have done it without you. Thank you to my beautiful mother and Phil for all of their love and support as well as my baby sister, Jackie, and baby, "Hey Baby", Gracie. I would also like to thank Vicki and Big and Little Jim Cate for keeping me in and out of line, respectively.

The members of the Warncke research group have also been very helpful during the course of this work. Special thanks to Miao Wang for his friendship, and hard work on the photolysis experiments. Thank you to Li Sun, Chen Zhu, Jeff Canfield, Olivia Groover, Adonis Bovell, Hanlin Chen, Bill Gunderson and Kaya Erbil for their friendship and support, and for making the lab a great place to work. I would also like to thank Ben and Nate for their hard work on the compressed photosynthesis project. A very special thank you goes to Jessica "The Mex" Hernandez for being such a great friend and always being there for me.

The members of my dissertation committee, Ivan Rasnik, Tim Lian, Laura Finzi and Eric Weeks have all been extremely supportive and helpful and have my sincere gratitude. I would like to thank the physics department faculty, graduate students and staff for making the Physics department at Emory such an enjoyable place. Thank you all so very much. A special thanks to Julie, Neil, Jessica and Adonis for their hard work with YEP.

For the friendship and good times, my many thanks to the Little Five Points Horseshoe Pit crew. Without you guys, I would have probably finished in half the time. Thank you to Richard "Dutch" Renes for throwing ringers when we needed them and Willie "Nascar Willie" for being a great neighbor. Also, many thanks to Eric "wiki wiki" Strickland and Dave Pattillo for being great friends. I would also like to give a very special thank you to Laura Bellinger for all of her support and encouragement along the way.

Table of Contents

List of Figures

Chapter 1: Introduction

Chapter 2: Construction of a UV/Visible Transient Absorption Spectrometer

Chapter 3: Static and Transient Absorption Studies of Adenosylcobalamin and Methylcobalamin in Ethanolamine Ammonia-Lyase: Influence of Substrate/Inhibitor binding on Cofactor Spectra and Radical Pair Recombination

Chapter 4: Characterization of Contributions of Protein and Chemical Coordinates to the Substrate Trigger of Cobalt-Carbon Bond Cleavage and Radical Pair Separation in the Ternary Complex of Adenosylcobalamin-Dependent Ethanolamine Ammonia-Lyase

Chapter 5: Developing a Biologically-Inspired Molecular Solar Energy Conversion Device: Reaction of Solution and Protein-Bound Cobalamin Cofactors with Carbon Dioxide and Halo-Organic Compounds

Appendix

List of Tables

Chapter 3: Static and Transient Absorption Studies of Adenosylcobalamin and Methylcobalamin in Ethanolamine Ammonia-Lyase: Influence of Substrate/Inhibitor Binding on Cofactor Spectra and Radical Pair Recombination

Chapter 4: Characterization of Contributions of Protein and Chemical Coordinates to the Substrate Trigger of Cobalt-Carbon Bond Cleavage and Radical Pair Separation in the Ternary Complex of Adenosylcobalamin-Dependent Ethanolamine Ammonia-Lyase

Chapter 5: Developing a Biologically-Inspired Molecular Solar Energy Conversion Device: Reaction of Solution and Protein-Bound Cobalamin Cofactors with Carbon Dioxide and Halo-Organic Compounds

Chapter 1: Introduction

1.1 The Coenzyme B_{12}-Dependent Enzyme Ethanolomine Ammonia Lyase

Coenzyme B_{12}-dependent enzymes catalyze radical mediated rearrangement reactions in both bacteria and mammals [1-3] that are necessary for life. This group of enzymes is unique in that they utilize highly reactive radicals to catalyze chemical reactions. The enzyme provides an active site that encloses and guides the highly reactive intermediate radicals involved. The enzymes also enhance the reaction rate, by 10^{11}-fold[4-6], and prevent undesired side reactions that could inactivate the enzyme.

Coenzyme B_{12} dependent enzymes are divided into the mutase and eliminase subfamilies. The mutase subfamily, Class I and Class III, is composed of enzymes that catalyze carbon skeleton rearrangement and amino group migration reactions. Methyl-malonyl CoA mutase[7], a metabolic enzyme found in humans and other mammals, is a member of the mutase subfamily. The eliminase subfamily, Class II, catalyze amino or hydroxyl migration and elimination to produce water or ammonia as a product. The work in this dissertation will focus on the Class II enzyme, ethanolamine ammonia-lyase (EAL) [EC 4.3.1.7; cobalamin (vitamin B_{12})-dependent enzyme superfamily [8-9]] from *Salmonella typhimurium.*[1,10] EAL catalyzes the conversion of aminoethanol and 2-aminopropanol to the corresponding aldehydes and ammonia in bacteria as part of glycerophospholipid metabolism.[11] EAL is composed of two protein subunits; a large subunit, EutB (453 residues, 49.4 kDa), and a small subunit; EutC (286 residues, 32.1 kDa). The protein exists as a hexamer of EutB/EutC dimers. The EutB protein, shown in Figure 1.1, has a $(\beta\alpha)_8$ TIM-barrel fold, and contains the active site and the cofactor and substrate binding sites, as determined through a comparative model for the subunit.[9] The

structure of EutB from *Listeria monocytogenes* has been recently determined by X-ray crystallography.[12] A crystal structure of EAL from *Escherichia coli*, with coenzyme B_{12} analogs and substrates, has also recently been reported and confirmed the comparative model structure.[13] The $(\beta\alpha)_8$ TIM-barrel fold of the EAL protein is a common scaffold for enzyme catalysis, present in more than 10% of all known protein structures.[14] The EAL protein has been shown to have the ability to function over a wide range of pH conditions, with at least 50% activity from 5.8 - 9.2 pH.[15-16]

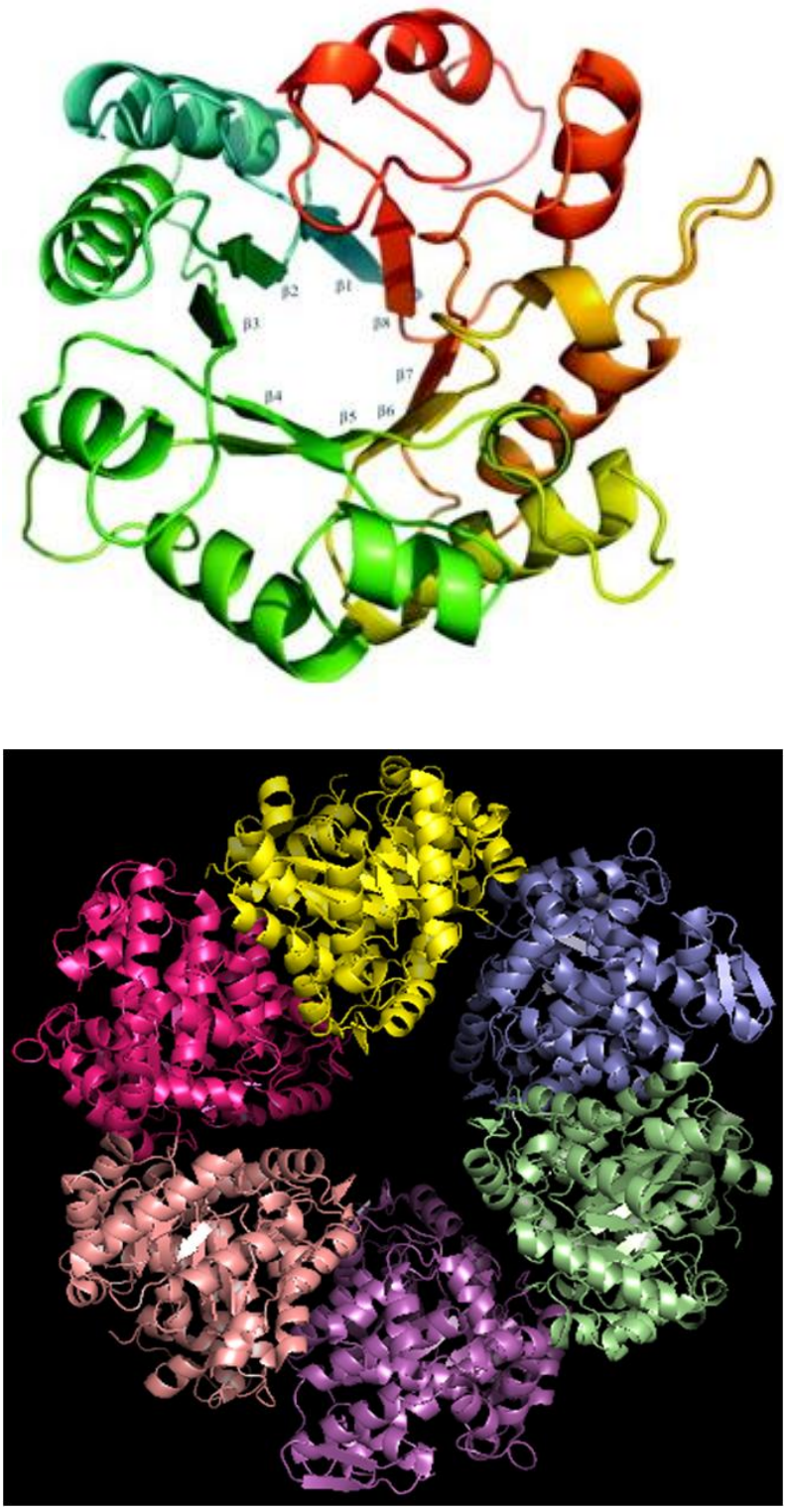

Figure 1.1. Comparative model of the structure of EutB from *S. typhimurium* ethanolamine ammonia-lyase (top)[9] and crystallized hexamer structure of the EutB subunit of EAL in *L. monocytogenes* (bottom).[12]

The cofactor, coenzyme $B_{12,}$ or adenosylcobalamin (AdoCbl), shown in Figure 1.2, is the source of the radical that is essential to the function of the EAL enzyme. The B_{12} cofactor is unique in that it is the only known biological molecule with a stable carbon-metal bond.[15,17] The cofactor is comprised of a corrin ring, made up of four pyrole subunits, whose nitrogen atoms coordinate a central cobalt atom. Amide groups are located on the outside of the corrin ring to facilitate binding of the β-axial face of the cofactor to the active site of the protein as shown in Figure 1.3. The central cobalt atom is bonded to a deoxyadenosyl group on the β-axial side of the molecule. The α-axial face of the cofactor is ligated by a 5,6-dimethylbenzimidazole group (DMBz) which is attached to an amide group on the corrin ring.

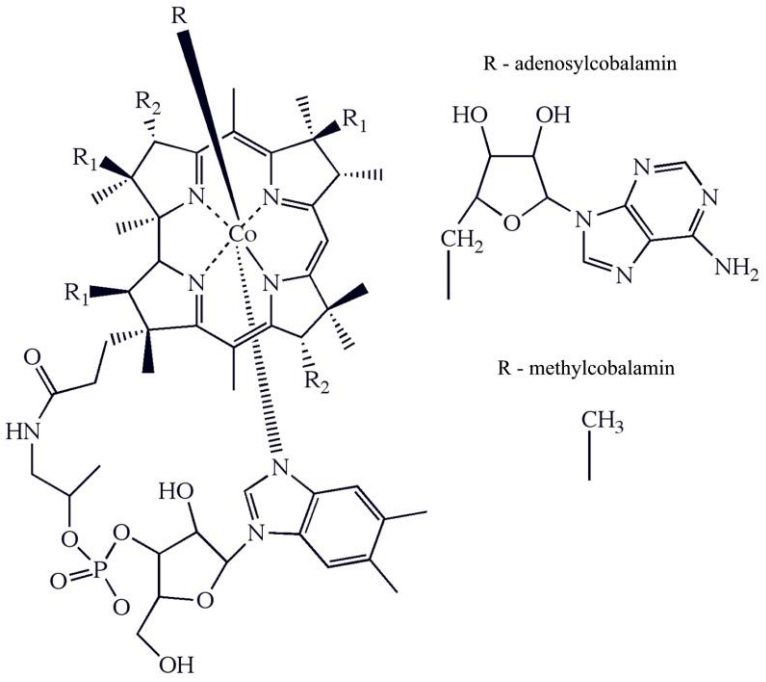

Figure 1.2. Depiction of the structures of AdoCbl and MeCbl. R represents the β-axial ligands, either 5'-deoxyadenosyl (top) or methyl (bottom). R1 and R2 represent acetamide and propionamide side chains. The dimethylbenzimidazole α-axial ligand of the coenzyme remains coordinated when the coenzyme is bound to EAL.[18-19]

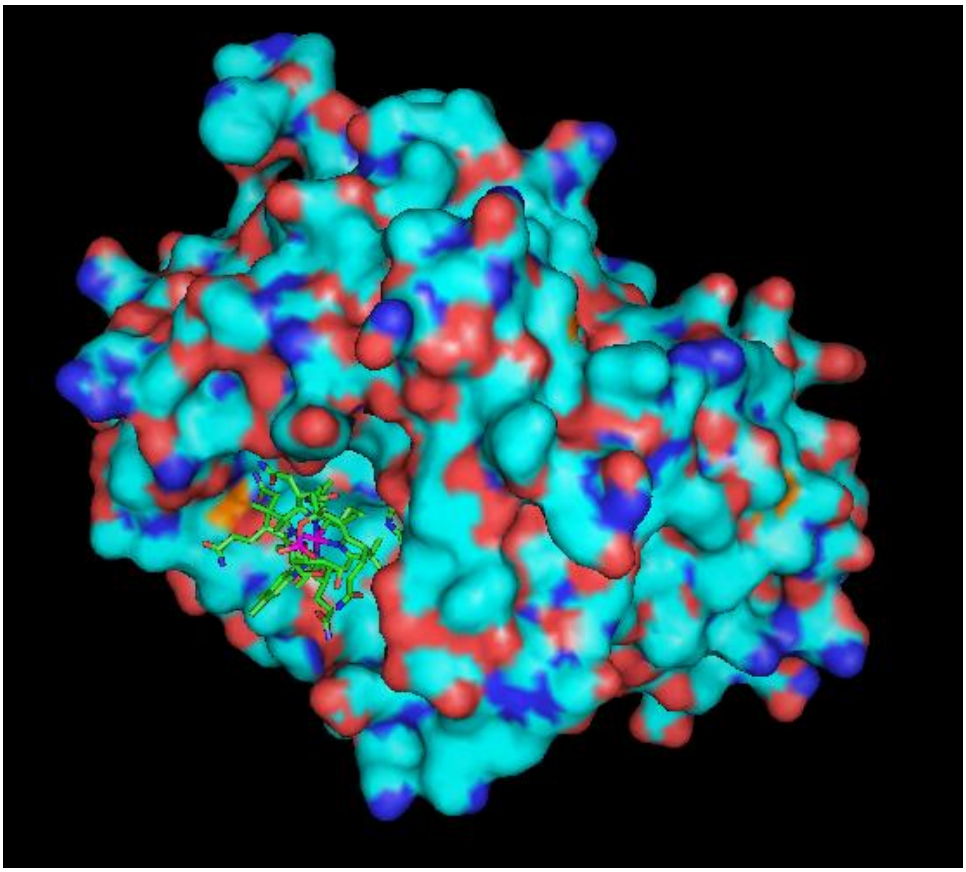

Figure 1.3. Space filled image of active site region in EAL with bound cofactor.[9]

The active ternary complex of EAL is formed following the binding of coenzyme B_{12} and a substrate molecule to EAL. The minimum mechanism[20-22] of EAL is shown in Figure 1.4. The first step in the native catalytic cycle of all AdoCbl-dependent enzymes is the thermally activated homolytic cleavage of the cobalt-carbon (Co-C) bond in AdoCbl, which results in the formation of the cob(II)alamin–5'-deoxyadenosyl radical pair.[1-3] The C5' radical center of the 5'-deoxyadenosyl moiety then migrates through the protein to abstract a hydrogen atom (HT1) from the substrate, to form the substrate radical (S•), which activates the substrate for rearrangement. High-resolution electron

paramagnetic resonance (EPR) spectroscopic studies of the cob(II)alamin-substrate radical pair, formed from (*S*)-2-aminopropanol [23-26] or aminoethanol,[27-29] have shown that the migration of the C5' radical center occurs over 5-7 Å and is illustrated in Figure 1.5. The substrate radical rearranges to form the product radical (P•). The product radical abstracts a hydrogen atom (HT2) from the 5'-deoxyadenosine to form the product and reform the 5'-deoxyadenosyl radical. The 5'-deoxyadenosyl radical migrates back across the active site to reform the intact cofactor, returning the cofactor to the cob(III)alamin state. The product is released making the substrate binding pocket available to bind a new substrate.

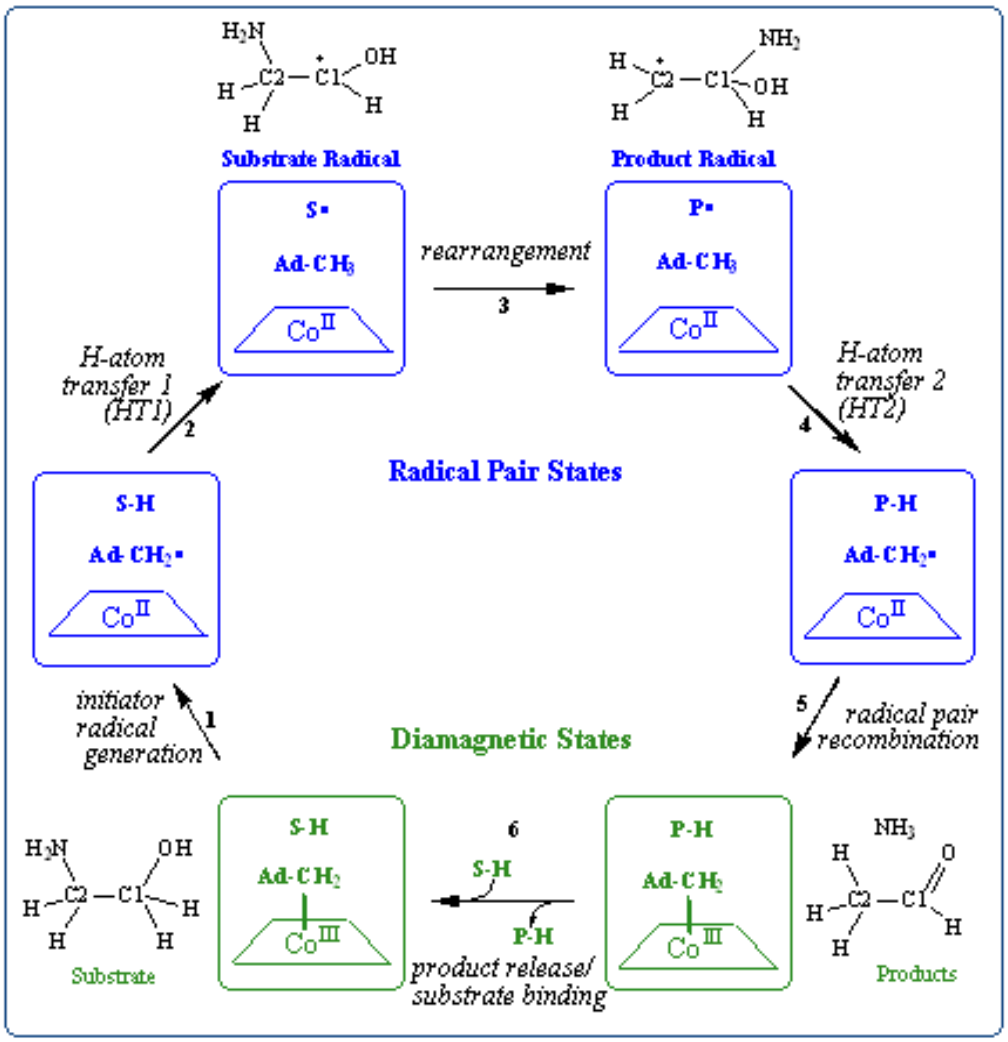

Figure 1.4. Proposed minimal mechanism of catalysis for vitamin B_{12} coenzyme-dependent EAL.[1,30] The paramagnetic radical pair states and diamagnetic states are indicated. The forward direction of reaction is indicated by arrows. For the substrate, (*S*)-2-aminopropanol **1**, the cycle is reversible.[20-22] The steps are: (1) radical pair separation, (2) first hydrogen atom transfer (HT1), (3) radical rearrangement, (4) second hydrogen atom transfer (HT2), (5) radical pair recombination, and (6) product release/substrate binding. Substrate-derived species are designated S-H (bound substrate, **1**), S$^{\bullet}$ (substrate radical, **2**), P$^{\bullet}$ (product radical, **3**), and PH (diamagnetic products, aldehyde **4** and ammonia). The 5'-deoxyadenosyl β-axial ligand is represented as Ad-CH_2- in the intact coenzyme, and as Ad-$CH_2^{\bullet}$ (5'-deoxyadenosyl radical) or Ad-CH_3 (5'-deoxyadenosine) following cobalt-carbon bond cleavage. The cobalt ion and its formal oxidation states are depicted, but the corrin ring and dimethylbenzimidazole α-axial ligand of the coenzyme[18-19] are not shown for clarity.

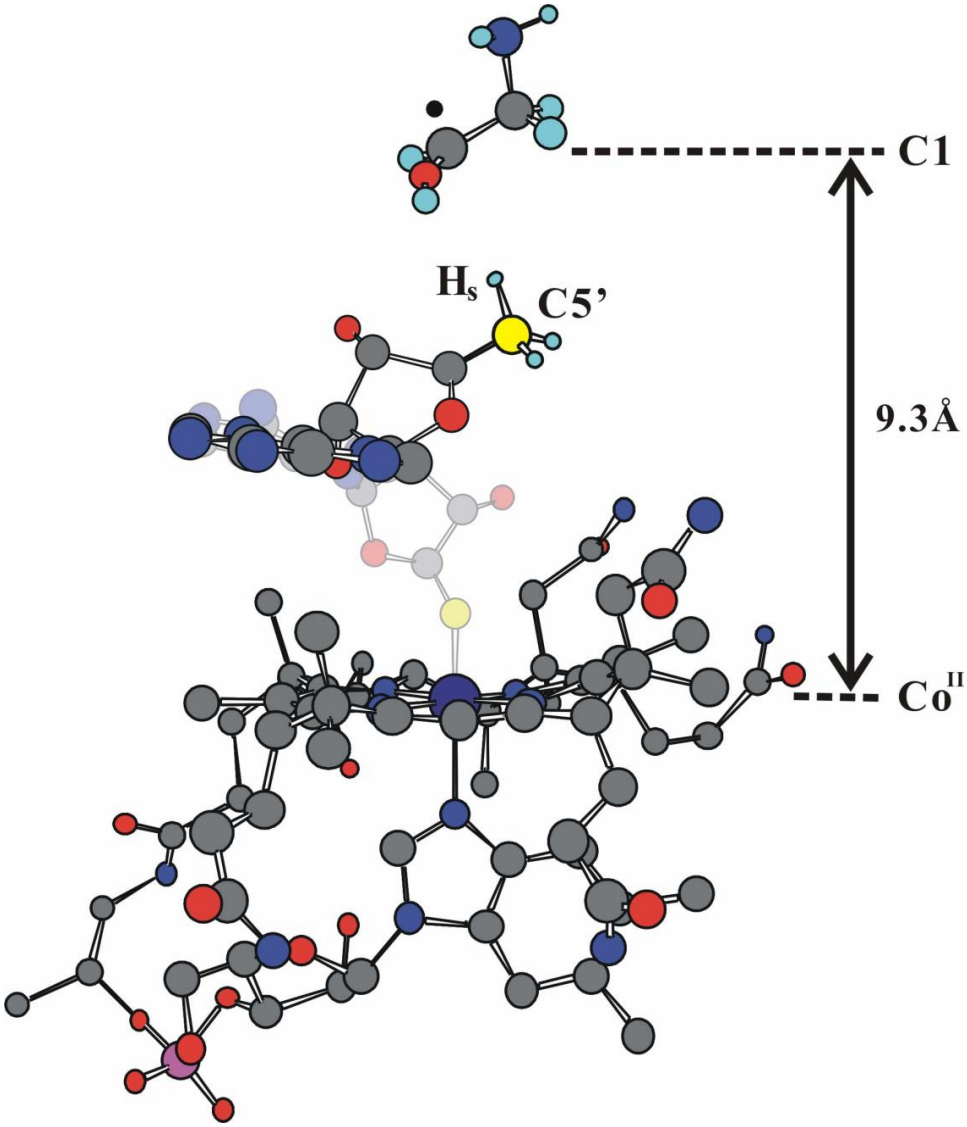

Figure 1.5. Model for the reactant geometries involved in cobalt-carbon bond cleavage, radical migration, and substrate radical formation in EAL.[24,27]

One of the central questions is how the enzyme system contributes to the cleavage of the Co-C bond, which is accelerated by $>10^{11}$-fold in the enzymes, relative to the cleavage in solution.[4,31-32] A long-standing issue in AdoCbl-dependent enzyme catalysis is the molecular mechanism of the rate acceleration[33-34], and how substrate binding,

which is required for cleavage, is coupled to the reaction.[1-3] The mechanism of the substrate binding-induced transformation (the "substrate trigger"), from the quiescent Co-C bond in the EAL holoenzyme to a state in the EAL/AdoCbl/substrate ternary complex, in which the Co-C bond lifetime is $<10^{-2}$ s at 298 K,[35] has not been characterized experimentally,[36] although a mechanism based on X-ray crystallographic structures of EAL has been proposed.[37]

1.2 Proposed Mechanisms for Cobalt-Carbon Bound Cleavage Enhancement

The rate of the cobalt-carbon bond cleavage rate in the enzyme system is enhanced by $>10^{11}$, as compared to the rate of cleavage of the free cofactor in solution.[32,38-39] This rate enhancement corresponds to a considerable lowering of the effective cobalt-carbon bond dissociation energy, from ~32 kcal/mol to ~17 kcal/mol after enzyme and substrate binding[40]. The lowering of the bond energy enhances the rate at which the cobalt carbon bond cleaves from once every 6 months to >100 times per second. The dramatic rate enhancement is necessary for the reaction to be efficient enough to support living organisms.

Chemomechanical Strain Hypothesis

Chemomechanical strain effects to the cofactor have been considered as a mechanism for the enormous rate enhancement of bond cleavage. A number of mechanisms that induce steric crowding, strain or corrin ring deformation to the cofactor upon enzyme

binding have been proposed.[5,41-49] These mechanisms, though different in their detail, are similar in that they result in the destabilization of the ground state energy of the cobalt-carbon bond and provide an enhancement to the bond cleavage rate.

The *trans*-effect hypothesis proposes that the mediation of the Co-C bond cleavage occurs through the α-axial ligand of AdoCbl, DMBz.[41-42] Evidence for the hypothesis originated in the correlation of the weakening of the bond dissociation energies of cobalt alkyl compounds with the steric bulk of the axial ligands.[5,43-45] This data has led to the hypothesis that upon binding of the AdoCbl cofactor to the EAL protein, the DMBz ligand sterically distorts the corrin ring upward, weakening the Co-C bond of the cobalt atom with the 5'-deoxyadenosyl group of the cofactor.[41]

Resonance Raman studies of cobalt alkyl compounds have showed that the α-axial ligand has a negligible effect on the Co-C bond energy.[50] Substitution of the DMBz ligand to imidazole, imidazolate or a water molecule resulted in minor shifts in the Raman peaks assigned to the Co-C bond, suggesting no substantial change in the strength of the bond. Evidence against the *trans*-effect hypothesis as the mechanism for catalysis of Co-C bond cleavage has also been provided by calculations[46-49] that show the Co-C bond strength is not significantly affected by the removal of the DMBz ligand.

It has also been proposed that the lowering of the Co-C bond energy of the cofactor is mediated through the 5'-deoxyadenosyl group on the β-axial face of the cofactor.[1,51-53] The mechanism is referred to as the *cis*-effect. It is hypothesized that protein residues inside the enzyme active site, interact with the 5'-deoxyadenosyl group to apply strain to the Co-C bond, which lowers the bond energy. Resonance Raman experiments using isotopic substitution to identify the cobalt-carbon stretch frequency have been carried out

for the cofactor as well as the cofactor-enzyme system using methylmalonyl-CoA mutase.[53] The difference in the frequencies was estimated to correspond to a ground state destabilization of the bond after binding to the enzyme of about ~0.5 kcal/mol.[52-53] This amount of ground state destabilization is insignificant to the almost 17 kcal/mol change necessary for the rate enhancement observed for the cofactor-enzyme-substrate system.[19] Isolation of the true ternary complex was not achieved in the experiments and leaves the possibility of triggering of the Co-C bond by the true substrate.

The chemomechanical mechanisms for catalysis are further complicated by the "substrate trigger model", which attributes the binding of the substrate to the enzyme as the trigger of the cobalt-carbon bond cleavage rate enhancement,[2,33,54] and that the binding of the cofactor to the much larger enzyme does very little to enhance the cleavage rate. The model proposes that the binding of the relatively small substrate induces conformational changes in the enzyme that destabilize the Co-C bond. The first evidence for the hypothesis came from X-ray crystallographic studies of the B_{12}-dependent enzyme, methylmalonyl-CoA mutase[54-55], in which a conformational change of the protein was observed in the crystal structure of the substrate inhibitor bound protein as compared to the holoenzyme. Similar effects have been observed in the B_{12}-dependent enzyme, diol dehydratases,[56] in which distortion of the Co-C(5')-C(4') bond angle of the cofactor was observed following binding of substrate inhibitor. These experiments were, however, performed with CNCbl, an AdoCbl analog, to avoid cleavage of the Co-C bond during X-ray irradiation, as well as substrate inhibitors, and do not provide substantial evidence to validate the hypothesis. Therefore, further

consideration is necessary to account for the lowering of the cobalt-carbon bond dissociation energy by ~17 kcal/mol.[2]

Dynamic Contributions to Catalysis

The search for universal features of catalytic mechanisms utilized by enzymes to achieve their enormous rate enhancements of up to 10^{20}–fold has evolved to focus on the nature of the free energy surface for the reactions, and the contributions to trajectories over this surface that are driven by protein motions, across a broad range of time scales.[57-58] The stabilization of specific protein conformational states, in response to the binding of substrates and analogs of intermediates, is well known.[59] Nuclear magnetic resonance (NMR) and X-ray crystallographic studies have revealed that the apoenzyme and reactant-bound forms of the enzyme, fluctuate among macroscopic conformations that are representative of protein structure states along the collective reaction coordinate for the enzyme reaction.[57,60-61] This "conformational sampling" among thermally averaged equilibrium structures, which involves side chains and secondary and tertiary structure elements throughout the protein, occurs on the micro- to millisecond time scale, and is thus commensurate with the time scales of the chemical steps in the reactions. Specific concerted protein motions have been proposed to enhance hydrogen atom transfer[62-63] and other reactions.[57,64] Faster protein motions, on the pico- to nanosecond time scale, that do not couple directly to slower chemical events, lead to an averaged potential for the reactants, and thus contribute to the free energy surface for the reaction.[57-58] Dynamical effects of promoting vibrations, that act on the sub-picosecond time scale in the transition state region, have also been proposed.[65] Experimental

observations of dynamical contributions to function in the ternary complex of enzyme, cofactor and substrate has been limited to the monitoring of both native and nonnative fluorescent probes in single molecule FRET experiments,[66-67] due to inability to synchronize the rapid turnover of enzymatic ternary systems. Though numerous experiments have provided evidence of dynamics affecting protein function, experiments have not been developed that probe dynamical contributions to the mechanism of catalysis in B_{12} dependent enzymes.

1.3 Photolysis of Cobalamins

The ultraviolet (UV)/visible absorption spectra of selected cobalamin derivatives are shown in Figure 1.6.[68-69] The absorption spectra are composed of two prominent regions that are the result of $\pi \rightarrow \pi^*$ transitions of the corrin ring. The α/β region of the spectra, from 475 to 575 nm, is characterized by an absorption coefficient, ε, between 8,000 and 10,000 $M^{-1}cm^{-1}$. The α/β band of the cobalamin spectra is a result of HOMO→LUMO transitions polarized along the long axis, C^5 to C^{15}, of the corrin ring.[46] The γ-band, located in the UV region of the spectra, is the result of transitions polarized along the short axis, Co to C^{10}, of the corrin ring. The weaker D and E transitions lie between the α/β and γ-band and are controversial in origin.[46] As shown in Figure 1.6, the β-axial ligand of the cobalamin molecule can affect the corrin ring electronic structure significantly and contribute to large changes in the UV/Visible absorption spectra. For example, the replacement of the adenosyl group in AdoCbl with a water molecule to form AquoCbl, enhances the absorbance at 350 nm by approximately a factor of 2.

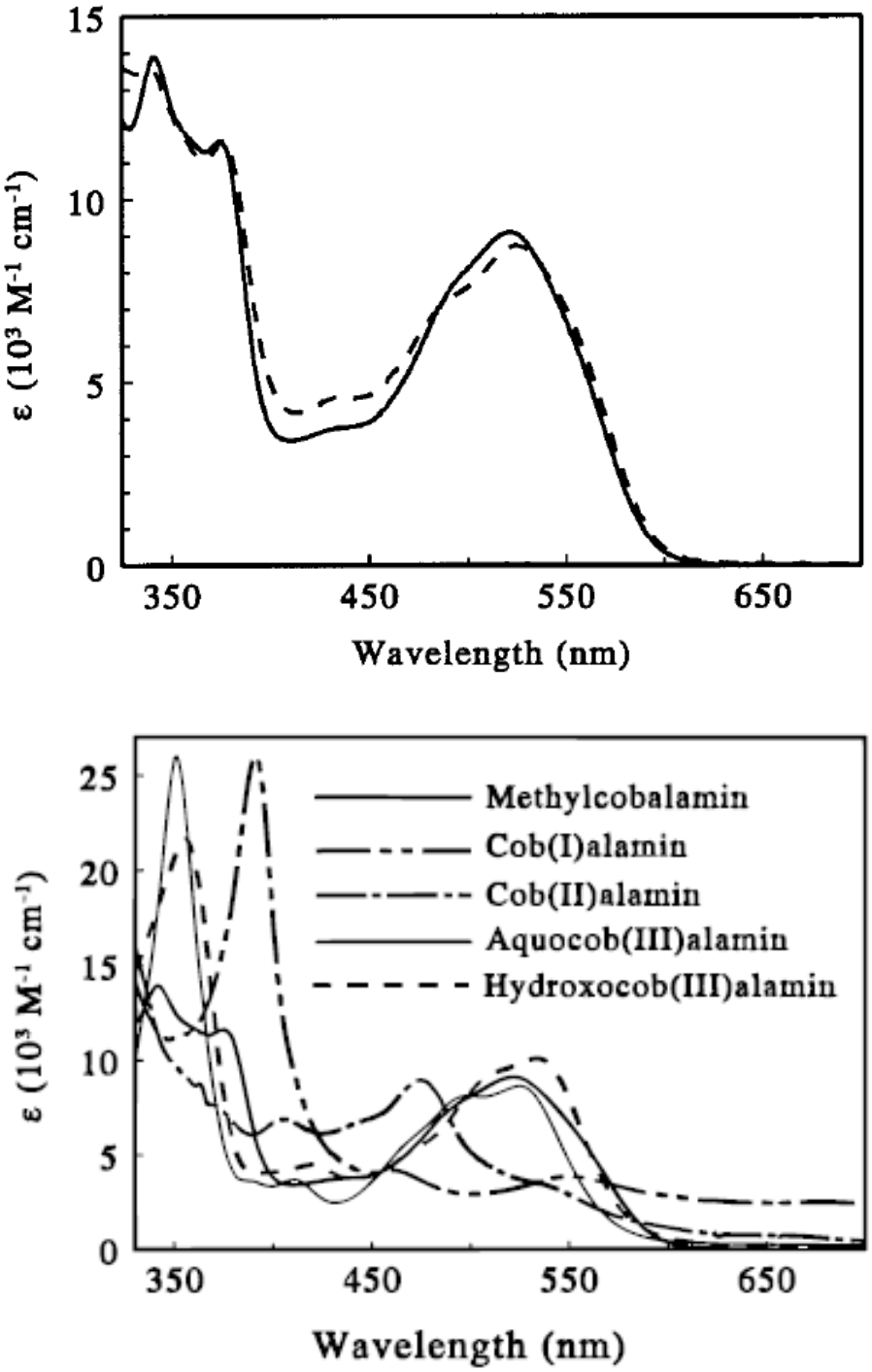

Figure 1.6. UV-visible absorption spectra of methylcobalamin (solid line) and 5'-deoxyadenosylcobalamin (dashed line) (top)[70] and spectra of methylcobalamin, cob(I)alamin, cob-(II)alamin, hydroxocob(III)alamin, and aquocob(III)alamin (bottom). The spectra have been scaled by using literature values of ε_{max}.[68-69]

The cobalt-carbon bond in the AdoCbl and MeCbl cofactor has been shown to be photolyzable with photon wavelengths ranging from 350 - 600 nm.[70-72] The photolysis of the Co-C bond forms a singlet radical pair state that has been characterized to be identical to the radical pair formed through bond thermolysis in the enzyme system.[73-74] Numerous studies of the kinetic processes following bond cleavage of the cofactor in solution have been performed by using an intense laser pulse to initiate bond cleavage.[5,45,69,71-73,75-82] Figure 1.7 shows a simplified kinetic scheme of the canonical states and steps involved in the photolysis experiment. Following photo-excitation, a fraction of the photoproducts relaxes to the ground state in $<10^{-9}$ s[70,81], forming the geminate cob(II)alamin-5'-deoxyadenosyl radical pair. The excited state formation and sequence of early photoproduct intermediates for alkylcobalamins in solution, which are not shown explicitly in Figure 1.7, have been described by Sension and coworkers.[70,83] The geminate radical pair state is one in which the cobalt-carbon bond has been cleaved and the atoms remain separated at approximately the original bond length. The geminate radical pair exists within a "cage" of surrounding solvent molecules, and can recombine promptly (geminate recombination), or diffuse apart (cage escape) and recombine on a slower time scale.[84] The radical pair formation and decay can be detected optically with relatively high sensitivity by monitoring the UV-visible absorption changes associated with the interconversion of the cobalamin between the Co^{III} state (visible wavelength maximum, λ_{max}=525 nm in water) and Co^{II} state (λ_{max}=470 nm in water). In studies of AdoCbl, MeCbl, and other alkylCbl in solution, time scales from electronic excited state formation and decay (femtoseconds) to solvent separation of the cob(II)alamin-radical pairs (milliseconds) have been monitored.[69-70,76,78-82,85-89] Following AdoCbl photolysis

in water, the geminate cob(II)alamin-5'deoxyadenosyl radical pair recombination and cage escape occur with rate constants of 1.4×10^{9} s^{-1} and 0.6×10^{9} s^{-1}, respectively, leading to a fraction (0.29) of radical pairs that escape the solvent cage.[70,88] The cage escape radical pair can recombine to reform the geminate radical pair, or can undergo radical-radical annihilation, internal rearrangement to form cycloadenosyl or other species, or react with solvent by hydrogen atom abstraction, which leads to irreversible cob(II)alamin formation.[81,90] An illustration of the steps following radical pair production and separation in solution and in the protein environment is shown in Figure 1.8.

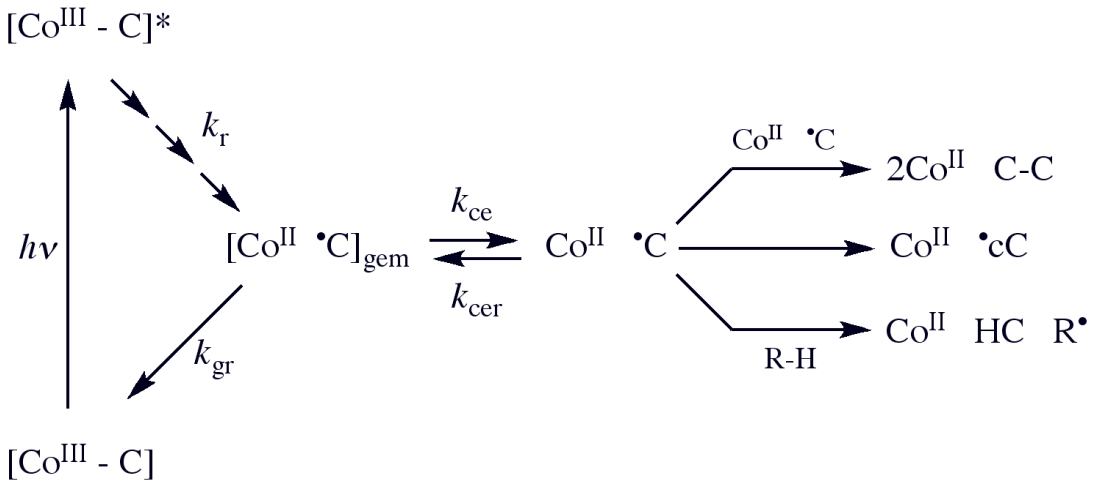

Figure 1.7. Simplified schematic diagram of the states and pathways of formation following photolysis of AdoCbl in solution. The cobalamin and 5′-deoxyadenosyl moiety are represented by cobalt (Co) and C5′-methylene center (C), as follows: [Co^{III}-C], intact coenzyme; [Co^{III}-C]*, excited singlet state; [Co^{II} •C]gem, geminate radical pair; Co^{II} gem •C, cage escape radical pair. The cage escape radical pair can recombine to reform the geminate radical pair, or can undergo radical-radical annihilation (top), internal rearrangement to form cycloadenosyl or other species (middle), or react with solvent (R-H) by hydrogen atom abstraction (bottom), which leads to irreversible cob(II)alamin formation.[81,91] Intermediate excited and relaxed states[70,82], which are not shown, are represented by the sequence of arrows leading from [Co^{III}C]*. Rate constants are defined as follows: k_r, excited to ground state relaxation; k_{gr}, geminate recombination; k_{ce}, cage escape; k_{cer}, reformation of geminate radical pair from cage escaped radical pair.

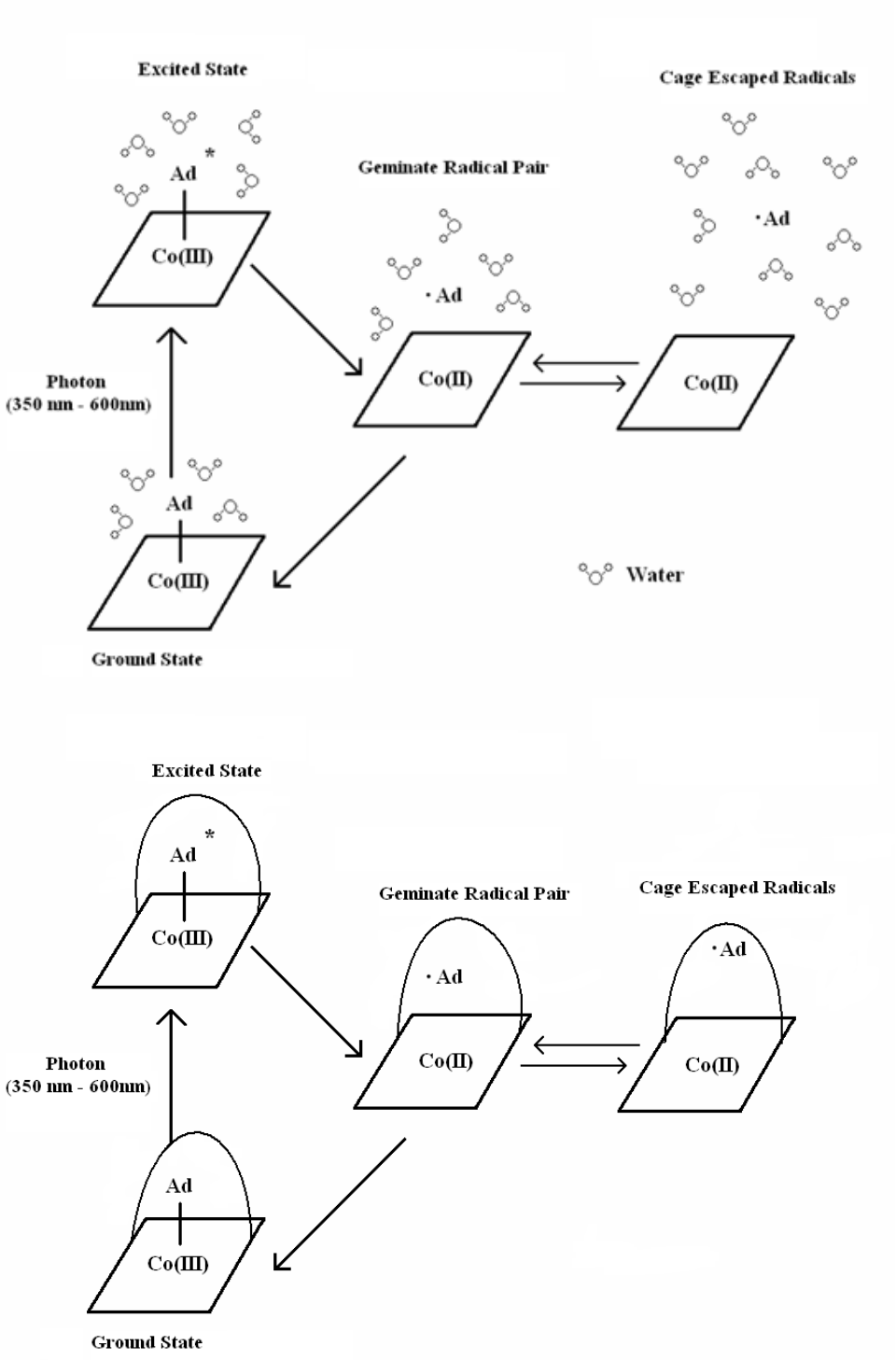

Figure 1.8. Depiction of adenosylcobalamin photolysis, recombination and geminate separation in solution (top) and inside the EAL binding site (bottom).

Photolysis of protein-bound AdoCbl provides a method for overcoming the large Co-C bond dissociation energy of ~32 kcal/mol[92] on a sub-nanosecond time scale. Calculations for methylcobalamin photolysis suggest that the separation of Co(II) and C5', r_{CoC}, in the ground state, following photocleavage and excited state relaxation, is 2.7-3.0 Å.[93] These r_{CoC} values correspond to calculated Co-C bond cleavage extents of >80%.[94-96] Thus, photolysis creates a mimick of the thermal cob(II)alamin-5'-deoxyadenosyl radical pair, whose fate can be used to probe the mechanism of the radical pair separation process. Quantitative time-resolved measurements of AdoCbl photolysis and recombination in proteins have thus far only been performed for AdoCbl-dependent glutamate mutase (GluM) on the ultrafast time scale (<9 ns).[75,97] The results showed that binding of AdoCbl to GluM led to a reduction of quantum yield of cob(II)alamin (at 9 ns) from 0.23 in solution to 0.05 in the protein. This was caused primarily by a decrease in the cage escape rate constant to 5-6 $\times 10^7$ s^{-1}, relative to the value of 5.7×10^8 s^{-1} reported for pure water.[75,97] The protein reduced the geminate recombination rate by only 30%[79]. These results show that AdoCbl is photolyzable in situ and that the protein influences (reduces) the quantum yield. However, these studies were restricted to ultrafast time scales that do not address recombination of the cage escaped radical pair. If the cage escaped 5'-deoxyadenosyl radical diffuses along the native radical pair separation coordinate[98-100] in the active site, then the time scale of recombination may be governed by the activation free energy barriers that control the native radical pair separation process on the micro- to millisecond time scales. The measurements in GluM were also carried out with holoenzyme in the absence of substrate. Therefore, the influence of substrate binding on the photoproduct yields and decay reactions was not addressed.

1.4 Outline of Dissertation

In order to address the mechanism of formation and stabilization of the cob(II)alamin-5'-deoxyadenosyl radical pair in the protein, we use pulsed-laser photolysis of the Co-C bond to prepare the radical pair population, followed by a UV-visible absorption probe of its time evolution. A home designed and constructed transient absorption spectrometer used to make these measurements is described in Chapter 2. This method overcomes the kinetic complexity and asynchrony of steady-state kinetic studies, and the evolution of the radical pair can be observed on time scales that are several orders of magnitude shorter than in previous stopped-flow studies of cob(II)alamin formation in the AdoCbl-dependent enzymes, methylmalonyl-CoA mutase[101], glutamate mutase[102], ribonucleotide triphosphate reductase[103], and ethanolamine ammonia-lyase [104].

In chapter 3, we report transient optical absorption measurements of the quantum yield and radical pair recombination kinetics following photolysis of AdoCbl on time scales from 10^{-7} to 10^{-1} s in solution and in EAL at room temperature. The influence of substrate on the quantum yield and radical pair recombination kinetics is assessed by using (*S*)-1-amino-2-propanol, an inactive substrate analog, which binds to the substrate binding site in EAL, but does not form the cob(II)alamin-substrate radical pair state. This analog has a methyl group at the pro-(*S*) position of stereospecific hydrogen atom abstraction from the carbinol carbon of the native substrate[105-106], which blocks the hydrogen atom transfer reaction. A branched kinetic mechanism is proposed to account for the results, in which the observed transients represent metastable cob(II)alamin-5'-deoxyadenosyl radical pair states. We conclude that the substrate analog partially fulfills

native function by suppressing non-productive reactions of the radical pair, but is not capable of inducing the full "substrate trigger" of Co-C bond cleavage that is characteristic of the native substrates.

In chapter 4 we report the results of visible light, pulsed-laser photolysis of the EAL ternary complex, formed with the substrate, (*S*)-2-amino-1-propanol. The ternary complex is formed and stabilized against thermal reaction on the time scale of the photolysis experiment in an optically transparent, fluid dimethylsulfoxide (DSMO)/water cryosolvent.[35,107] We observe that substrate binding to holo-EAL under conditions of kinetic competence for thermally-activated turnover at 240 K[35] does not significantly perturb the absorption spectrum of AdoCbl, and that the optically-detected photoproduct amplitudes and recombination rates in holo-EAL and the ternary complex do not differ significantly. Continuous visible irradiation also has no effect on the kinetics of thermally-activated cob(II)alamin-substrate radical pair formation, or the subsequent equilibrium level of this state at 246 K, as detected by EPR spectroscopy. The interpretation of these results requires a model in which rate-determining protein-cofactor interactions guide the cleavage of the Co-C bond, at every microscopic step of radical pair separation. The Co-C bond cleavage catalysis in EAL is characterized by a diagonal trajectory across a free energy landscape defined by coupled chemical and protein coordinates.

The last chapter of this dissertation, Chapter 5, focuses on developing a compressed photosynthesis subunit from the the B_{12} cofactor and EutB subunit of the EAL enzyme system for the reduction of carbon dioxide (CO_2) and toxic halo-organic compounds. We find that a significant increase in the reduction rate of the cofactor by

Ti(III) citrate to the Co^{I} state is achieved following the removal of the DMBz axial ligand of the cofactor. Removal of the ligand also permits photo-initiated reduction of cofactor. The interaction of the Co^{I} state with CO_2 and chloroacetonitrile is also characterized. The experiments demonstrate the reduction of the cofactor to the Co^{I} state while bound to the EAL and the isolated EutB protein, and thus the ability to assemble the reactive protein complex.

Chapter 2: Construction of a UV/Visible Transient Absorption Spectrometer

2.1 Transient Absorption Spectroscopy: Principles

Transient-absorption spectroscopy is an optical technique used to resolve in time the absorption spectrum of a sample, following a very fast perturbation of the sample that results in a spectral change. The change in absorbance at a particular wavelength, as in the case considered here, or of the entire spectrum, is measured as a function of time following the perturbation of the sample by the pulse, which results in the creation of new species. In the case considered here, the perturbation is optical excitation, which is typically produced by a pulsed laser or flash lamp with a time width much smaller than the lifetime of the transient state or species of interest. The change in the absorption spectrum induced by the excitation pulse is typically monitored using a continuous wave light source, for time scales greater than 10 ns, or a pulsed laser source, as in the case of sub-nanosecond pump-probe studies. Transient absorption spectroscopy has been applied to a number of physical systems and is capable of extracting information on photo-initiated chemical events, such as bond breaking, electron transfer, on a wide range of time scales, from 10^{-15} to 10 s of seconds.[71,81,85-86,108]

The absorbance of a molecule, A_1, at a given wavelength, is quantified by Beer's Law,[109] which describes the absorption of a species at a given concentration.

$$A_1 = \varepsilon_1 b c_1 \qquad (2.1)$$

In equation (2.1), c_1 is the total concentration of the absorbing species [Molar], b is the path length [cm] and ε_1 is the molar absorptivity [M^{-1} cm^{-1}], of the species at a particular

wavelength. The absorbance, A_1, is measured experimentally by monitoring the intensity of the incident monitoring beam, I_o, and the intensity of the beam after transmission through the sample, I_{trans} , and is given by equation (2.2)

$$A_1 = -\log\left(\frac{I_{trans}}{I_o}\right) \tag{2.2}$$

The absorbance, A_1, can be can be rewritten in terms of the transmittance,

$$T = \left(\frac{I_{trans}}{I_o}\right), \tag{2.3}$$

and then combined with equations (2.1) and (2.2) to express the transmittance value in terms of the extinction coefficient, path length and concentration, as shown in equation (2.4).

$$T = \frac{I_{trans}}{I_o} = 10^{-\varepsilon_1 b c_1} \tag{2.4}$$

The ratio of the intensity of the transmitted beam to the initial beam, shown in equation (2.4), is typically measured experimentally to collect static absorption spectra and used to find the absorbance of the sample.

The absorbance can be expressed in a form that describes a sample which contains two molecular species with unique absorption spectra, as is a typical case following photolysis:

$$A_{new} = b(\varepsilon_1 c_{1new} + \varepsilon_2 c_2) \tag{2.5}$$

In equation (2.5), b is the path length, ε_1 and ε_2 are the molar absorptivity [M^{-1} cm^{-1}] coefficients of the respective species at the monitoring wavelength and c_{1new} and c_2 are their respective concentrations. The concentration of the species considered is given as c_{1new} and c_2 with c_{1new} representing the same species as c_1, but in depleted concentration due to photo-induced transformation to the c_2 species. The absorbance A_{new} is related to the initial intensity, I_o, and final intensity, $I_{transnew}$ of the monitoring beam as shown in equation (2.6).

$$A_{new} = -\log\left(\frac{I_{trannew}}{I_o}\right) \tag{2.6}$$

The transmission of a sample with two unique species present can then be expressed as shown in equation (2.7).

$$T = \frac{I_{trannew}}{I_o} = 10^{-(\varepsilon_1 b c_{1new} + \varepsilon_2 b c_2)} \tag{2.7}$$

Equations (2.4) and (2.7) can be combined to express the ratio of the transmitted intensity of the probe beam after photolysis with two species originating from a single species as shown in equation (2.8).

$$T = \frac{I_{trans}}{I_{transnew}} = 10^{(-\varepsilon_1 bc_1 + \varepsilon_1 bc_{1new} + \varepsilon_2 bc_2)} \tag{2.8}$$

Given that the difference in the absorbance value of the two species at a given wavelength can be expressed as the difference extinction coefficient, $\Delta\varepsilon$, as shown in equation (2.9),

$$\Delta\varepsilon = \varepsilon_2 - \varepsilon_1 \tag{2.9}$$

and that the total concentration of all species present in the sample following photolysis is

$$c_{1new} = c_1 + c_2 \tag{2.10}$$

equation (2.8) can be rewritten as

$$\frac{I_{transtotal}}{I_{transnew}} = 10^{\Delta\varepsilon c_2 b} \tag{2.11}$$

Equation (2.11) conveniently relates the change in the monitoring beam intensity at a given wavelength to the concentration of the new species created from photolysis. The intensity of the photons in the monitoring beam is proportional to the voltage measured from a photomultiplier tube (PMT) used to detect the beam, and therefore, the values $I_{transtotal}$ and $I_{transnew}$ can be replaced with the respective PMT voltages, v_{total} and v_{new}. The

concentration of the new species formed from photolysis can be expressed as shown in equation (2.12).

$$c_2 = \log \frac{\left(\frac{v_{total}}{v_{new}} \right)}{\Delta \varepsilon} \tag{2.12}$$

Values of the difference in molar absorptivity, $\Delta\varepsilon$, can be measured experimentally from static spectra of the two species individually, which are obtained separately. Typically, for transient absorption measurements, the voltage, v_{total}, is measured from the baseline reading of the sample before photolysis and v_{new} values are recorded following photolysis. This allows for the concentration of the new species to be monitored as a function of time following photolysis.

The efficiency of photoproduct production can give valuable information about the excitation characteristics of the molecule, chemical processes immediately following photolysis, as well as the environment of the species being examined. The efficiency at which photoproducts are produced is typically quantified as the quantum yield (QY), and is defined as the concentration of photoproduct species divided by the number of absorbed photons.

$$QY = \frac{[P]_{product}}{[h\upsilon]_{abs}} \tag{2.13}$$

Quantification of the yield of photo-product produced following a pulsed photolysis experiment must be performed at low excitation pulse energy to exclude multiple photon absorptions per molecule. The excitation pulse energy is chosen by measuring the concentration of photoproduct of the sample as a function of pulse energy to identify the single photon excitation region, where there is a linear correlation of incident photons with the number of photoproducts produced. The concentration of photoproducts is found by using the previously derived relation in equation (2.12). The concentration of incident photons, $[h\nu]_{incident}$, is obtained from the following expression,

$$[h\nu]_{incident} = \frac{E_{pulse}}{E_{photon} V_{beam} N_A} \tag{2.13}$$

where E_{photon} is the photon energy at, V_{beam} is the pump excitation volume, N_A is Avogadro's number, and E_{pulse} is the laser pulse energy. The value of $[h\nu]_{abs}$ is obtained from $[h\nu]_{incident}$ after scaling by the probability of photon absorbance, which is given by (1-T) and found using the concentration of the initial sample calculated from the static absorption spectrum taken before photolysis.

2.2 Mechanical and Optical Setup

The transient absorption spectrometer (TAS) was designed and constructed in order to produce and detect optical transients in protein samples which commonly have experimentally unfavorable characteristics. Protein frequently has low solubility that

necessitates low sample concentrations to reduce unwanted light scattering caused by aggregation, which decreases signal to noise. In some cases, such as the photolysis of protein-bound cofactors, ligands with small dissociation constants (weak binding) require samples to contain only a fraction of cofactor per protein binding site, in order to minimize free cofactor in solution. This effect further reduces concentration of species that are monitored in the sample. Samples can also have photolysis reactions that are irreversible, making sample volume replenishing necessary between excitations. Low QY values also make photoproduct detection difficult. The transient absorbance spectrometer described here has a sensitivity (signal to noise ratio of 2) to change in absorbance, ΔA, of $7x10^{-3}$ per shot, and is able to monitor wavelength changes over the visible region from 300-650 nm ± 1 nm, and has a time range from 10^{-9} - 10^{1} of seconds. A schematic of the constructed TAS is shown in Figure 2.1. The components from the schematic and labeling from the legend of Figure 2.1 will be referred to in the following description of the TAS.

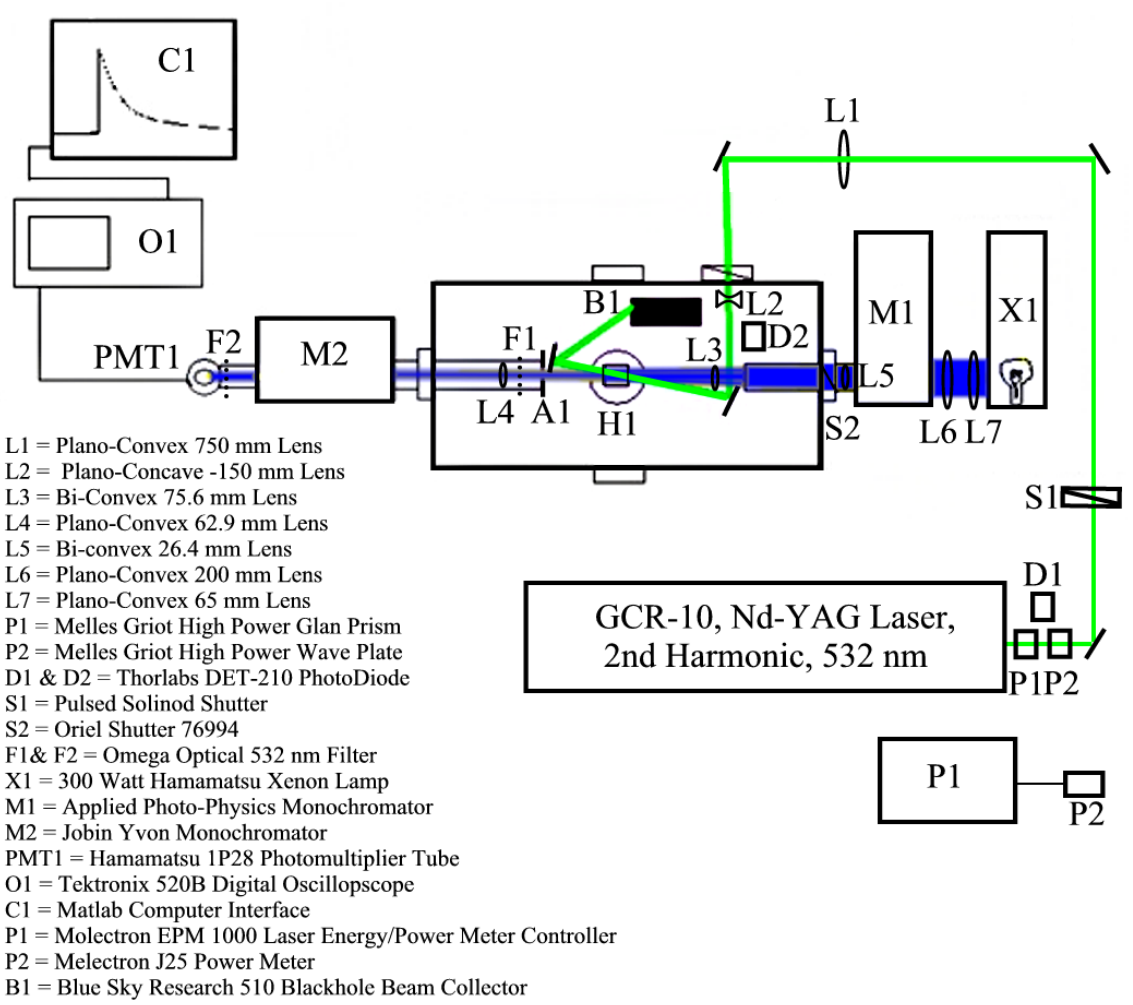

Figure 2.1. Mechanical and optical schematic of transient absorption spectrometer.

Transient Absorption Spectrometer Housing and Sample Holder

The TAS housing was designed and constructed to minimize the amount of stray light reaching the sample compartment, in order to minimize unfavorable photolysis events and spurious light detection. The complete TAS system is shown in Figure 2.2. The entrance and exit ports of the TAS housing where threaded to accommodate optical

lens tubes and have adapters designed for the mounting of components directly to the TAS housing. An aluminum beveled lid to the TAS housing was also designed and constructed along with a smaller sample holder cover for use during experiments which required access to the interior of the TAS. The TAS was equipped with a tapped sub-floor under which cooling, air and sample lines, stirrer power and BNC connections are located. Two BNC connections were also installed above the sub-floor for connection to a fast photodiode used for oscilloscope triggering. The TAS box, monitoring beam lamp and monitoring beam monochromators were equipped with height adjustable feet as well as custom clamps to secure them to the optical table. The entire TAS housing, flanges, adapters, sub-floor, and detection housing were anodized flat black to minimize optical reflections and stray light collection.

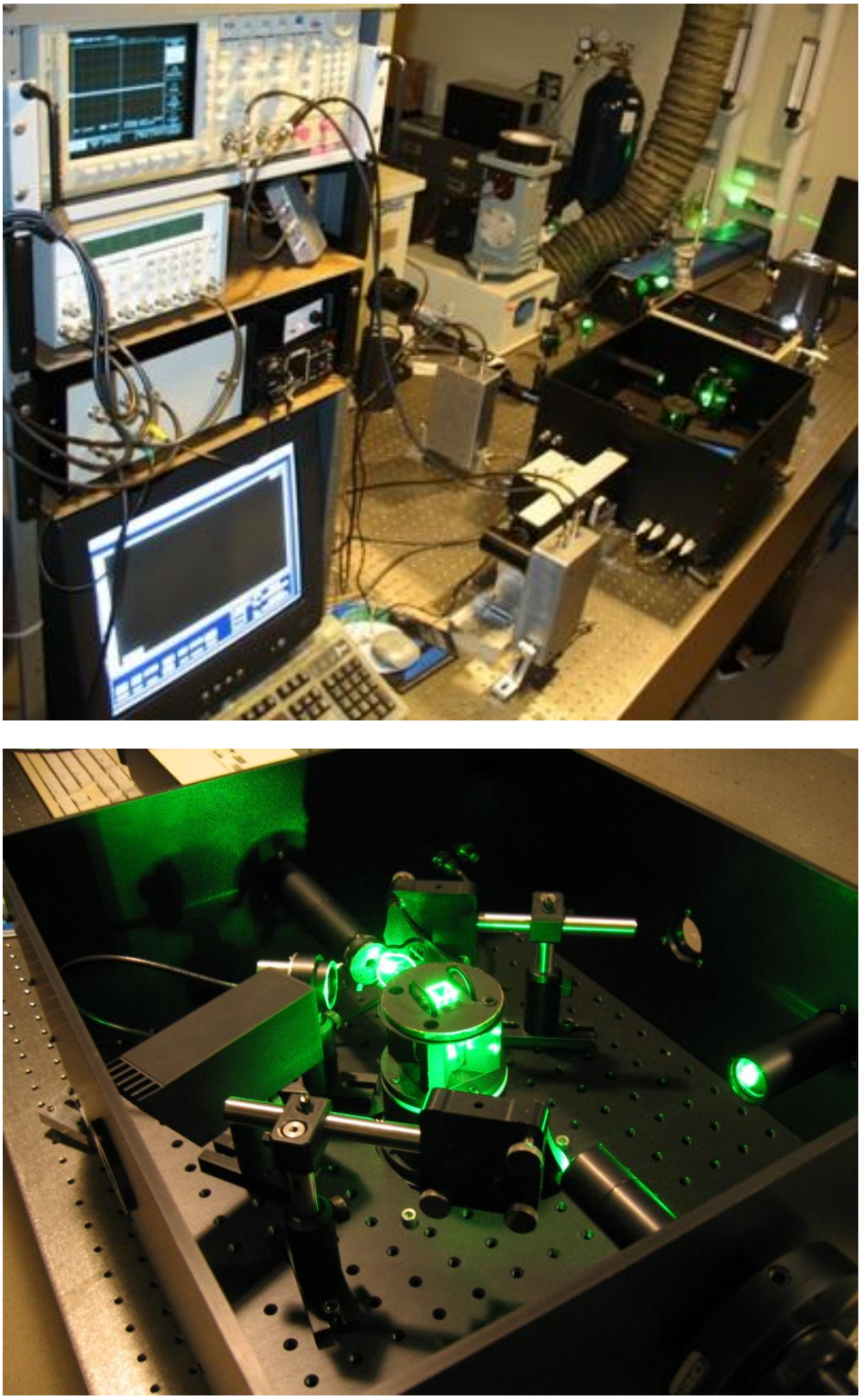

Figure 2.2. Image of transient absorption spectrometer optical assembly. Full view (top), close up view of sample compartment (bottom).

The sample holder was constructed of brass for optimal thermal properties. It securely holds the sample via a set of metal springs and provides optical access to the sample from all four sides. The edges of the sample holder were milled at near 45 degree angles to permit overlap of the monitoring and probe beams in a parallel orientation, while maintaining mechanical and thermal contact with the cuvette. The sample holder was also equipped with a liquid flow cooling system, computer controlled magnetic stirrer, sample and air flow lines, and sample cover. The setup allows for temperature controlled measurements, continuous or static sample flow, and dry air saturation of the sample cell and/or the entire TAS housing.

Sample Excitation

The second harmonic output (532 nm) of a Nd:YAG laser (SpectraPhysics GCR-10, Figure 2.1), with pulse energy adjusted by a glan prism polarizer/half-wave plate, is used as the excitation source of the TAS. The Q-switching provides a 10 ns pulse width (full width at half max), a repetition rate of 10 Hz and an energy output which can be attenuated from 0-60 mJ/pulse. Typical photolysis experiment pulse energies used were 1 -10 mJ/pulse. The excitation beam is directed along its path by a series of high energy threshold mirrors (Spectra Physics, 0441-6070 Dichroic Mirror). A computer controlled home designed and constructed solenoid shutter (Figure 2.1-S1) controls admittance of a single excitation pulse into the spectrometer; this permits data collection for samples associated with low solubility (concentration), low quantum yield, and irreversible photo-processes, by allowing the sample probe volume to be replenished between photo-excitations. The diameter of the excitation beam is adjusted to be about twice that of the

monitoring beam to insure adequate beam overlap, typically 2 mm and 1 mm respectively, to eliminate transient diffusion effects. The excitation beam is directed through a beam reducer consisting of a convex lens located outside the TAS assembly (Figure 2.1-L1) and a diverging lens (Figure 2.1-L2) located inside the TAS assembly inside a threaded optical lens tube. The excitation beam is then collected by mirror and reflected parallel along the axis of the probe beam, overlapping the probe beam as it passes through the sample holder (Figure 2.1-H1). The excitation beam is reflected by a mirror located near the adjustable aperture (Figure 2.1-A1) and is directed into a beam dump (Thorlabs "Blackhole", Figure 2.1-B1). The beam dump minimizes reflection of the used excitation beam back into the TAS assembly box limiting stray light collection.

Probe Beam Configuration

The probe beam of the TAS, used to monitor induced absorption changes of samples, was produced by a 300 Watt Xenon lamp (Hamamatsu Super-Quiet L2480, Figure 2.1-X1), which provides a low noise monitoring beam from 200 nm to 1200 nm as shown in Figure 2.3. The light from the lamp was focused by a pair of 1.5 inch converging lenses (Figure 2.1-L6, L7) onto the entrance of a monochromator, "lamp monochromator", (Applied Photo-Physics F-34, Figure 2.1-M1) which produced a variable bandwidth probe beam, 2 nm – 50 nm. During typical operation, the lamp monochromator entrance and exit slits were adjusted to 8 mm and 1 mm, respectively, to maximize beam intensity with nominal wavelength resolution. A home constructed aluminum pinhole aperture, approximately 0.5 mm diameter, was mounted at the exit slit of the lamp monochromator. The pinhole was used to approximate the emerging beam as

a point source to insure a uniform, circular image of the probe beam at the sample. The wavelength profile of the probe beam exiting the lamp monochromator, in this configuration, was measured to have a spectral width of approximately 7 nm, full width at half max. The lamp monochromator eliminates both high and low energy photons not monitored during the experiment that might otherwise adversely affect the sample through unnecessary photolysis, UV photo-damage, or infrared heating. The reduced bandwidth probe beam exiting the lamp monochromator is collected and collimated by a converging lens (Figure 2.1-L5) housed within a home constructed threaded lens tube designed to affix directly onto the outside of a shutter (Oriel model 76994, Figure 2.1-S2), which can be manually or computer controlled. The probe beam passes through the shutter, which is mounted onto the outside of the TAS housing, and continues into the TAS sample compartment, where it is focused by a converging lens (Figure 2.1-L3) into the sample holder (Figure 2.1-H1). Alignment of the probe beam onto the center of the sample holder and adjustment of the probe beam diameter at the sample can be performed by adjusting the converging lens position, (Figure 2.1-L3). After passing through the sample holder, the probe beam continues through a small adjustable aperture (Figure 2.1-A1), approximately three inches beyond the sample holder, mounted onto a threaded optical lens tube mount (Thorlabs, Inc.). The aperture is adjusted to optimize the collection of probe beam light while minimizing the collection of stray light. A 532 nm laser line filter (Omega Optical, XLK08, Figure 2.1-F1) is mounted behind the adjustable aperture to assist in the rejection of laser light scattered by the sample. After passing through the filter the probe beam light is collected by a converging lens (Figure 2.1-L41) and focused onto the entrance of a second, detector monochromator (Jobin Yvon H-20,

Figure 2.1-A1), to reduce scattered excitation light collection and produce a detection bandwidth of 1 to 2 nm. The aperture, filter, and collection lens are housed inside a threaded optical tube lens mount that is screwed directly into the inside of the TAS housing, in order to further reduce stray light collection. The second monochromator is attached to the outside of the TAS box via a home designed threaded attachment flange. The probe beam passes through a second 532 nm laser line filter (Omega Optical, XLK08, Figure 2.1-F2) before exiting the detector monochromator and entering the PMT housing.

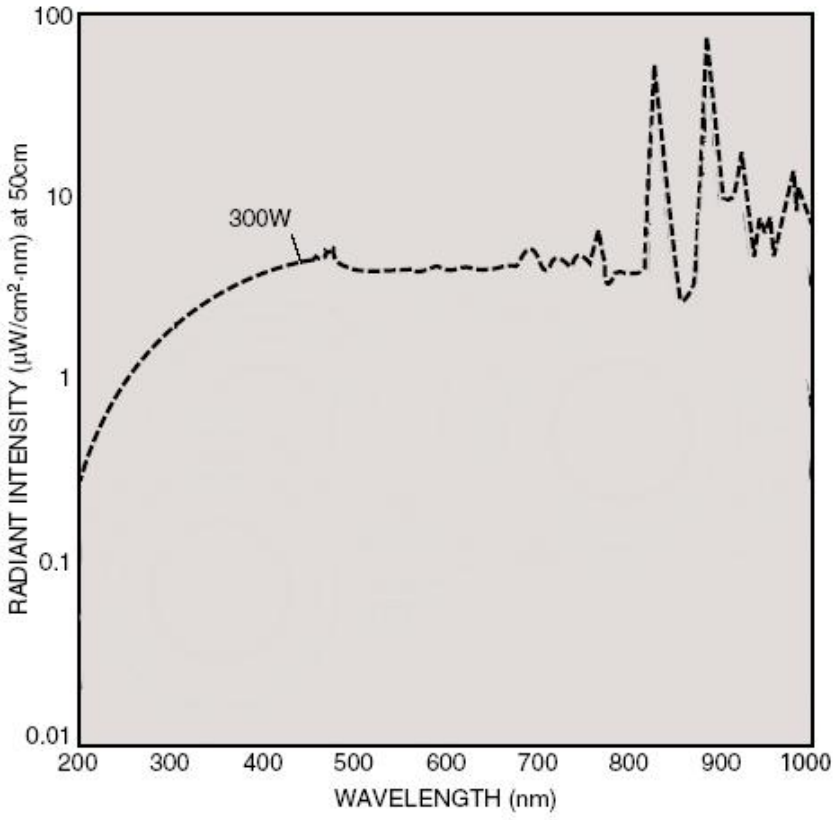

Figure 2.3. Spectrum of 300 W Xenon probe lamp, Hamamatsu Corporation.

Probe Beam Detection

The probe beam of the TAS is detected by a PMT (Hamamatsu model 1P28) which has high detection efficiency in the visible region from 300-650 nm, Figure 2.4. The PMT is housed within a home designed and constructed PMT holder, Figure 2.5. The PMT holder was constructed to be light tight, accommodate 1 inch diameter optics or laser reject filters, and mount directly to the detector monochromator exit port. The base of the PMT holder attaches to the PMT 5 dynode stage amplification detection circuit, Figure 2.6. Two custom detection circuit designs were a gift from Professor Thomas Netzel (Georgia State University), and corresponded to a 9 stage dynode and a 5 stage dynode version (Appendix 1). Integrated circuit boards were designed in the Emory electronics shop, shown in Appendix 1 for the 5 and 9 dynode versions, and constructed and mounted inside a shielded housing with the appropriate PMT socket and adapter to accommodate the PMT holder shown in Figure 2.5. The detection circuit uses a series of capacitor banks which supply a large surplus of detection current to the PMT. The circuits were designed to increase signal stability and provide high signal to noise detection from the PMT. The time response of the PMT is chosen considering the time scale of the experiment and the time between data points, with a home constructed termination box. The resistance values of the termination box, 300 Ohm, 3,000 Ohm and 30,000 Ohm, result in RC time constants for the PMT of, 0.1 μs, 1 μs, and 10 μs, respectively. A 50 ohm BNC connector terminator (Tektronix) is used to set the time constant of the PMT during fast time scale studies of 10 ns. The output of the photomultiplier tube is digitized and temporarily stored in a digital sampling oscilloscope (Tektronix, TDS 520B, Figure 2.1-O1).

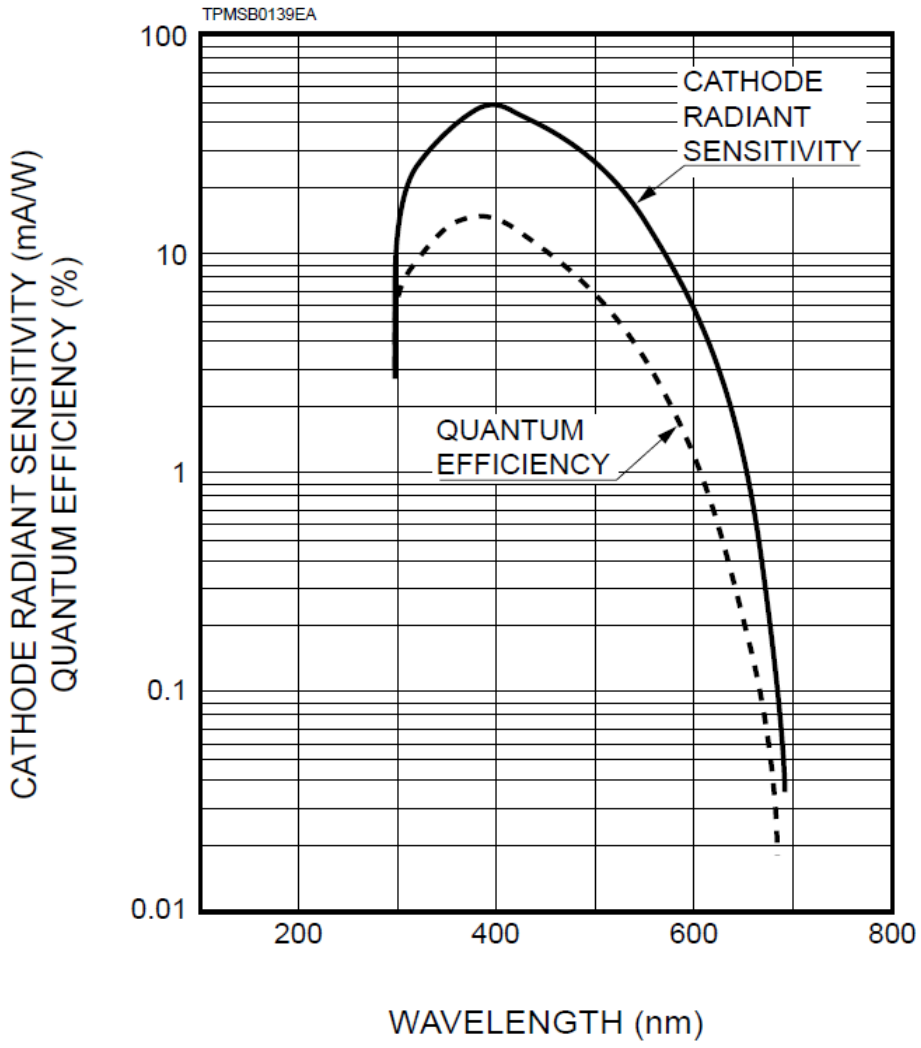

Figure 2.4. Quantum efficiency curve of Hamamatsu 1P21 photo-multiplier tube.

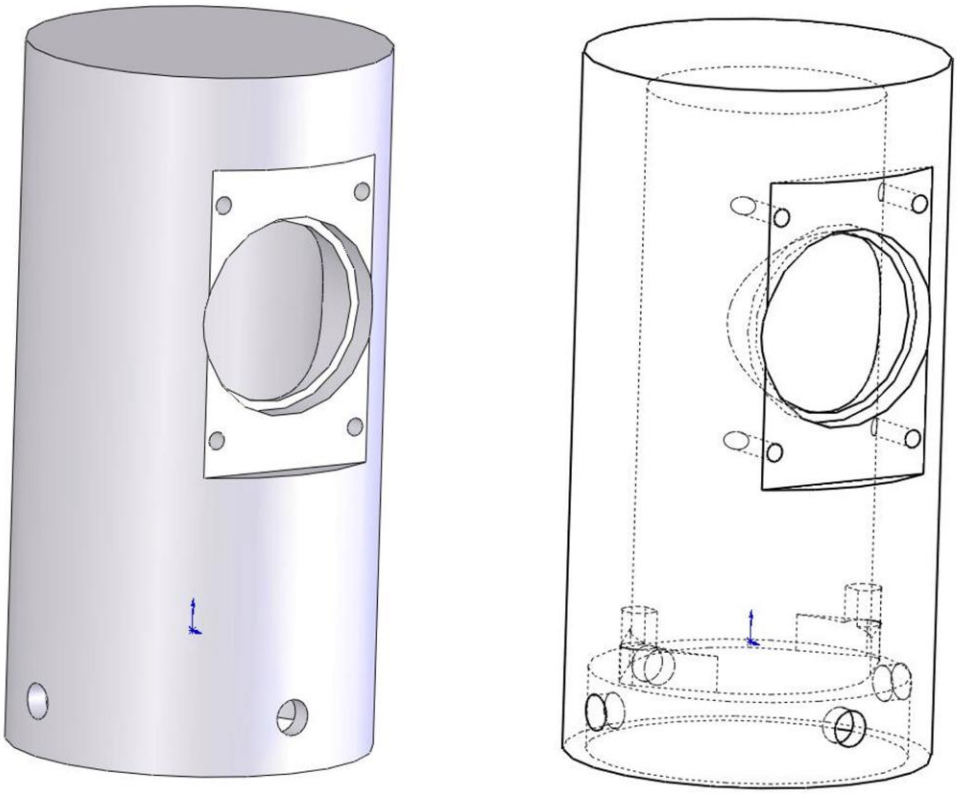

Figure 2.5. Schematic of photo-multiplier tube housing.

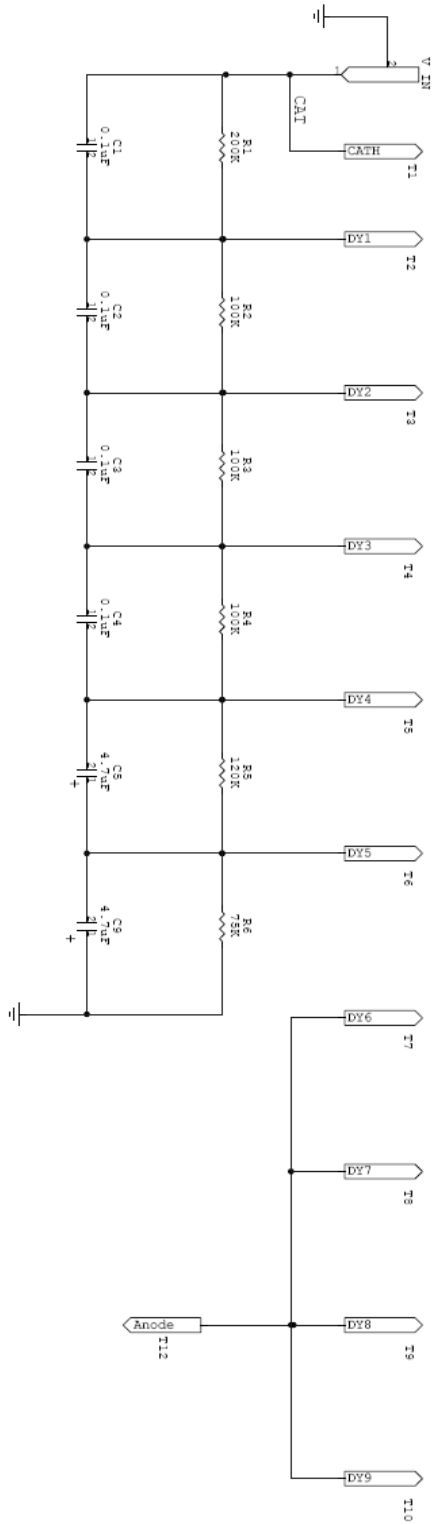

Figure 2.6. High current 5 dynode photo-multiplier tube detection circuit.

2.3 Instrument Control and Data Acquisition

Timing and Interface

The timing control and data acquisition of the TAS system is controlled through home designed LabVIEW (National Instruments) program that, through a GPIB/IEEE-488.2 interface, directly controls a four channel digital delay/pulse generator (Standford Research, DG 535, Figure 2.7) as well as the digital sampling oscilloscope (Tektronix, TDS 520B, Figure 2.1-O1, Figure 2.7). A schematic of the timing control and data acquisition of the TAS, as well as electrical connections, are shown in Figure 2.7 and a detailed command description of the Labview program is shown in Appendix 2. The user interface of the Labview control program is shown in Figure 2.8. The Labview interface controls the output level and delay times of the output signals of the delay/pulse generator. The timing diagram of the delay/pulse generator is shown in Figure 2.9. The T_0 start time of the delay/pulse generator is triggered by the output of a fast photodiode (Thorlabs, DET-210, Figure 2.1-D1 and Figure 2.11) monitoring the Q-Switched 10 Hz output of the Nd-YAG laser. The fast photodiode is used instead of the Q-Switch monitor output of the laser, owing to the increased time accuracy of the diode. A computer controlled, home designed and constructed solenoid shutter (Figure 2.1-S1 and Figure 2.7) controls admittance of a single excitation pulse into the spectrometer. The shutter requires a minimum of 1.5 A to open and therefore could not be controlled solely by the delay/pulse generator's TTL pulse output. A power transistor switch, shown in Figure 2.10, was designed and constructed to drive the solenoid shutter by amplifying the

voltage and current of a TTL pulse output of the delay/pulse generator. The positive TTL pulse, CD, is used to switch on a NAND gate (National Instruments DS75452) powered by a +5 V, 100 mA semiconductor voltage regulator (LN421-T7805CT). The NAND gate provides current amplification substantial enough to switch on a PNP power transistor (TIP32) in series with a +24 V, 3.6 A linear regulated power supply (Power One DC Power Supply) and the solenoid of the shutter to ground. Both the PNP power transistor and the +5 V voltage regulators were fitted with home constructed heat sinks due to the large power dissipation associated with the circuit. A feedback diode is also used to ensure minimal inductive feedback upon transistor turn off and fast closure of the shutter. Upon testing, the shutter was shown to open and close in 25 ms and could remain open on the minutes time scale. The opening time is fast enough to allow a single laser pulse from the 10 Hz pulse train to be selected to interact with the sample. The delay time in opening of the shutter was taken into account in the timing sequence of the delay/pulse generator, which was set by the Labview program. The turn-on time of the power transistor switch is estimated to be on the order of 25 ns, indicating that the limiting time factor of the shutter is the solenoid used to open the shutter. The delay/pulse generator TTL output, B, is set by the Labview program to determine the length of the "time to wait" between shutter opening and thus photolysis events.

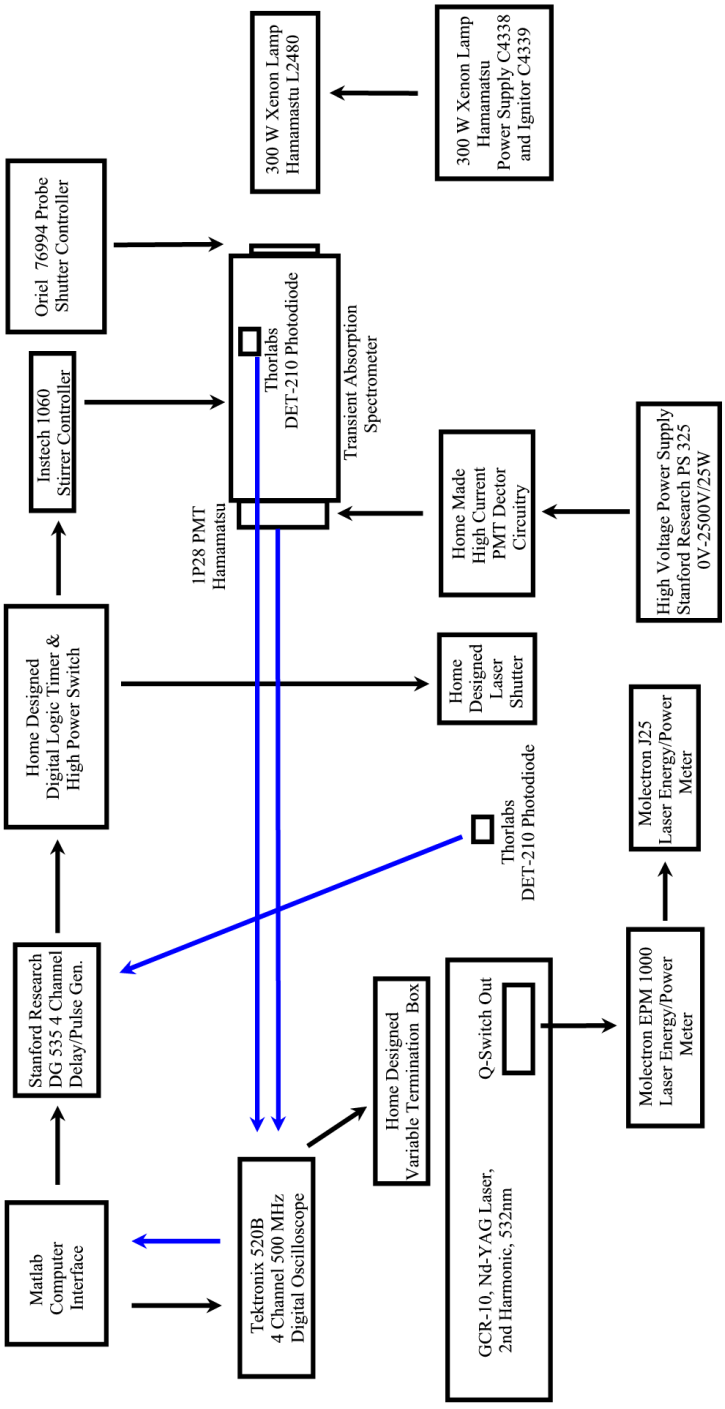

Figure 2.7. Transient absorption spectrometer electronics, detection and control flow chart.

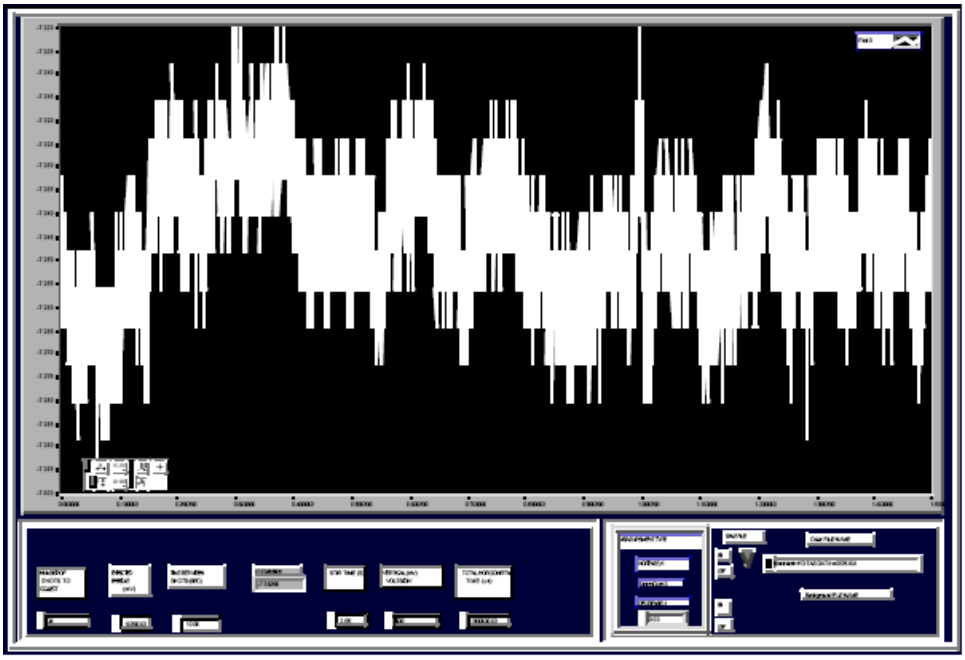

Figure 2.8. Screen shot of Matlab interface.

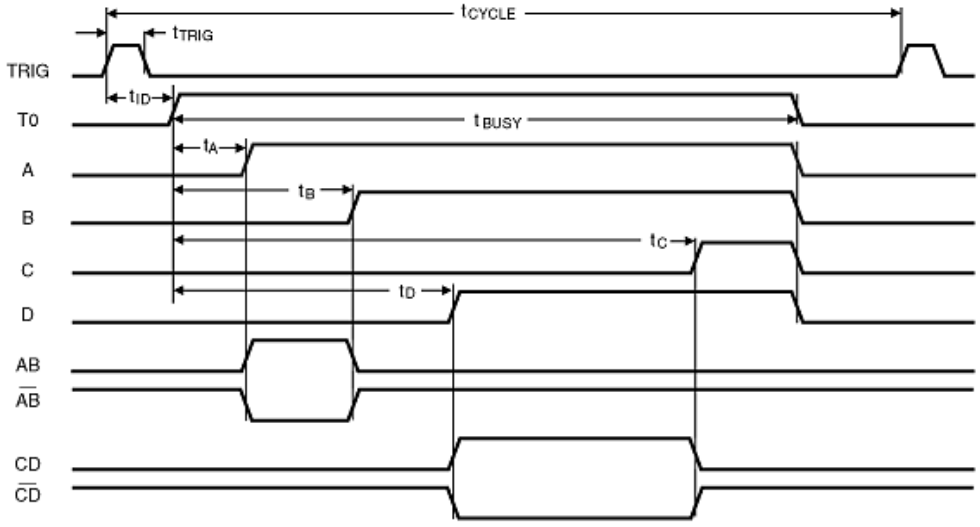

Figure 2.9. Timing diagram from Stanford Instruments DG535 pulse generator.

Logic circuitry, shown in Figure 2.10, which is controlled by the Labview program, was also designed to control the stirring time after photolysis by the magnetic stirrer installed at the base of the sample holder. Precise control of the stirrer was needed to permit stirring of the protein sample following excitation and to allow enough time for the sample to settle before the next excitation event. The length of time to stir the sample is selected on the front panel of the Labview program and sets the A outputs of the delay/pulse generator, which sets the length of the stir time. The A and T_0 outputs from the delay/pulse generator were used to switch on an exclusive OR gate (ON-Semiconductors, SN74LS86). The exclusive OR gate is turned on when the A output is low and the T_0 output is high. The exclusive OR gate output switches on a NOR gate (National Semiconductors, DS75453) which has its output wired in series with a fast signal relay (Omron G5V-2). The activation of the NOR gate completes the circuit of the fast relay solenoid flipping the relay switch, giving the stirrer motor (Instech 1060, Figure 2.7) current to ground through the NOR gate. The relay solenoid and stirrer motor were wired with feedback diodes in parallel to ensure fast response. The stirrer circuitry was constructed in the same box as solenoid shutter circuitry and is equipped with BNC input for TTL signals from the delay/pulse generator and RCA and output connections for the stirrer motor and power supply connections.

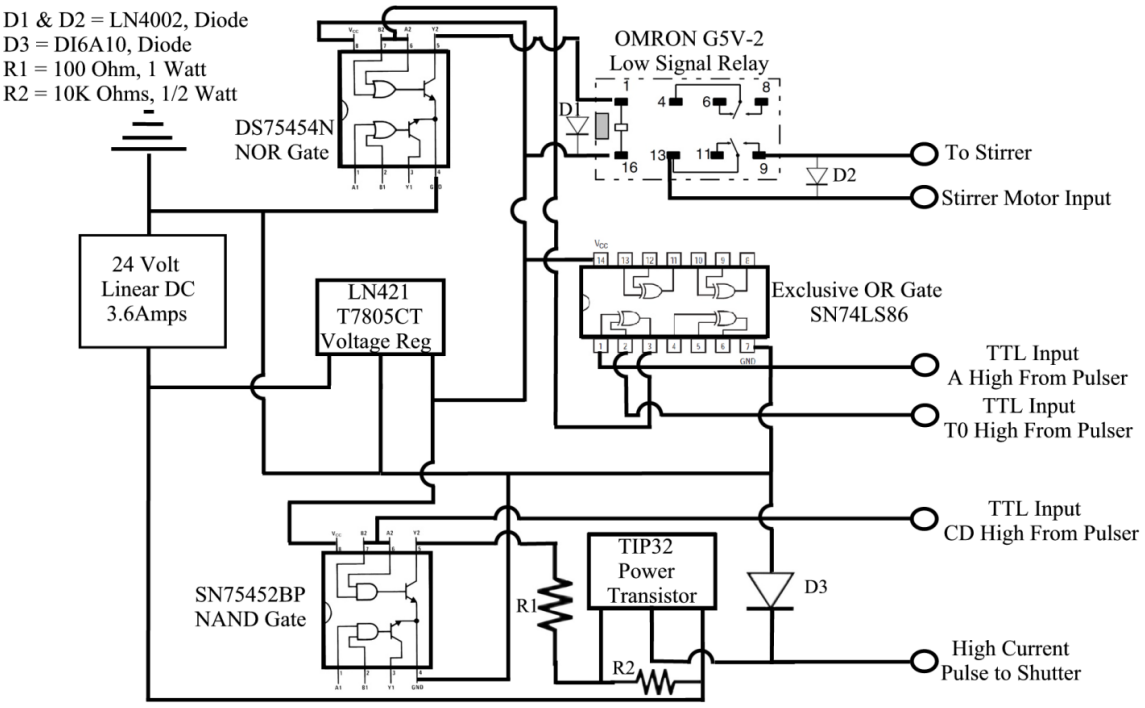

Figure 2.10. Logic, high current fast transistor switch and stirrer controller circuit diagram.

The Labview interface also controls the digital sampling oscilloscope, Tektronix, TDS 520B, (Figure 2.1-O1 and Figure 2.7) which collects and records the transient absorption data. The control program allows the user to set the number of photolysis events to average, the stir time after photolysis, the wait between shots, the detection voltage resolution and the time scale to monitor. The program first interfaces with the oscilloscope and delay/pulse generator to set the required parameters needed to monitor and record the intensity level of the transmitted monitoring beam through the sample. An estimate of the expected baseline voltage is input by the user to achieve a more accurate reading. The measured baseline level is then stored and used to set the offset of the oscilloscope for transient data collection. The program includes code that sets the

position of the baseline of the monitoring beam on the oscilloscope, by considering whether a decreased, increased or unknown absorption change is expected. It also sets a delay time scale, by considering the horizontal time base chosen, in order to shift the transient curve to the left on the oscilloscope screen to optimize the record length of the oscilloscope, which is 15,000 data points. The individual spectrum is collected, recalibrated by any voltage offsets applied during detection, and a set of time points is created within the Labview program and combined into a 2 x 15,000 ASCII file which contains time in the first column and voltage in the second. The single spectrum is then transferred to the computer for storage. The program continues until the selected number of averages is collected and all data is saved into a single file for each run. Data analysis algorithms, which select data points to calculate baseline voltages immediately before the photolysis event, calculate the change in optical density following photolysis, and calculate the concentration of photoproducts, as well as average the runs and save the spectra as .mat files. The algorithms were written by using Matlab (Natick, MA) routines that were run on PC computers.

Chapter 3: Static and Transient Absorption Studies of Adenosylcobalamin and Methylcobalamin in Ethanolamine Ammonia-Lyase: Influence of Substrate/Inhibitor Binding on Cofactor Spectra and Radical Pair Recombination

Synopsis

UV-visible absorption spectrum of the B_{12} cofactor, Adenosylcobalamin (AdoCbl) and Methylcobalamin (MeCbl), is used to monitor the electronic perturbations induced on the cofactor upon binding to EAL and to monitor substrate and substrate analog binding induced conformation changes of the enzyme that affect the cofactor. Photolysis is used to monitor the kinetics of the 5'-deoxyadenosyl radical migration on time scales of catalytic reactions in the absence and presence of substrate analog in ethanolamine ammonia-lyase. Measurements were made in aqueous solution at room temperature. This is the first observation of the kinetics of radical pair recombination of long lived, >100 ns, radical pairs inside a coenzyme B_{12}-dependent enzyme active site. The monitoring of the photo-induced long lived radical pair formed from bond homolysis of adenosylcobalamin in the enzyme was studied using transient absorption spectroscopy, from nanoseconds to milliseconds, to examine the 5'-deoxyadenosyl radical's migration inside the active site, as well as the quantum yields of the long lived species. This work investigates both the effects of substrate analog binding on the electronic structure of cofactor, as well as the recombination of the radical pair inside the enzyme.

3.1 Materials and Methods

Sample Preparation

EAL was purified from the *Escherichia coli* over expression strain incorporating the cloned S. *typhimurium* EAL coding sequence[110] essentially as described[111], with the exception that the enzyme was dialyzed against buffer containing 100 mM HEPES (pH 7.5), 10 mM potassium chloride, 5 mM dithiothreitol, 10 mM urea, and 10% glycerol[77]. Enzyme activity was determined as described[112] by using the coupled assay with alcohol dehydrogenase/NADH. The specific activity of the purified enzyme with aminoethanol as substrate was 35-45 μmol/min/mg.

Adenosylcobalamin (AdoCbl), Methylcobalamin (MeCbl), (*S*)-1-amino-2-propanol, (*R*)-1-amino-2-propanol, (*S*)-2-amino-1-propanol and 2-Aminoethanol were purchased from commercial suppliers (Sigma Chemical Co). Samples of enzyme (20-100 μM active sites) with cofactor (10-50 μM) bound were prepared and sonicated at 277 K to reduce light scattering. Samples with substrate analog bound were prepared as above with 10 mM of the substrate analog (*S*)-1-amino-2-propanol present. Anaerobic solutions of AdoCbl were prepared by placing small volumes of cofactor stock solution under vacuum, followed by backfilling with argon before addition to anaerobic buffer. Argon bubbling for 1 h was utilized to degass the buffer solution. Components were injected into a 3 ml quartz anaerobic cuvette with a sealed septum that had been flushed with argon for at least 5 min prior to sample mixing.

Static Absorption Spectroscopy

Static absorption spectra from 300 nm to 650 nm were collected by using a Shimadzu UV-1601 absorption spectrometer with 0.5 nm wavelength accuracy. Spectra were collected before and after transient absorption measurements and again after laser

saturation of the sample. A scattering base line of each enzyme sample was taken before the addition of cofactor. All measurements were performed at 295 ±1 K.

Transient Absorption Spectroscopy

Transient absorption measurements were performed by using a transient spectrophotometer of home design and construction. The spectrometer is described in detail in Chapter 2. Transient absorption of the cob(II)alamin state was monitored at 470 nm (probe) following laser pulse photolysis at 532 nm. Measurements were made with 0.1-10 μs dwell times and corresponding time constants of 0.01-1 μs. All measurements were performed at 295 ±1 K.

3.2 UV/Visible Absorption Spectra of Cobalamins Following Binding to EAL with and without Substrate and Substrate Analogs

Pre-Photolysis Absorption Spectra of Adenosylcobalamin and Methylcobalamin Complexes

UV-visible absorption spectra collected for AdoCbl in buffered aqueous solution and for AdoCbl bound to EAL in the absence and presence of (*S*)-1-amino-2-propanol are shown in Figure 3.1. The wavelengths of selected absorption bands are presented in Table 3.1. The spectrum of AdoCbl in solution is similar in form as reported previously[88] and is characterized by the prominent visible α- and β- transitions at 525 nm, and 490 nm, respectively, and by ultraviolet γ-bands at 340 nm and 377 nm[113]. The spectral features

of the cobalamins have been assigned in detail to electronic transitions in the corrin ring of the cofactor by Brunhold and coworkers [46,113]. The binding of AdoCbl to EAL (Figure 3.1) results in wavelength shifts in the absorption spectra, relative to AdoCbl in aqueous solution, and are presented in expanded wavelength scale of the visible and UV spectral regions in Figure 3.2. The spectra of the cofactor shows a 2.5 nm and 1.0 nm hypsochromic shifts of the 525 nm and 377 nm absorbance maxima, and the 5.3 nm bathochromic shift of the 340 nm maximum. These changes in the AdoCbl spectrum indicate that the cofactor binding site in EAL alters the electronic properties of the cofactor to a limited degree. Changes in the spectra could arise from changes in the polarity of the protein environment that surrounds the cofactor[68], specific interactions of the corrin ring with protein residues, or the conformation of the bound cobalamin, or a combination of these effects. Small changes in the AdoCbl spectrum have also been noted for AdoCbl binding to coenzyme B_{12}-dependent glutamate mutase[114].

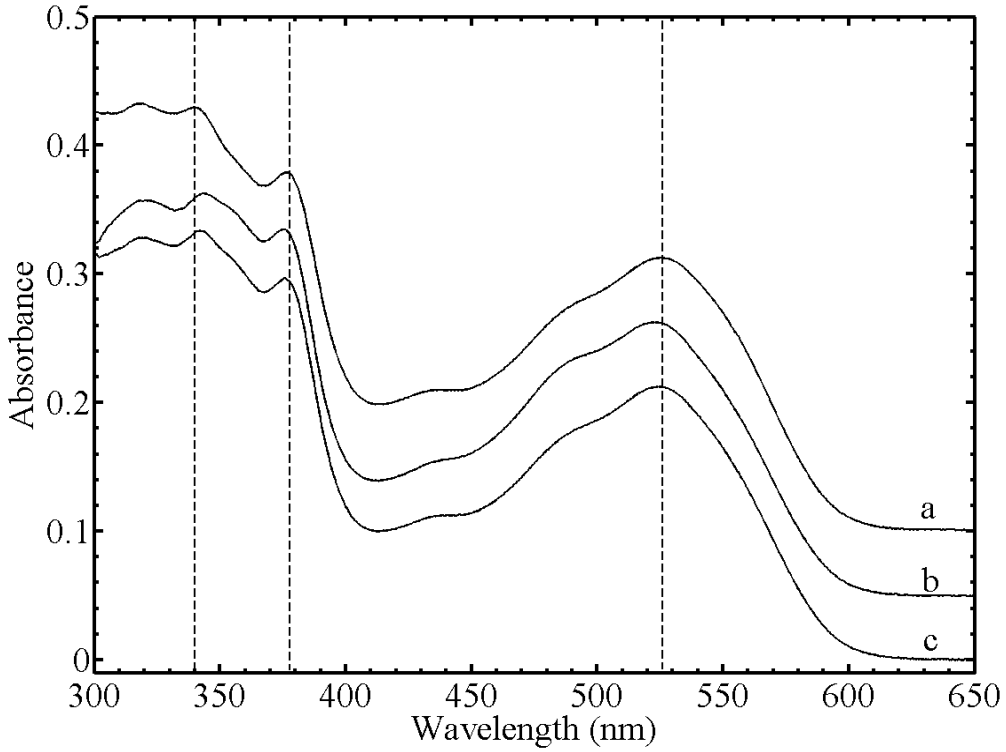

Figure 3.1. Absorption spectra of AdoCbl (25 μM) taken at room temperature. (a) Solution. (b) in EAL. (c) in EAL with (*S*)-1-amino-2-propanol (10mM) bound. Dashed line is set to peak of AdoCbl in solution near 525 nm and 375 nm. Protein or protein plus inhibitor absorption spectra were subtracted following cofactor binding and scaled to 525nm peak of AdoCbl in solution and offset for comparison. Spectra were recorded in 10 mM potassium phosphate buffer at pH 7.5.

Table 3.1. Selected wavelengths of maximum absorbance of AdoCbl and MeCbl in solution and in EAL, in the presence and absence of substrates and substrate analogs.

Cobalamin[a]	**Substrate or Analog**[b]		**Spectral Peak**	
		525 nm	**375 nm**	**340 nm**
Adenosylcobalamin in solution	-	525.25	376.5	339.75
Adenosylcobalamin + EAL	-	522.75	375.5	344.5
Adenosylcobalamin + EAL	(*S*)-1-Am-2-PrOH	524.25	375.75	342.5
Methylcobalamin in solution	-	522.0	374.5	342.0
Methylcobalamin + EAL	-	514.75	375.75	340.25
Methylcobalamin +EAL	2-Aminoethanol	513.25	374.5	340.5
Methylcobalamin +EAL	(*S*)-2-Am-1-PrOH	513.75	375.0	340.5
Methylcobalamin + EAL	(*S*)-1-Am-2-PrOH	511.5	374.0	341.0
Methylcobalamin + EAL	(*R*)-1-Am-2-PrOH	510.0	373.5	341.0

[a]Solution: Anaerobic 10 mM potassium phosphate, pH=7.5; [AdoCbl or MeCbl]=25 µM. Enzyme: Aerobic ethanolamine ammonia-lyase in 10 mM potassium phosphate, pH=7.5. [AdoCbl or MeCbl]=25 µM, corresponding to 0.5:1 Cobalamin/active sites.

[b]Substrates (10mM): 2-aminoethanol, (*S*)-2-amino-1-propanol. Inhibitors (10mM): (*S*)-1-amino-2-propanol, (*R*)-1-amino-2-propanol.

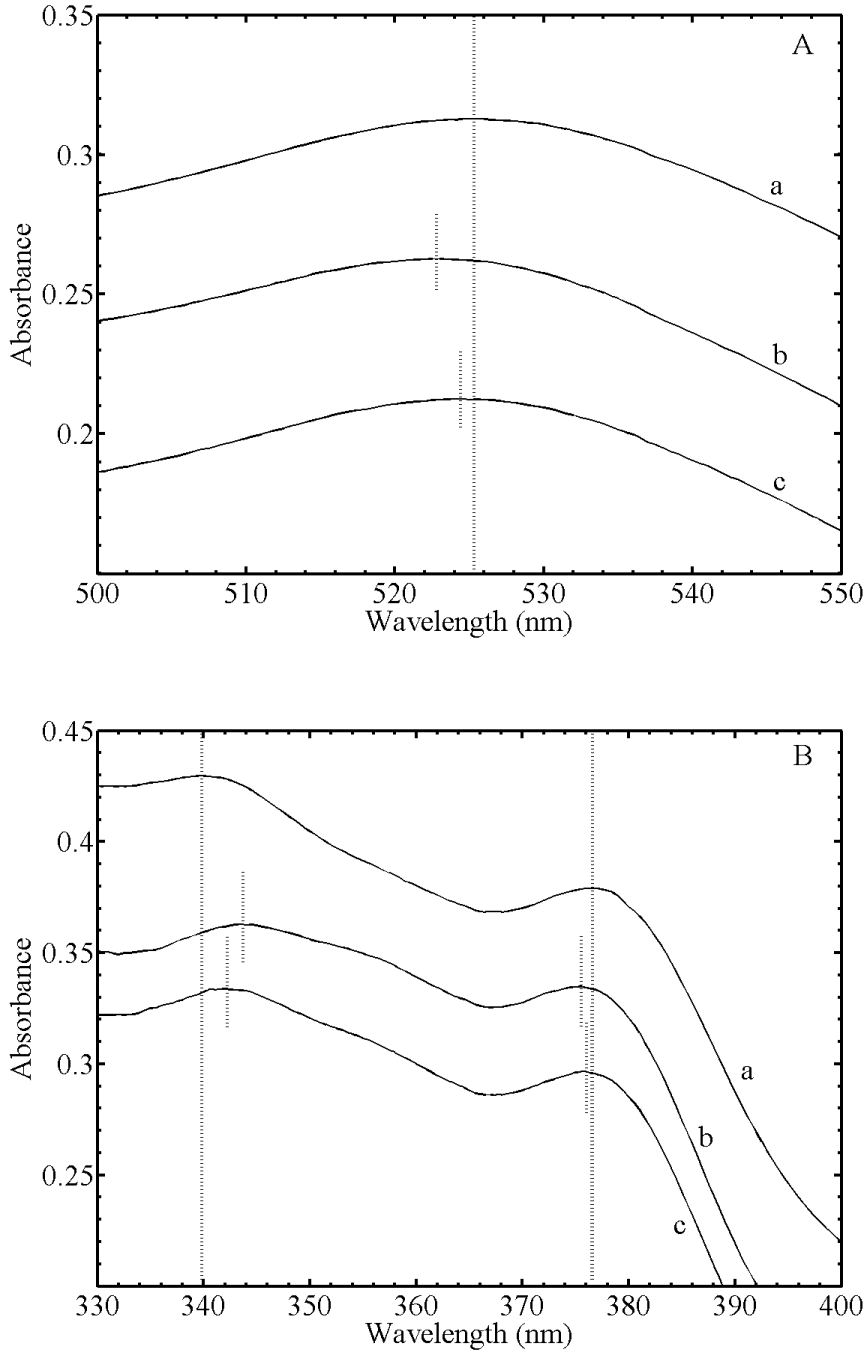

Figure 3.2. Absorption spectra of AdoCbl (25 μM) from Figure 3.1 over selected wavelength ranges at higher wavelength resolution. Panel: (A) 500-550 nm and (B) 330-400 nm. (a) Solution. (b) in EAL. (c) in EAL with (*S*)-1-amino-2-propanol (10mM) bound.

Binding of the substrate inhibitor, (*S*)-1-amino-2-propanol, to the EAL holoenzyme complex results in bathochromic shifts of 1.5 nm and 1 nm of the 525 nm and 375 nm bands, and a 2 nm hypsochromic shift of the 340 nm band, relative to the holoenyzme absorption maxima and are shown in Figure 3.1 and 3.2. These spectral shifts are in the direction opposite to those induced by AdoCbl binding to EAL, and are smaller in magnitude. The (*S*)-1-amino-2-propanol binding induced shifts in the AdoCbl UV-visible spectrum indicates that the substrate minimally induces a structural change in the protein which perturbs the electronic structure of the cofactor, relative to AdoCbl in holo-EAL. The possibility exists that the substrate inhibitor does not fully induce the changes in the protein-cofactor interactions which destabilize the cobalt-carbon bond energy of AdoCbl.

UV-visible absorption spectra collected for MeCbl in buffered aqueous solution, and for MeCbl bound to EAL in the absence and presence of the substrate analog, (*S*)-1-amino-2-propanol, (*R*)-1-amino-2-propanol, (*S*)-2-amino-1-propanol bound and the natural substrate, aminoethanol are shown in Figure 3.3. The wavelengths of selected absorption bands are presented in Table 3.1. The spectrum of MeCbl in solution is identical to that previously reported[88]. As for AdoCbl, the spectrum is characterized by the visible α- (522 nm), β- (490 nm) and γ- (342 nm, 375 nm) band transitions. The binding of MeCbl to EAL leads to shifts in the wavelength maxima of the absorption bands, as observed for the binding AdoCbl to EAL. Figure 3.4 shows hypsochromic shifts of 7.2 nm and 1.7 nm for the 522 nm and 342 nm absorbance maxima, and a 1.3 nm bathochromic shift of the 375 nm maximum. The changes observed in the MeCbl

spectrum indicate that the cobalamin binding site in EAL perturbs the electronic properties of the cofactor only slightly, relative to solution.

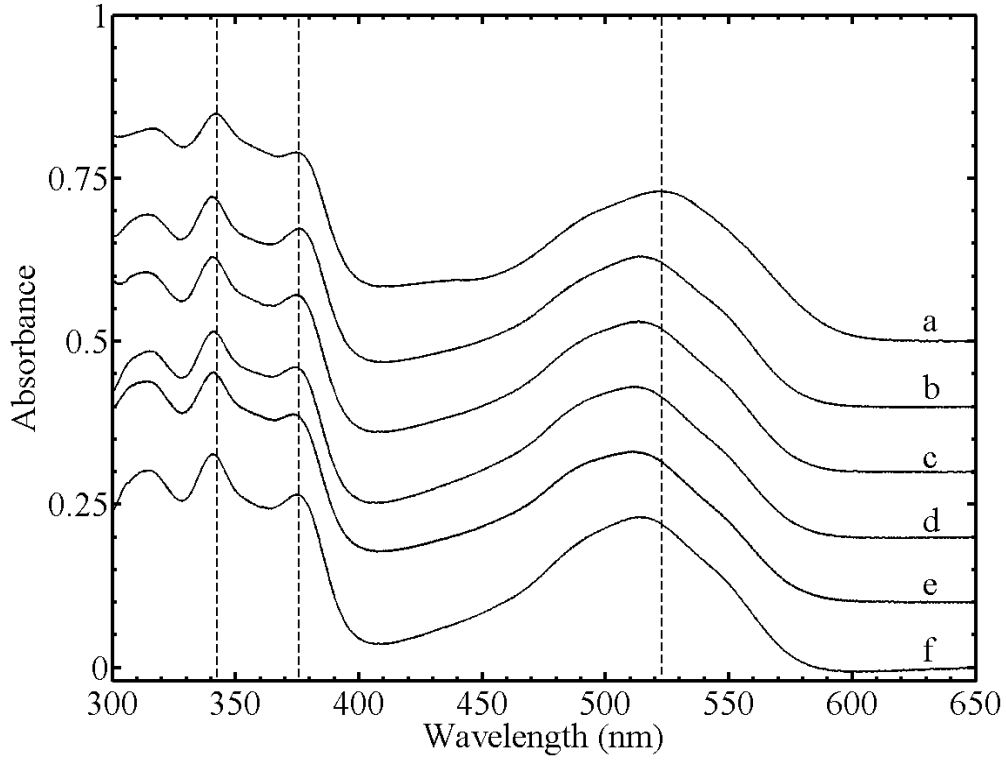

Figure 3.3. Absorption spectra of MeCbl (25 μM) at room temperature. (a) in solution. (B) in to EAL. (C) in to EAL with aminoethanol bound. (d) in to EAL with (*S*)-1-amino-2-propanol bound. (e) in to EAL with (R)-1-amino-2-propanol bound. (f) in to EAL with (*S*)-2-amino-1-propanol bound. Substrate or substrate analog concentration 10mM. Protein or protein plus substrate/inhibitor absorption spectra were subtracted following cofactor binding and scaled to 525nm peak of MeCbl in solution and offset for comparison. Dashed line is set to peak of MeCbl in solution near 525 nm and 375 nm. All spectra were recorded in 10 mM potassium phosphate buffer at pH 7.5.

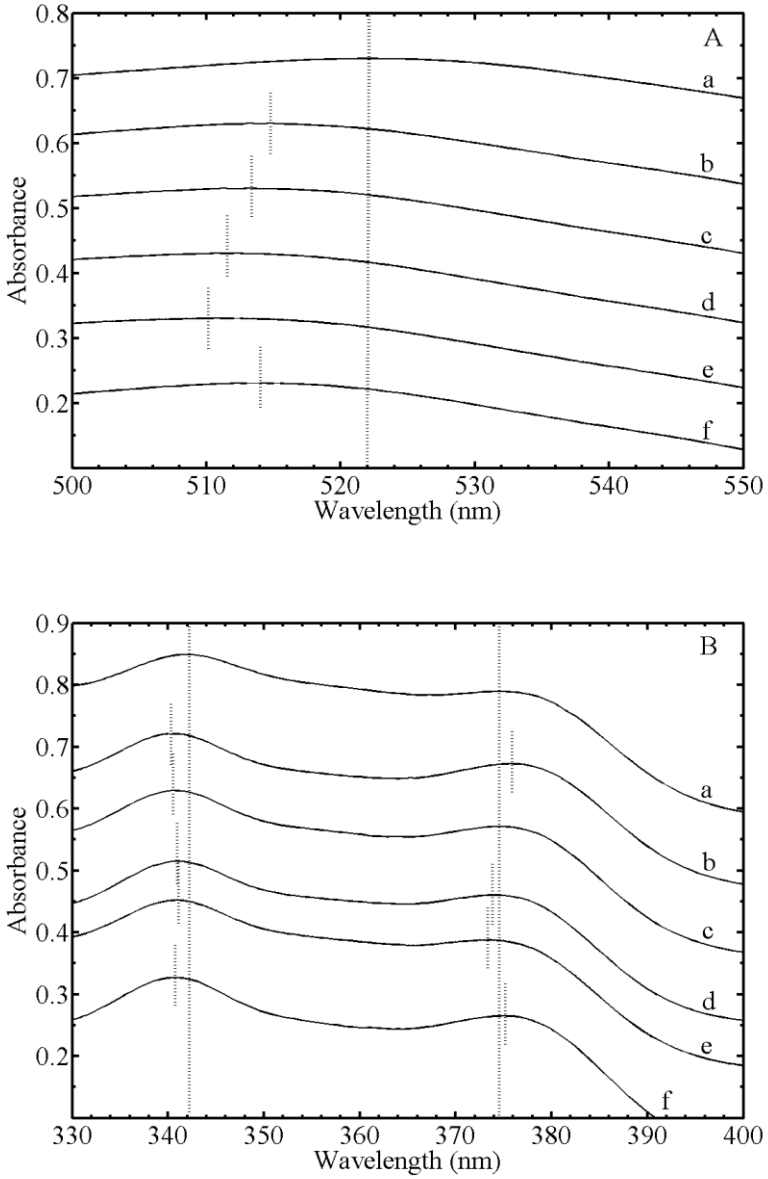

Figure 3.4. Absorption spectra of MeCbl from Figure 3.3 over selected wavelength ranges at higher wavelength resolution. (A) 500-550 nm. (B) 330-400 nm. (a) in solution. (B) in to EAL. (C) in to EAL with aminoethanol bound. (d) in to EAL with (*S*)-1-amino-2-propanol bound. (e) in to EAL with (R)-1-amino-2-propanol bound. (f) in to EAL with (*S*)-2-amino-1-propanol bound. Substrate or substrate analog concentration of 10mM.

MeCbl is not an active cofactor for the EAL system but retains the binding characteristics of the AdoCbl cofactor. The inactivity of MeCbl, while bound to EAL, allows for the monitoring of absorption spectra following the binding of substrates without enzyme turnover occurring. Table 3.1 shows that the binding of substrates and substrate analogs to the MeCbl-EAL complex cause shifts in the MeCbl spectrum. The absorption spectra of MeCbl bound to EAL with substrate and substrate inhibitors bound is shown in Figure 3.3. The direction of the shifts induced by binding of the substrates and analogous is the same as for the AdoCbl-EAL complex with bound (*S*)-1-amino-2-propanol, but the magnitudes of the shifts are significantly greater for the MeCbl complexes. The binding of the native substrate, 2-aminoethanol, to the holoenzyme resulted in bathochromic shifts of 1.5 nm and 1.3 nm for the 522 nm and 375 nm regions respectively, and a hypsochromic of 0.2 nm for 342 nm bands. Similar shifts where observed upon binding of the substrate (*S*)-2-amino-1-propanol, 1 nm, 0.8 nm, 0.2 nm for the 522 nm, 375 nm and 342 nm bands respectively. Binding of the substrate-analog inhibitors, (*S*)-1-amino-2-propanol and (*R*)-1-amino-2-propanol, to the holoenzyme, have the most significant effect on the MeCbl absorption spectra upon. Bathochromic shifts of 3.3 nm, and 1.8 nm where observed for the 522 nm and 375 nm bands and a hypsochromic shift of 0.7 nm in the342 nm band. The presence of bound (*R*)-1-amino-2-propanol leads to bathochromic shifts of 4.8 nm and 2.3 nm of the 522 nm and 375 nm bands, and a 0.7 nm hypsochromic shift of the 342 nm band, in the MeCbl absorption maxima.

The methyl group of MeCbl, which has a van der Waals radius of 2 Å is smaller than the deoxyadenosyl group of AdoCbl, and is not capable of polar or hydrogen

bonding interactions. Therefore, it is essentially non-interactive with the protein interior. Therefore, the shifts in MeCbl spectra introduced by substrate/analog binding arise from a perturbation of the cobalamin ring and/or axial DMBz ligand conformation induced by the protein. In either case, this interaction must be mediated by a protein conformational adjustment that propagates over the approximately 10 Å distance [24,27] between the substrate binding site and the corrin macrocycle.

The small changes in the absorption spectra with both AdoCbl and MeCbl, as cofactors for EAL, suggest that the binding of substrate to the enzyme changes the protein conformation such that the electronic structure of the cofactor is influenced, but not to the extent needed to "trigger" the protein for function. This evidence for one or more protein structural perturbation chains between the substrate and the corrin macrocycle binding sites does not directly verify the substrate trigger hypothesis. It does, however, indicate that long-range substrate-induced structural changes, which might contribute to the catalysis of Co-C bond cleavage, are present in EAL. The possibility does exist that the substrate inhibitor does not fully induce the changes in the protein-cofactor interactions that destabilize the cobalt-carbon bond energy of Adocbl and that the protein conformational changes induced by the native substrates where not able to induce changes in nonfunctioning cofactor MeCbl.

Post-Photolysis Absorption Spectra of Adenosylcobalamin and Methylcobalamin Complexes

The photoproduct difference spectra (post-photolysis minus pre-photolysis) for AdoCbl in anaerobic solution and AdoCbl in EAL in aerobic solution are presented in

Figure 3.5 and 3.6, respectively. The difference spectra for AdoCbl in anaerobic solution shown in Figure 3.5 is characterized by the loss of the AdoCbl α-band around 525 nm (negative feature) and the rise of long wavelength maximum of cob(II)alamin around 470 nm (positive feature). The comparable spectral features indicate that the difference spectrum for AdoCbl photolysis in EAL in aerobic solution in Figure 3.6 represents AdoCbl minus cob(II)alamin, because it is the same as the reference AdoCbl minus cob(II)alamin difference spectrum obtained in anaerobic solution (Figure 3.5). Small differences in the line shape and peak positions are caused by the different cofactor environments in aqueous solution and in EAL, as found for other AdoCbl-dependent enzymes.[33-34,115]

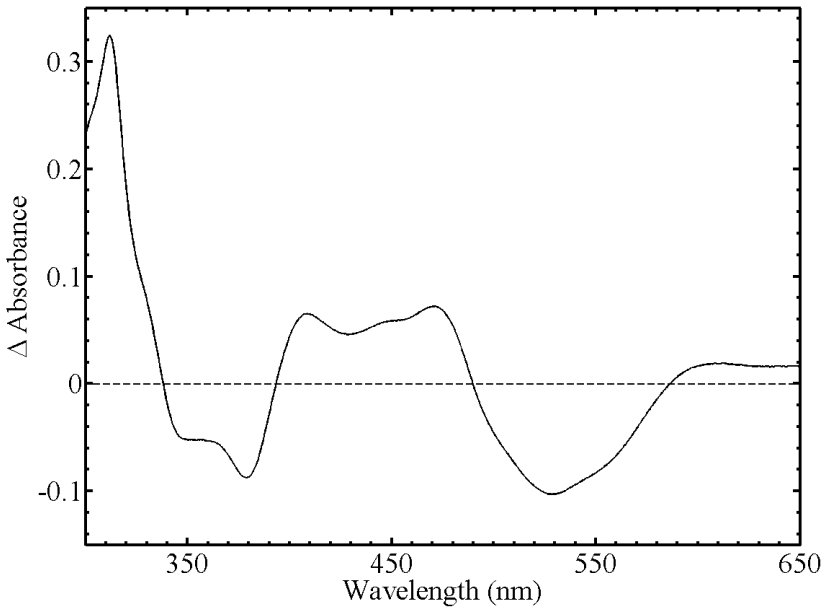

Figure 3.5. Absorption difference spectra of photolyzed minus pre-photolysis AdoCbl (25μM) in anaerobic solution.

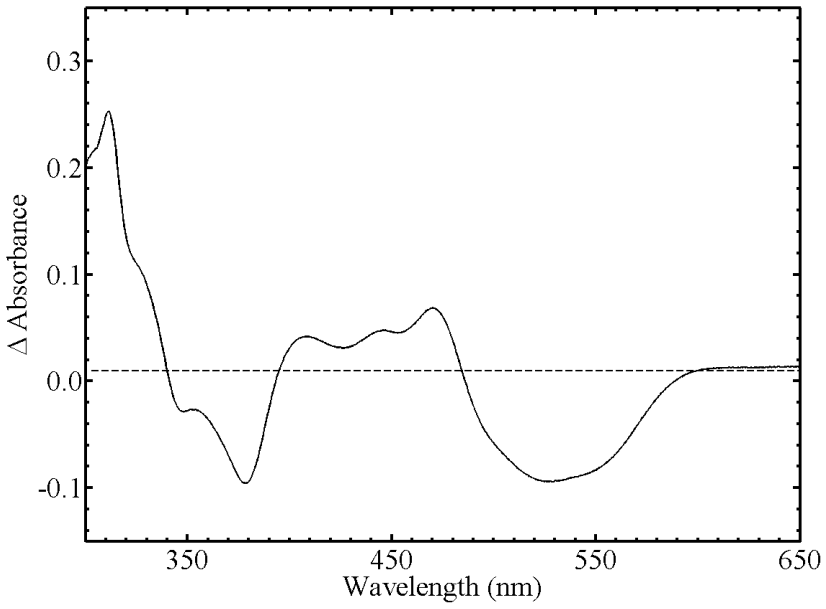

Figure 3.6. Absorption difference spectra of photolyzed minus pre-photolysis AdoCbl (25μM) in EAL in aerobic solution.

The post-photolysis difference spectrum of AdoCbl in aerobic solution is presented in Figure 3.7 and MeCbl bound to EAL in aerobic solution is shown in Figure 3.8. Both spectra show a loss in absorbance in the α-band around 525 nm and an increase in the γ-band at 350 nm which is characteristic of aquocob(III)alamin formation. The corresponding aerobic solution difference spectrum for aquocobalamin minus AdoCbl] in Figure 3.7 confirms that aquocob(III)alamin is the MeCbl photoproduct on the $>10^{-3}$ s time scale in EAL. Hogenkamp and coworkers have previously shown that aquocob(III)alamin arises from the reaction of cob(II)alamin with dioxygen (O_2).[116] The results therefore show that the binding of the native AdoCbl cofactor in EAL leads to a state in which O_2 is prevented from interacting with the photoproduct cob(II)alamin. In contrast, the binding of the non-native MeCbl does not confer the property of O_2 insensitivity.

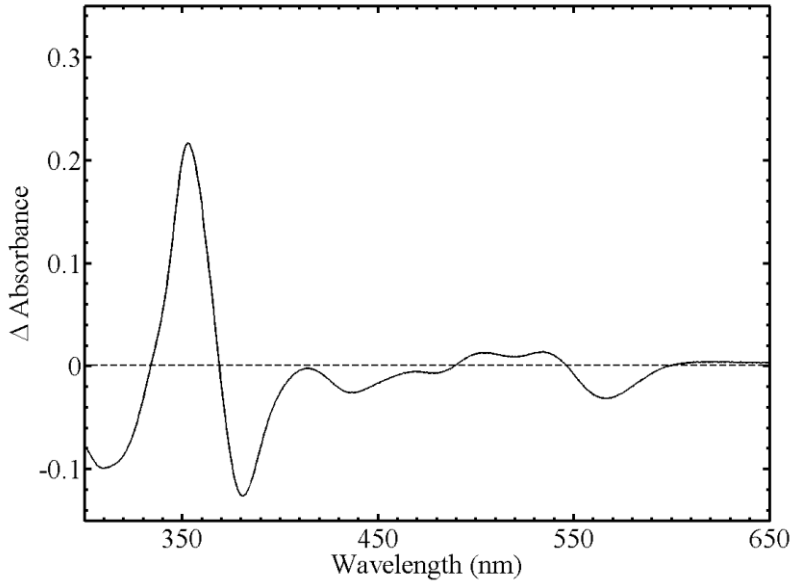

Figure 3.7. Absorption difference spectra of photolyzed minus pre-photolysis AdoCbl (25μM) in aerobic solution.

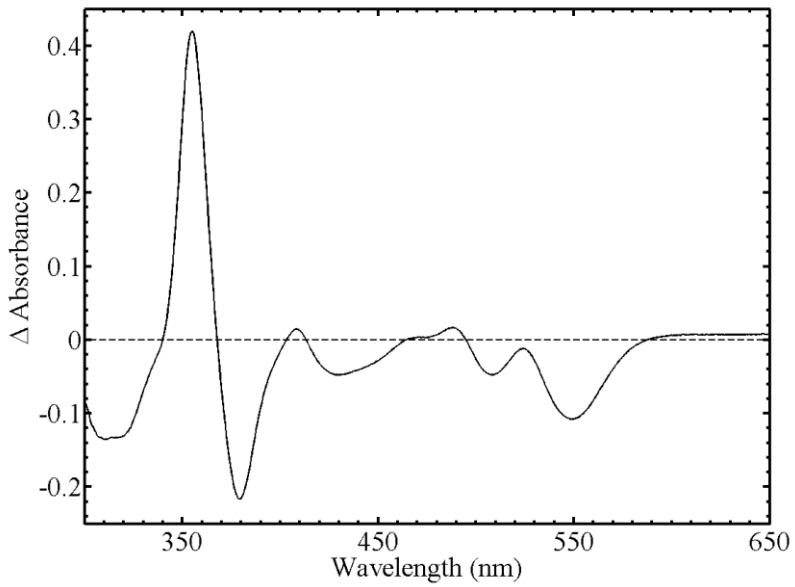

Figure 3.8. Absorption difference spectra of photolyzed minus pre-photolysis MeCbl (25μM) in EAL in aerobic solution.

The post-photolysis spectra of cob(II)alamin derived from AdoCbl in EAL are stable on the minutes time scale under aerobic conditions, in both the presence and the absence of bound substrate analog. Therefore, the protein protects the active site region from contact with dioxygen (O_2), on a time scale that is >10,000-fold the turnover frequency per site (k_{cat} per site) of approximately 50 s^{-1}. This is essential for maintaining multi-turnover reactivity of EAL under aerobic conditions. Post-photolysis static spectra reveal that when MeCbl is bound to EAL, the cob(II)alamin is not protected from O_2 and forms aquocob(III)alamin on the minutes time scale. The O_2 may bind near to the cobalamin in the MeCbl-EAL complex, in the region that would be occupied by the 5'-deoxyadenosyl moiety of AdoCbl.

3.3 Quantum yield of cob(II)alamin formation following photolysis of AdoCbl and MeCbl in solution and in EAL

Quantum Yield Measurements of Adenosylcobalamin in EAL with Substrate Inhibitor

The quantum yield of photolysis of AdoCbl was determined on the 10^{-7} s time scale under different conditions by using low pulse energy (≤2 mJ) excitation from the 532 nm output of the pulsed-Nd-YAG laser, and a continuous-wave probe at 470 nm. The low energies were selected to prevent multiple photon absorption by AdoCbl, as described in Chapter 2. The ratio of the concentration of AdoCbl to EAL active sites was ≤ 0.5, to avoid interference from free cofactor. A dissociation constant (K_D) for AdoCbl binding to EAL of 0.5 μM is estimated from the Michaelis constant[111], which indicates

that, under the conditions of the experiments, the free cofactor represents 4% of the total cofactor in the sample. The quantum yield values are presented in Table 3.2. The measured quantum yield at 10^{-7} s for AdoCbl photolysis in 10 mM potassium phosphate buffer at pH 7.5 of 0.23 ± 0.01 is comparable to previously reported aqueous solution, room temperature values of 0.23± 0.04 (excitation wavelength, λ_{ex}=532, 355 nm)[88] and 0.24 ±0.04 (λ_{ex}=400, 520 nm).[70]

Table 3.2. Quantum yield of cob(II)alamin at 10^{-7} s following photolysis of AdoCbl or MeCbl in anaerobic solution and in aerobic solutions of EAL in the absence and presence of the substrates and substrate analogs.

Cobalamin	**Substrate or Analog[a]**	**Environment**	**Quantum Yield[b]**
Adenosylcobalamin	-	Solution	0.23 ±0.01
	-	EAL	0.08 ±0.01
	(*S*)-1-Am-2-PrOH	EAL	0.04 ±0.01
Methylcobalamin	-	Solution	0.37 ±0.02
	-	EAL	0.13 ±0.01
	2-Aminoethanol	EAL	0.12 ±0.03
	(*S*)-2-Am-1-PrOH	EAL	0.13 ±0.02
	(*S*)-1-Am-2-PrOH	EAL	0.09 ±0.02
	(*R*)-1-Am-2-PrOH	EAL	0.10 ±0.01

[a]Substrates: 2-aminoethanol, (*S*)-2-amino-1-propanol. Substrate analogs (inhibitors): (*S*)-1-amino-2-propanol, (*R*)-1-amino-2-propanol.

[b]Average of $N \geq 3$ determinations, ±standard deviation.

Binding of AdoCbl by EAL leads to a 3-fold reduction in the quantum yield at 10^{-7} s relative to solution, to a value of 0.08 ±0.01. Reduction in the yield of cob(II)alamin at 9 ns has been previously reported for photolysis of AdoCbl bound in glutamate mutase, relative to solution.[75] The yield at 9 ns in glutamate mutase was 0.05 ±0.03.[75] Table 3.2 shows that, in the presence of bound (*S*)-1-amino-2-propanol, the quantum yield of cob(II)alamin at 10^{-7} s is reduced by 50%, relative to the quantum yield in the holoenzyme.

Quantum Yield Measurements of Methylcobalamin in EAL with Native Substrates and Substrate Inhibitors

Table 3.2 also presents the values of the quantum yield of cob(II)alamin following photolysis of MeCbl in solution and in EAL under different conditions. For measurements of MeCbl bound to EAL, the ratio of the concentration of MeCbl to EAL active sites was ≤ 0.5, to avoid interference from free cofactor. If the K_D for MeCbl binding to EAL is estimated as 1 μM, the free cofactor represents 8% of the total cofactor in the sample. Table 3.2 shows that MeCbl displays a higher quantum yield than AdoCbl in solution. This has been attributed to the smaller size of the methyl group, which allows more rapid cage escape, relative to the larger 5'-deoxyadenosyl group.[70,89] Binding of MeCbl in EAL reduces the quantum yield by 2.8-fold relative to solution, which is comparable to the 2.9-fold reduction observed for AdoCbl photolysis in EAL relative to solution. This result is consistent with the decreased rate of steady-state photolysis of MeCbl bound in methionine synthase, relative to MeCbl in solution.[117]

The value of 0.37 ±0.02 for the MeCbl quantum yield in Table 1 is comparable to previously reported values of 0.33 ±0.12 (λ_{ex}=527 nm; pulsed)[81], and 0.35 ±0.03 (λ_{ex}=442 nm; continuous-wave)[89], in which the rise in amplitude of the 470 nm band of cob(II)alamin following photolysis in anaerobic solution was detected and used to determine the quantum yield. The 470 nm band has also been used to detect cob(II)alamin in other MeCbl photolysis studies.[78,118] In contrast, by using broad band detection (460-640 nm) and deconvolution analysis of time-dependent spectra, Sension and coworkers report that the quantum yield at 9 ns in pulse-probe experiments declines at longer wavelengths (0.34 ±0.04 for λ_{ex}=400 nm; ~0.14 for λ_{ex}=520 nm).[70] This is consistent with the trend of λ_{ex}-dependent MeCbl quantum yields reported previously for photolysis under aerobic conditions.[119-120] While the detailed explanation for the discrepancies in quantum yield values for λ_{ex}>500 nm is not clear, it does not alter the principal conclusions of the present work.

Table 3.2 also shows the effect of the true substrates, aminoethanol and (*S*)-2-amino-1-propanol, the inactive substrate analog, (*S*)-1-amino-2-propanol, and the mechanism-based inactivator, (*R*)-1-amino-2-propanol[121], on the quantum yield of cob(II)alamin following photolysis of MeCbl in EAL. The quantum yield is the same for the four compounds (0.09-0.13) to within one standard deviation, and is essentially unaltered from the quantum yield for MeCbl alone. This result contrasts with the 50% reduction in the quantum yield for AdoCbl with (*S*)-1-amino-2-propanol bound in EAL.

3.4 Time-dependence of photoproduct cob(II)alamin following photolysis of AdoCbl and MeCbl in solution and in EAL

Adenosylcobalamin

Figure 3.9 shows the transient kinetics of cob(II)alamin on the millisecond time scale, following photolysis of AdoCbl in the buffered aqueous solution, and in EAL in the absence and presence of bound (*S*)-1-amino-2-propanol. For these experiments, a relatively high laser pulse energy of 10 mJ/pulse was used to enhance the population of cob(II)alamin, by photolyzing AdoCbl that had undergone geminate recombination on the timescale of the 10 ns laser pulse width. Measurements of the decay on shorter time scales of at least 0.1 μs do not show additional kinetic transients. The kinetics in Figure 3.9 therefore represent the events that occur on the time scale of ≥ 0.1 μs for each condition. This is consistent with previous studies of AdoCbl photolysis in solution.[81,89] The time dependence of the cob(II)alamin photoproduct concentration in solution was fit by a second-order decay plus a constant function. The second-order character of the transient decay was confirmed by the linear dependence of the decay half-time on AdoCbl concentration[122], as shown in Figure 3.10. The linear fit in Figure 3.10 leads to a second-order rate constant of 3.5×10^{9} $M^{-1}s^{-1}$, which is consistent with the reported diffusion-limited rate of cob(II)alamin recombination with the 5'-deoxyadenosyl radical.[81] The constant component of the fit of the solution decay in Figure 3.9 represents cob(II)alamin "stranded" by the rapid radical-radical recombination reaction of 5'-deoxyadenosyl radicals. The radical-radical annihilation reaction proceeds with second-order rate constants of approximately 3×10^{9} $M^{-1}s^{-1}$,[81] and therefore, competes favorably with recombination of cob(II)alamin with 5'-deoxyadenosyl radicals. The second-order and constant components of the time-dependent cob(II)alamin signal in solution confirm that the observed cob(II)alamin is the cage escape photoproduct.

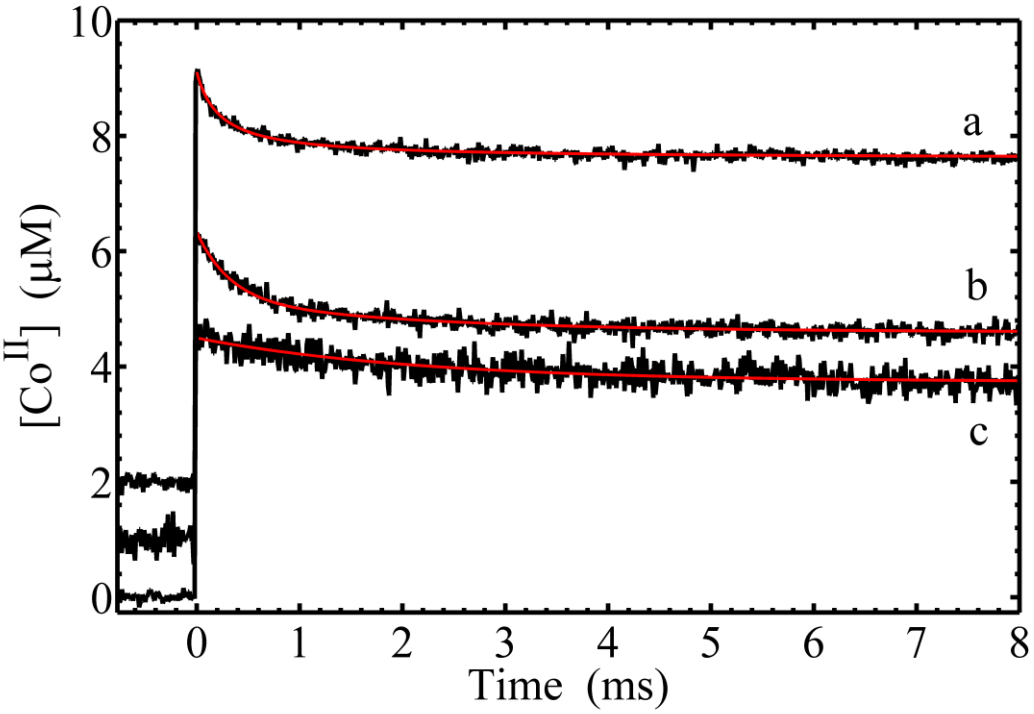

Figure 3.9. Time dependence of cob(II)alamin concentration following pulsed laser photolysis of AdoCbl, and overlaid best-fit functions (red). Cob(II)alamin concentration was obtained from the absorbance at 470 nm. (a) Anaerobic solution; second-order plus constant fit function. (b) In EAL in aerobic solution; biexponential plus constant fit function. (c) In EAL in aerobic solution, with (*S*)-1-amino-2-propanol bound; monoexponential plus constant fit function. The decay has been multiplied by a factor of 2.0 to account for the two-fold higher concentration AdoCbl in (b) relative to (c). The fitting parameters are presented in Table 3.3.

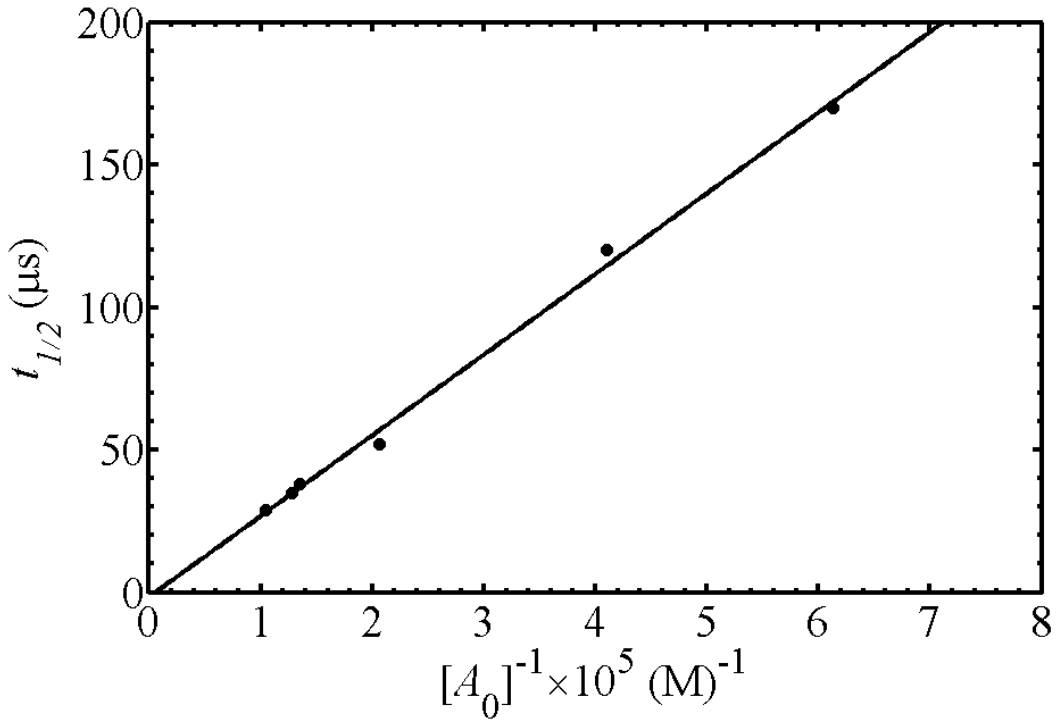

Figure 3.10. The half-time of cob(II)alamin decay as a function of inverse concentration of cob(II)alamin photoproduct following AdoCbl photolysis in anaerobic solution. The best-fit line corresponds to a second-order rate constant of 3.53×10^9 $M^{-1}s^{-1}$. *Fitting parameters*: Slope=2.83×10^{-10}, ordinate intercept=-1.29×10^{-6}, R^2=0.9963.

Figure 3.9 shows that the decay of the long-lived cob(II)alamin photoproduct following photolysis of AdoCbl bound to EAL also displays transient and constant components. The transient decay was well fit by using a biexponential plus constant function. The single exponential plus constant function did not provide a satisfactory fit to the transient decay (Figure 3.11 and Figure 3.12,). A proportion of 19% of the long-lived cob(II)alamin decays with a lifetime of 0.46 ms and a second component (13%) decays with a lifetime of 2.4 ms. The remaining 68% of the cob(II)alamin does not recombine on the longest time scales observed by transient absorption, or by subsequent

recording of the static spectra of the photolyzed samples (≤ 300 s). The kinetics and amplitudes of the decay are not influenced by changing the concentrations of AdoCbl or EAL. The presence of the spin trap, 5,5-dimethyl-1-pyrroline-N-oxide (DMPO) in the solution with holo-EAL does not influence the decay kinetics, and no spin-trapped, paramagnetic DMPO-adduct species were detected in the solution around the protein following photolysis by using electron paramagnetic resonance (EPR) spectroscopy. These results indicate that the observed cob(II)alamin recombines with the 5'-deoxyadenosyl radical within the protein interior. Therefore, the transients correspond to first-order kinetic processes.

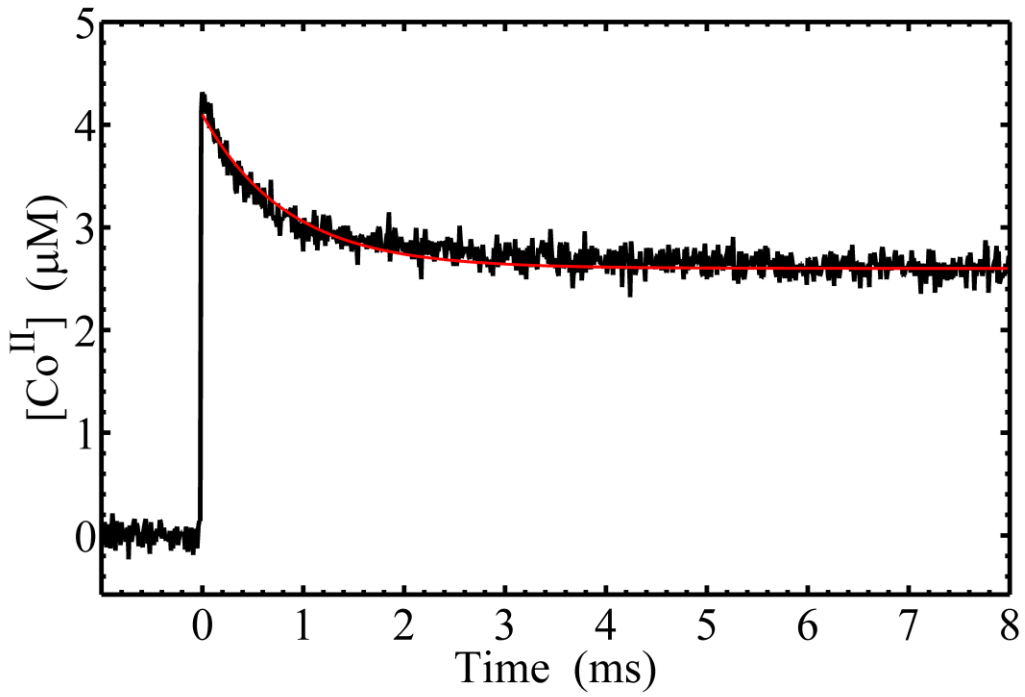

Figure 3.11. Time dependence of cob(II)alamin concentration following pulsed laser photolysis of AdoCbl bound to EAL, and overlaid best-fit monoexponential plus constant decay function (red). *Fitting parameters*: First-order rate constant, 1.2×10^{3} s^{-1}; normalized transient amplitude, 0.37; normalized constant amplitude, 0.63.

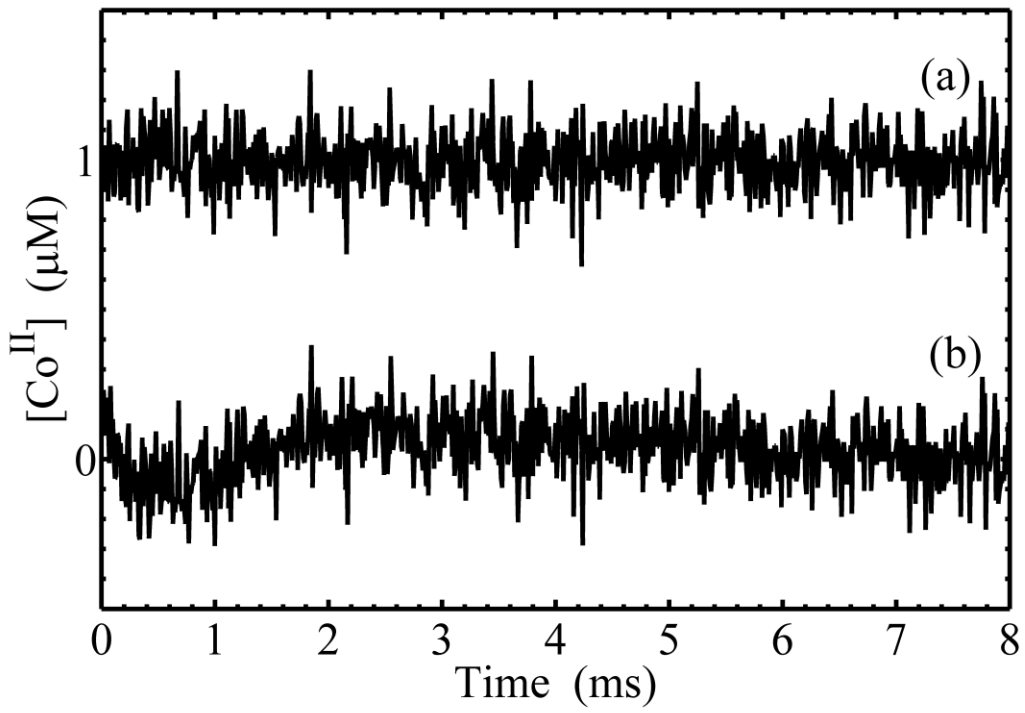

Figure 3.12. Residuals of fits of the time dependence of cob(II)alamin concentration following pulsed laser photolysis of AdoCbl bound to EAL. (a) Residuals of biexponential plus constant fit function. (b) Residuals of monoexponential plus constant fit function. Trace (a) has been offset from trace (b) by a constant addend of 1 μM. Figure 3.9 shows the biexponential plus constant fit, and Figure 3.11 shows the monoexponential plus constant fit.

Figure 3.9 shows the time dependence of the long-lived cob(II)alamin photoproduct state in EAL in the presence of bound (*S*)-1-amino-2-propanol. The transient decay can be fit by using a single exponential function plus a constant. A biexponential function did not lead to a significantly better fit (Figure 3.13). The fit shows that the cob(II)alamin signal decays with a lifetime of 2.2 ms, which accounts for 27% of the long-lived cob(II)alamin. A proportion of 73% of the cob(II)alamin did not

recombine at ≤ 300 s. The results show that (*S*)-1-amino-2-propanol selectively influences the cob(II)alamin photoproduct species, by eliminating the fast decay process, and by reducing the amplitude of the constant phase relative to the slow phase.

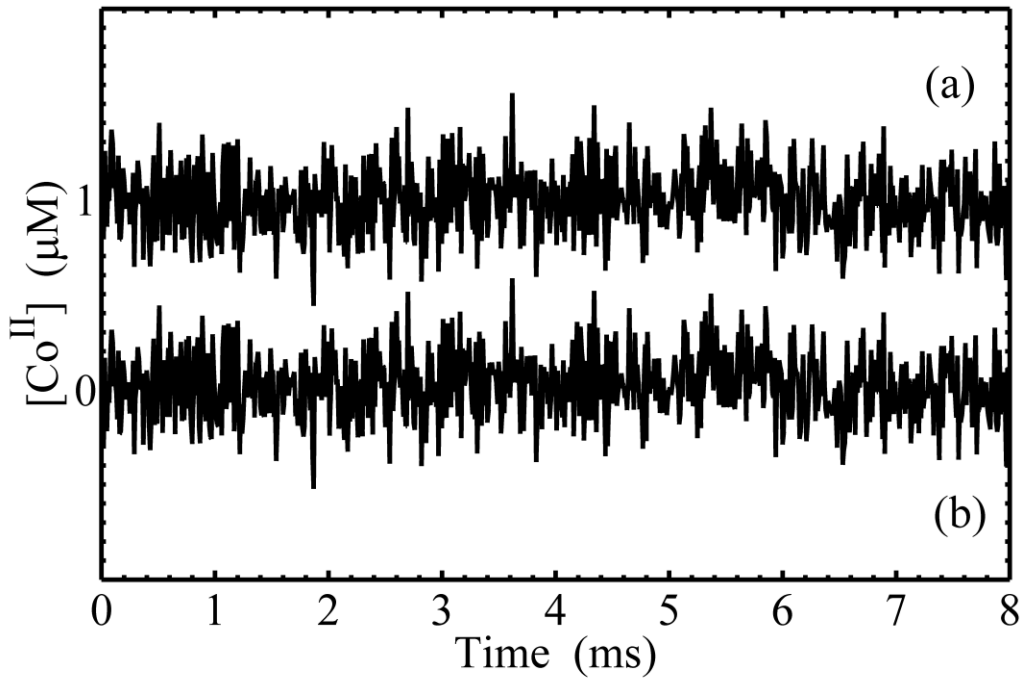

Figure 3.13 Residuals of fits of the time dependence of cob(II)alamin concentration following pulsed laser photolysis of AdoCbl in EAL with (*S*)-a-amino-2-propanol bound . (a) Residuals of monoexponetial plus constant fit function. (b) Residuals of biexponetial plus a constant fit function. Trace (a) has been offset from trace (b) by a constant addend of 1 μM. Figure 3.9 shows the monoexponential plus constant fit.

Methylcobalamin

Figure 3.14 and Figure 3.15 show the transient kinetics of cob(II)alamin on the millisecond time scale, following photolysis of MeCbl in anaerobic aqueous solution and in EAL in aerobic solution, respectively, at high laser pulse energy (10 mJ/pulse). Measurements on shorter time scales show that the kinetics in Figure 3.14 represent the

events that occur on the time scale of ≥ 0.1 μs for each condition. The time dependence of cob(II)alamin photoproduct in solution in Figure 3.14 was fit by a second-order decay plus a constant function. As observed for AdoCbl in solution, the transient kinetics were second-order, with a rate constant of 5.7×10^{9} $M^{-1}s^{-1}$, and the constant component of the fit represents cob(II)alamin "stranded" by the rapid radical-radical recombination reaction of methyl radicals.[81]

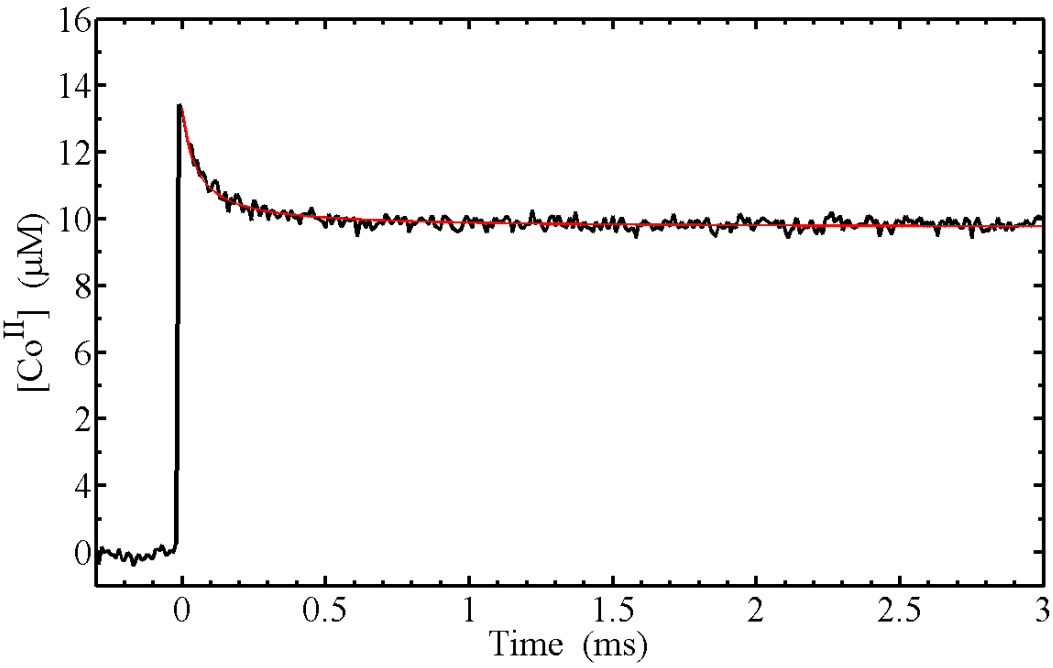

Figure 3.14. Time dependence of cob(II)alamin concentration following pulsed laser photolysis of MeCbl (30 μM), and overlaid best-fit functions (red) in anaerobic solution; second-order plus constant fit function. Second-order rate constant, 5.7×10^{9} $M^{-1}s^{-1}$; normalized transient amplitude, 0.28; normalized constant amplitude, 0.72.

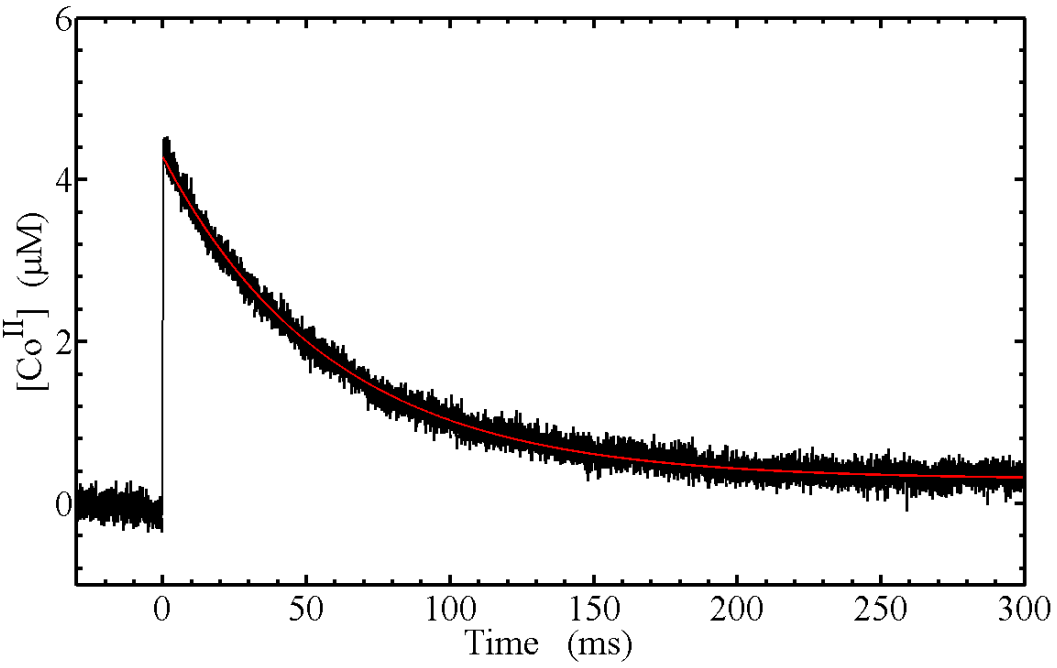

Figure 3.15. Time dependence of cob(II)alamin concentration following pulsed laser photolysis of MeCbl (30 μM) in EAL (60 μM), and overlaid best-fit functions (red) in aerobic solution; first-order plus constant fit function. *Fitting parameters*: First-order rate constant, 1.7×10^{1} s^{-1}; normalized transient amplitude, 0.93; normalized constant amplitude, 0.07.

Figure 3.15 shows that the millisecond decay of the long-lived cob(II)alamin photoproduct following photolysis of MeCbl bound to EAL in aerobic solution displays a monoexponential decay, with first-order rate constant of 17 s^{-1}. This contrasts with the biphasic transient and constant components of the cob(II)alamin decay in EAL following photolysis of AdoCbl (Figure 3.9). An exponential decay for cob(II)alamin is also observed following MeCbl photolysis in EAL in the presence of bound (*S*)-1-amino-2-propanol (22 s^{-1}) and aminoethanol (12 s^{-1}).

The photoproduct difference spectra (post-photolysis minus pre-photolysis) presented in Figure 3.8 provide an explanation for the difference in AdoCbl and MeCbl decay kinetics. The MeCbl photoproduct spectrum in EAL in aerobic solution in Figure 3.8 displays a negative feature of relatively low amplitude around 550 nm, and a strong positive feature at 350 nm. The spectrum does not show the characteristic loss of the $\alpha\beta$-band maximum at 525 nm (negative feature) and the rise of the 470 nm band of cob(II)alamin (positive feature) that are observed for AdoCbl photolysis in EAL under aerobic conditions, and for AdoCbl photolysis in anaerobic solution, as shown in Figure 3.5 and Figure 3.6, respectively. The absorption at 350 nm [λ=20 mM^{-1} cm^{-1}][89] is characteristic of aquocob(III)alamin. Aquocob(III)alamin and AdoCbl have comparable absorbance in the visible region. The corresponding aerobic solution difference spectrum for [aquocobalamin minus AdoCbl] in Figure 3.7 confirms that aquocob(III)alamin is the MeCbl photoproduct on the $>10^{-3}$ s time scale in EAL.

3.5 Discussion

Model for the Formation and Reaction of Cage Escaped Co^{II}-Radical Pair Populations Following AdoCbl and MeCbl Photolysis in EAL

Three cage escape photoproduct states are identified from the different components of the decay of cob(II)alamin that are observed in the transient absorption measurements (Figure 3.9; Table 3.3), as follows: (a) fast transient (corresponding to photoproduct population, P_f), (b) slow transient (photoproduct population, P_s), and (c) constant amplitude (photoproduct population, P_c). Figure 3.16 shows the kinetic model

that is proposed to account for the formation and time dependence of the cob(II)alamin photoproduct states in holo-EAL, in which three pathways from the geminate radical pair state lead to formation of cage escape photoproducts, which remain within the protein interior. We favor this branched reaction mechanism of separate paths from the geminate radical pair to the P_f, P_s, and P_c states, because it is the most simple mechanism that is consistent with the data. A mechanism in which cage escape leads to sequential formation of the P_f and then P_s states is not favored, because the decay rate constant assigned to P_s in holo-EAL is maintained in the absence of P_f in (*S*)-1-amino-2-propanol bound holo-EAL. This is not expected for a sequential mechanism, $A_1 \leftrightarrows A_2 \leftrightarrows A_3$, where A_1 denotes the geminate radical pair and A_2, A_3 are sequential cage escape states, because the two relaxation rate parameters, λ_1 and λ_2, for the linear two-step mechanism are functions of all four rate constants [$\lambda=\lambda(k_{ij}, k_{ji})$ where i=1, 2, 3, j=1,2,3, $i\neq j$, and the k_{ij} and k_{ji} are the forward and backward rate constants for each step, respectively].[122] In the general case, this mechanism leads to the prediction that the single relaxation rate constant, which is measured upon elimination of the terminal state, is different from λ_1 and λ_2.

Table 3.3. Relative amplitudes and observed recombination rate constants for cage escape populations in holo-EAL and in holo-EAL with bound (*S*)-1-amino-2-propanol.

Condition	Population	Rel. Amplitude	k_{decay} (s^{-1})
EAL•AdoCbl	P_f	0.19 ±0.05	2.2 (±0.4) $\times 10^3$
	P_s	0.13 ±0.05	4.2 (±1.5) $\times 10^2$
	P_c	0.68 ±0.08	-
EAL•AdoCbl •Substrate Analog	P_f	0	-
	P_s	0.27 ± 0.11	4.5 (±1.3) $\times 10^2$
	P_c	0.73 ±0.11	-

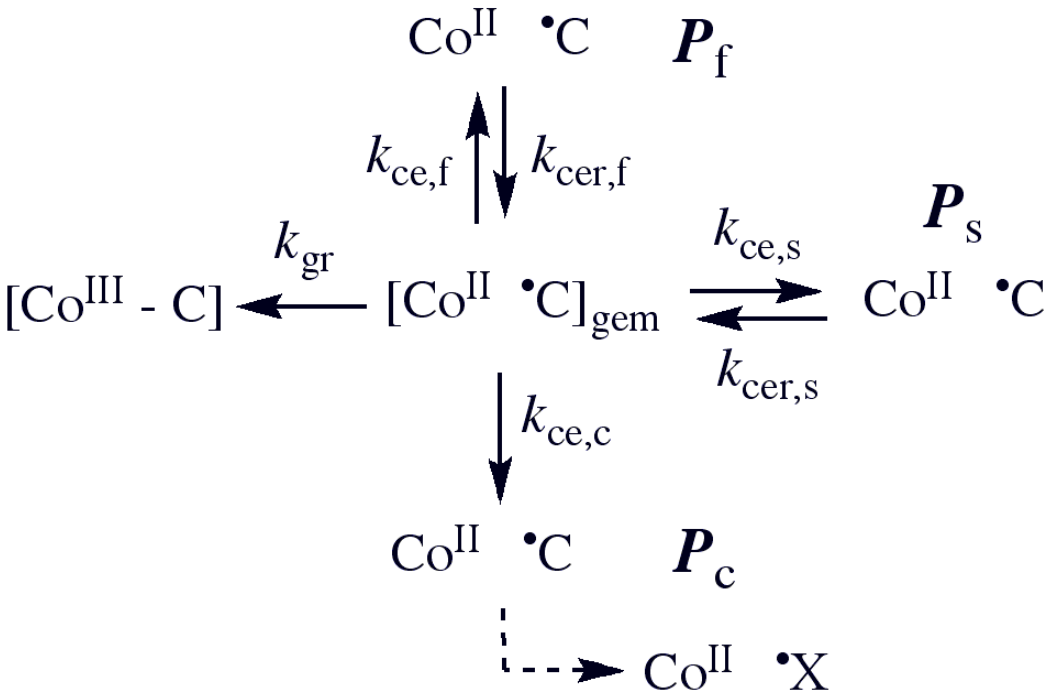

Figure 3.16. Proposed kinetic scheme for reactions of the cob(II)alamin-5'-deoxyadenosyl radical pair states following formation by photolysis in EAL.

The post-photolysis results show that the binding of the native AdoCbl cofactor in EAL leads to a state in which O_2 is prevented from interacting with the photoproduct cob(II)alamin. In contrast, the binding of the non-native MeCbl does not confer the property of O_2 insensitivity and shows the formation of aquo(III)cobalamin. The monoexponential, as opposed to second-order, decay of cob(II)alamin following MeCbl photolysis suggests a reaction with O_2 that is bound in the protein interior prior to the laser pulse and the decay does not reflect simple migration of the radical inside the protein interior. Hogenkamp and coworkers have previously shown that aquocob(III)alamin arises from the reaction of cob(II)alamin with dioxygen (O_2).[116]

Substrate Analog Binding Influences the Cage Escape Process

Table 3.4 shows the quantum yields for the states, P_f, P_s, and P_c in holo-EAL. These values were obtained by scaling the relative amplitudes in Table 3.3 by using the quantum yield value of 0.08 ±0.01 (Table 3.2). Table 3.4 also shows the quantum yields in holo-EAL in the presence of bound (*S*)-1-amino-2-propanol. The absence of the P_f state, and the decrease in amplitude of the P_c state relative to P_s (see Table 2) in the presence of (*S*)-1-amino-2-propanol, accounts for the substrate analog-induced decrease in the quantum yield of the cage escape population. Therefore, the decrease in quantum yield of the total cage escape population is caused by an effect of (*S*)-1-amino-2-propanol on the cage escape rate constant, rather than by an effect on the sub-nanosecond quantum yield of the geminate radical pair state, or by a change in the rate constant for geminate recombination. The latter two effects would cause a uniform decrease in the amplitudes of all three *P* states, with preservation of the relative amplitudes.

Table 3.4. Absolute quantum yield value at 10^{-7} s and estimated rate constants and activation energies for cage escape cage for different escape populations in holo-EAL and in holo-EAL with bound (*S*)-1-amino-2-propanol.

Condition	Population P_i	f_i	$k_{ce,i}$ (s^{-1})[a]	$E_{a,ce,i}$ (kcal/mol)[a]
EAL•AdoCbl	P_f	0.015 ±0.004	2×10^7	8
	P_s	0.010 ±0.004	2×10^7	8
	P_c	0.054 ±0.009	6×10^7	7
EAL•AdoCbl	P_f	0	-	
•Substrate Analog	P_s	0.011 ±0.005	1×10^7	8
	P_c	0.029 ±0.009	3×10^7	7

[a] k_{ce} calculated by assuming $k_{gr} = 1\times10^{-9}$ s^{-1}.

We speculate that P_f and P_c may represent states on non-productive pathways of the cob(II)alamin-5'-deoxyadenosyl radical pair reaction. If so, this would indicate that one role of protein changes induced by substrate binding is to suppress non-productive pathways of radical pair reaction.[123] The P_c state may represent an intermediate in which the 5'-deoxyadenosyl radical has undergone internal radical rearrangement, or has reacted with the protein by hydrogen atom abstraction or radical substitution. These are reactions with chemical precedent in solution homolyses.[90] P_s, whose yield is not suppressed by substrate analog binding, may thus resemble a productive radical pair state.

The quantum yield of methyl radical production was also significantly decreased in the presence of substrates and substrate analogs as shown in Table 3.2. The quantum yield was measured to be the same for the four compounds (0.09-0.13) to within one standard deviation, and was essentially the same as the quantum yield for MeCbl alone. This result is in contrast with the 50% reduction in the quantum yield for AdoCbl with (*S*)-1-amino-2-propanol bound in EAL. The absence of a significant substrate or substrate analog effect on MeCbl photolysis quantum yield suggests that the influence of (*S*)-1-amino-2-propanol on AdoCbl quantum yield is caused by an effect on the 5'-deoxyadenosyl moiety.

Estimation of Cage Escape Rate Constants and Activation Free Energy Barriers

The rate constants for cage escape in EAL can be estimated from the measured quantum yield values, if a value for the geminate recombination rate constant (k_{gr}) is assumed. The work of Sension and coworkers has shown that the geminate recombination rate constants for the cob(II)alamin - 5'-deoxyadenosyl radical pair are comparable in a variety of solvents, as shown by the following values: pure water (1.43×10^{9} s^{-1})[79], ethylene glycol (1.34×10^{9} s^{-1})[79] and the protein in glutamate mutase (1.08×10^{9} s^{-1})[75]. From these measurements, it was concluded that the rate constant for geminate recombination is "at most weakly dependent on solvent"[76], even for different alkyl axial ligands.[76] If it is assumed that the geminate recombination rate constant in EAL is 1×10^{9} s^{-1} (Arrhenius activation energy barrier, $E_{a,gr}$=5 kcal/mol), then the quantum yield values for P_f, P_s, and P_c (f_f, f_s, and f_c, respectively) can be used in the

following system of equations to solve for the corresponding cage escape rate constants ($k_{ce,f}$, $k_{ce,s}$, and $k_{ce,c}$, respectively), as follows:

$$\phi_i = \frac{k_{ce,i}}{k_{gr} + k_{ce,f} + k_{ce,s} + k_{ce,c}} \qquad \text{[Eq. 4]}$$

In Eq. 4, the index, *i*, corresponds to *f*, *s*, or *c*. The values of the three $k_{ce,i}$ and the corresponding Arrhenius activation energies, $E_{a,i}$, are presented in Table 3.4.

The decays of P_f and P_s through the geminate radical pair each proceed by a two step mechanism, in which k_{ce}, k_{cer} represent an equilibration step prior to the essentially irreversible geminate recombination (k_{gr}). The estimated k_{ce} values are 16- to 90-fold slower than k_{gr}, and therefore, $k_{gr}>>k_{ce}$. Under these conditions, a steady-state approximation is appropriate for the geminate radical pair during the decay, and the observed monoexponential decay rate constant is equal to k_{cer} to within approximately 1%.[122] The k_{cer} values in Table 3.3 correspond to E_a values of 13-14 kcal/mol. Therefore, if a cob(II)alamin-5'-deoxyadenosyl radical pair successfully escapes from the cage, then it is stabilized, by kinetic and/or thermodynamic factors, against recombination, for times that are commensurate with the lifetimes of hydrogen atom transfer reactions between carbon atoms (E_a≈13-14 kcal/mol).[124] Hydrogen atom transfer from the substrate C-H to the C5' radical center follows radical pair separation in EAL.

Implications for the Substrate Trigger Mechanism of Cob(II)alamin-5'-Deoxyadenosyl Radical Pair Formation in EAL

The competition between geminate recombination and cage escape controls the microsecond quantum yield. The two reactions occur on a time scale of 10^{-9}-10^{-7} s, and on the scale of relatively short cobalt-to-carbon distances [*r*(Co-C)]. These distances lie between the equilibrium Co-C bond length of 2.0 Å and approximately 4 Å, which corresponds to the diameter of one methylene carbon atom. Influences of substrate analog binding on cage escape are therefore characterized by changes in protein-coenzyme interactions that act at relatively short *r*(Co-C) values. (*S*)-1-amino-2-propanol binding effects cage escape at short *r*(Co-C) values, as demonstrated by the elimination of P_f and the decrease in P_c relative to P_s. However, substrate analog binding to EAL fails to increase the quantum yield, as predicted, based on the requirement of substrate binding for Co-C bond cleavage and radical pair separation (the "substrate trigger model"). We do not believe that this is because (*S*)-1-amino-2-propanol does not support the hydrogen atom transfer, because the time and *r*(Co-C) distance scales of the hydrogen atom transfer are ~10^{-3} s[35,104] and ~7 Å[24,27], respectively. Rather, the substrate analog may not fully induce the changes in protein-cofactor interactions that alter the cob(II)alamin-5'-deoxyadenosyl radical pair energetics (increased stabilization free energy, or decreased cage escape activation free energy barrier) that are characteristic of the true substrates, owing to steric disruption of substrate-protein interactions by the 1-methyl group. According to the mechanism in Figure 3.16, and the assumed value for k_{gr} of 1×10^{9} s^{-1} [76], a decrease in the value of $E_{a,s}$ by 3 kcal/mol would increase the quantum yield of P_s to 0.5, from the observed value of 0.01. Thus, it is reasonable that a specific interaction of the protein with the true substrate would be reflected in an enhanced quantum yield. This proposal will be tested, and described in Chapter 4, by performing

the photolysis measurements on the EAL•AdoCbl•substrate ternary complex, which is stabilized against turnover, in a recently developed cryosolvent system.[35]

Chapter 4: Characterization of Contributions of Protein and Chemical Coordinates to the Substrate Trigger of Cobalt-Carbon Bond Cleavage and Radical Pair Separation in the Ternary Complex of Adenosylcobalamin-Dependent Ethanolamine Ammonia-Lyase

Synopsis

In order to further address the "substrate trigger" mechanism of cobalt-carbon (Co-C) bond activation and cleavage and the role of concerted protein motions in radical mediated catalysis, the ternary complex of [enzyme•AdoCbl•substate] with bound substrate has been stabilized on the time scale of the absorption experiments in a fluid dimethyl sulfoxide/water cryosolvent at 230-248 K. The quantum yield and kinetics of decay of cob(II)alamin formed by pulsed-laser photolysis of adenosylcobalamin (AdoCbl) in the ternary complex have been studied by using transient (10^{-7} – 1 s time scale) and static ultraviolet-visible absorption spectroscopy. The paramagnetic photoproducts of pulsed and continuous wave photolysis were monitored by using continuous-wave X-band EPR spectroscopy at 120 K.

4.1 Materials and Methods

Materials

All chemicals were obtained from commercial sources and were used without further purification. Adenosylcobalamin, (*S*)-1-amino-2-propanol and (*S*)-2-amino-1-propanol were purchased from Sigma-Aldrich Chemical Co. EAL was purified from the *Escherichia coli* over expression strain incorporating the cloned S. *typhimurium* EAL coding sequence[110] essentially as described,[111] with the exception that the enzyme was

dialyzed against buffer containing 100 mM HEPES (pH 7.5), 10 mM potassium chloride, 5 mM dithiothreitol, 10 mM urea, and 10% glycerol,[77] and neither Triton X-100 nor urea were used during the purification. Enzyme activity was determined as described[112] by using the coupled assay with alcohol dehydrogenase/NADH. The specific activity of the purified enzyme with aminoethanol as substrate was 20-30 μmol/min/mg.

Enzyme Sample Preparation

Adenosylcobalamin, (*S*)-1-amino-2-propanol and (*S*)-2-amino-1-propanol were purchased from Sigma-Aldrich Chemical Co. The preparation of EAL in the cryosolvent system has been described in detail.[35] Briefly, samples with a 2.0-fold excess of EAL enzyme active sites (60 μM active site concentration) with cofactor (30 μM) were prepared in water buffered with 10 mM potassium cacodylate (pH 7.1), to form holoenzyme at 295 K. A cryosolvent pH value of 7.1 at this stage leads to a pH value of 7.5 ±0.4 at 230-240 K in the low temperature cryosolvent.[35] Potassium cacodylate buffer was used, owing to the relatively small temperature dependence of the pK_a.[107] The solution was sonicated at 277 K to minimize light scattering. Small volumes of 70% (volume/volume, v/v) dimethysulfoxide (DMSO)/water, which represented less than 15% of the volume of the holoenzyme-containing solution, were then added with continuous slow stirring, in four steps, at decreasing temperatures from 273 to 240 K. The solution was then transferred, with the protection of cold isopentane, to a quartz cuvette containing a solution of 54% (v/v) DMSO/water at 240 K, to achieve a final 50% (v/v) DMSO/water solution of EAL holoenzyme. The quartz cuvette was positioned in the low

temperature optical cryostat, which was mounted inside either the transient, or the static, absorption spectrometer. The substrate, (*S*)-2-amino-1-propanol, or substrate analog, (*S*)-1-amino-2-propanol, at a concentration of 5 mM final concentration in 50% (v/v) DMSO/water cryosolvent, was introduced after further lowering of the temperature to 230 K. The system was then incubated at 230 K for at least 5 min to allow substrate equilibration with the active site. All procedures were performed under a dim red safe light.

Adenosylcobalamin Sample Preparation

Anaerobic solutions of AdoCbl in cryosolvent were prepared by nitrogen gas bubbling for 15-30 min at 295 K, in a 3 ml quartz anaerobic cuvette through a septum. A positive pressure of nitrogen (3 psi) was maintained inside the cuvette during subsequent manipulations. The temperature of the sample was then lowered to either 230 (static spectrum acquisition experiments) or 240 K (photolysis experiments).

Low Temperature Optical Cryostat

A low temperature (77 K to 300 K) cryostat system was designed and constructed for optical monitoring of the cryosolvent system. Dry nitrogen gas was flowed through a stainless-steel heat exchanging coil which was immersed in liquid nitrogen. A home-made temperature controller, based on a 1/16 din MICROMEGA® autotune PID temperature/process controller (Omega CN77000), heats the cold nitrogen gas to the

desired temperature by using an electric heating element along the nitrogen gas pathway. The temperature is monitored by using a T-band thermocouple (Omega 5STRC-TT-T-30-36). The nitrogen gas flows through a home designed and constructed brass cuvette holder, shown in Figure 4.1, where the sample is held in a quartz cuvette (Hellma QS 282 1.000 ml). An outer housing, shown in Figure 4.2 and Figure 4.3, is used to eliminate the moisture condensation along the optical path. The pre-cooled nitrogen gas is used to purge the inside of the outer housing after passing through the sample holder. Two on-axis heated quartz windows provide optical access to the cooled sample. The system has >90% transmittance from 250 nm to 2500 nm at 230 K. The top of the housing is covered by a glass hatch for easy sample access. The temperature stability at 230 K is ± 1 K over a 2 h time interval. This system is used with both the transient and static absorption spectrometers.

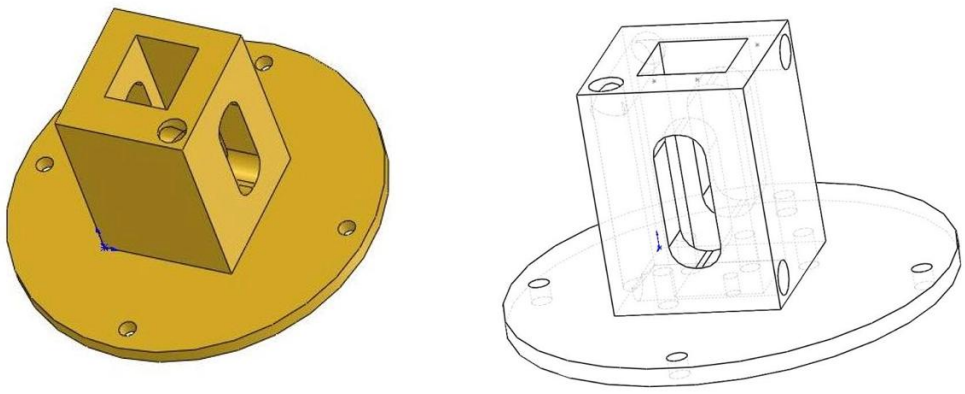

Figure 4.1. Schematic of brass cuvette holder used with cold nitrogen cooling system.

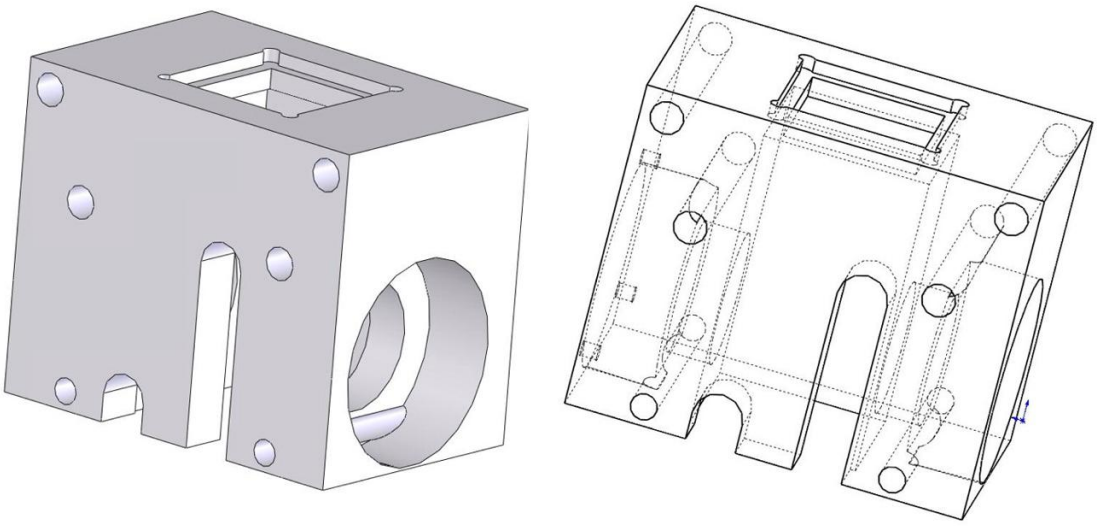

Figure 4.2. Schematic of outer housing used with the Low Temperature Optical Cryostat.

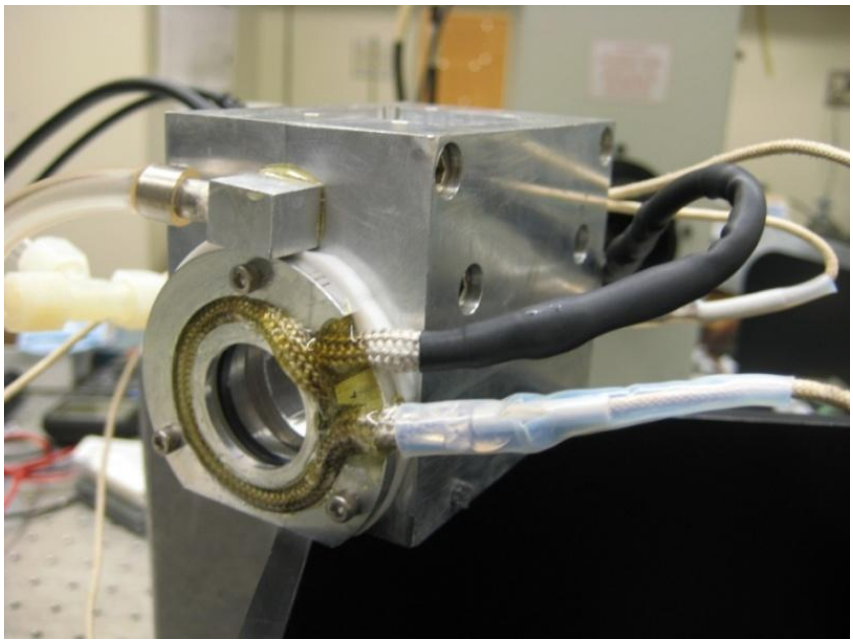

Figure 4.3. Image of assembled outer housing, cold nitrogen flow, heated quartz windows of the low temperature optical cryostat.

Low Temperature Static Absorption Spectra

Low temperature static absorption spectra from 300 nm to 650 nm were collected by using a Shimadzu UV-1601 absorption spectrometer (0.5 nm wavelength accuracy), which was fitted with the low temperature optical cryostat. The average of three spectra were taken for all low temperature spectra. Three enzyme sample spectra without cofactor were taken and averaged for a background scattering baseline, and this baseline was later subtracted from the holoenzyme and ternary complex spectra. All measurements were performed at 230 ±1 K.

Low Temperature Transient Absorption Spectroscopy

Transient absorption measurements were made by using the low temperature optical cryostat, and a transient spectrophotometer of home design and construction, which has been previously described.[125] The transient absorption spectrometer has a sensitivity to change in absorbance (*A*) of 2×10^{-3} over 300-650 nm, and a deadtime of ≤20 ns. The second harmonic output (532 nm) of a Nd:YAG laser (SpectraPhysics GCR-10; 10 ns pulse width), with pulse energy adjusted by a glan prism polarizer/half-wave plate, was used as actinic source. The spectrometer's pump and probe pulse timing sequences and data collection were controlled by a Macintosh computer with LabVIEW software (National Instruments) via a GPIB/IEEE-488.2 interface. Data fitting and analysis was performed by using Matlab (Natick, MA) or OriginPro (OriginLab Corporation, Northampton, MA), routines that were run on PC computers. Transient

absorption of the cob(II)alamin state was monitored at 470 nm (probe) following laser pulse photolysis at 532 nm. Measurements were made with a 100 μs dwell time between the acquisition of data points and a corresponding time constant for the detector of 10 μs. All measurements were performed at 240 ±1 K.

EPR Spectroscopy of Cob(II)alamin-Substrate Radical Pair Formation

X-band continuous-wave EPR spectra were obtained by using a Bruker E500 ElexSys EPR spectrometer, equipped with a Bruker ER4123 SHQE X-band cavity. Temperature was controlled with a Bruker ER4131VT liquid nitrogen/gas flow cryostat system, with ER4121VT-1011 evaporator/transfer line, ER4121VT-1013 heater/thermocouple, and 26 liter liquid nitrogen reservoir. EAL samples in 41% v/v DMSO/water cryosolvent were prepared for EPR spectroscopy in 2 mm outer diameter EPR tubes (Wilmad/Lab Glass, 712-SQ-250M), as described briefly above and previously.[35] Holo-EAL was mixed with the substrate, (*S*)-2-amino-1-propanol, at 230 K. As described in Results, photolysis of the ternary complex at 230 K was carried out by using the focused 532 nm output of the pulsed Nd-YAG laser (50 mJ/pulse, 10 Hz, 90 seconds). A subsequent experiment was performed in which the reaction of the ternary complex to form the cob(II)alamin-substrate radical state was initiated by a temperature step from 230 K to 245 K. During the rise of the cob(II)alamin-substrate radical EPR signal, the sample was subjected to a protocol of intermittent irradiation by using the filtered output (250 nm – 380 nm) of a 200 W mercury lamp (Oriel Optics Corp., C-60-

30). All samples where frozen in liquid nitrogen following photolysis and EPR measurements were performed at 120 K, under dim light.

Quantum Yield Measurements

Quantum yield measurements were obtained by using laser pulse energies of ≤ 3 mJ, in order to eliminate multiple photon absorption by AdoCbl during the laser pulse. The 470 nm probe beam was used to detect the formation of cob(II)alamin. Quantum yield measurements were made with a 1.0 μs dwell time and a time constant of 0.1 μs. The quantum yield (*QY*) is defined as the concentration of cob(II)alamin photoproduct formed by the laser pulse, divided by the absorbed photon (*hv*) concentration, $[hv]_{abs}$. Details of the calculation of φ values have been described.[125]

Temperature-Dependence of the First-Order Rate Constant

The temperature dependence of the first order rate constant, *k*, is given by the Arrhenius expression:[122]

$$k(T) = Ae^{\frac{-E_a}{RT}} \tag{4.1}$$

where E_a is the activation energy, *R* is the gas constant, and *A* is a prefactor that represents the value of *k* as $E_a \rightarrow 0$. The value of *A* is typically approximated as $\frac{k_B T}{h}$,

where k_B and h are the Boltzmann and Planck constants, respectively, and T is absolute temperature.

4.2 UV/visible Absorption Spectra of Holoenzyme and Ternary Complex at 230 K

The absorption spectra of AdoCbl at 230 K in the 50% v/v DMSO-water cryosolvent, and for AdoCbl in holo-EAL and in the ternary complex with (*S*)-2-amino-1-propanol bound, are presented in Figure 4.4. The AdoCbl spectra show the characteristic visible wavelength absorption maximum (α/β band) and the UV maximum (γ-band).[33] The spectrum from the ternary complex does not contain the cob(II)alamin signal, which confirms that the ternary complex is under kinetic arrest on the minutes time scale of the spectrum acquisition.[35] In the cryosolvent system at 240 K, the λ_{max} value of the α/βband was found to be 528.3 ± 0.3 nm for free AdoCbl, 527.7 ± 0.2 nm for holo-EAL, and 527.9 ± 0.3 nm for the EAL ternary complex. The λ_{max} value of the γ band was found to be 377.0 ± 0.1 nm for free AdoCbl, 376.9 ± 0.1 nm for holo-EAL, and 376.9 ± 0.1 nm for the EAL ternary complex. There is a subtle hypsochromic shift of 0.6 ±0.4 nm of the α/βband following AdoCbl binding to the apo-enzyme, which is caused by the different cofactor environments in aqueous solution and in EAL, as found for other AdoCbl-dependent enzymes.[33-34,115] No significant shift in the positions or absorbance values of the visible or UV absorption maxima of AdoCbl are observed following binding of the substrate to holo-EAL. However, there are subtle changes in the spectrum of AdoCbl in the ternary complex, relative to holo-EAL. These include an approximately

3 Å bathochromic shift of the shoulder around 475 nm, and a change in the line shape of the minor peak feature around 425 nm. These changes provide UV-visible spectroscopic evidence that the substrate binds to EAL at low temperature, which is in agreement with the kinetic evidence for substrate-holo-EAL binding at low temperature.[35]

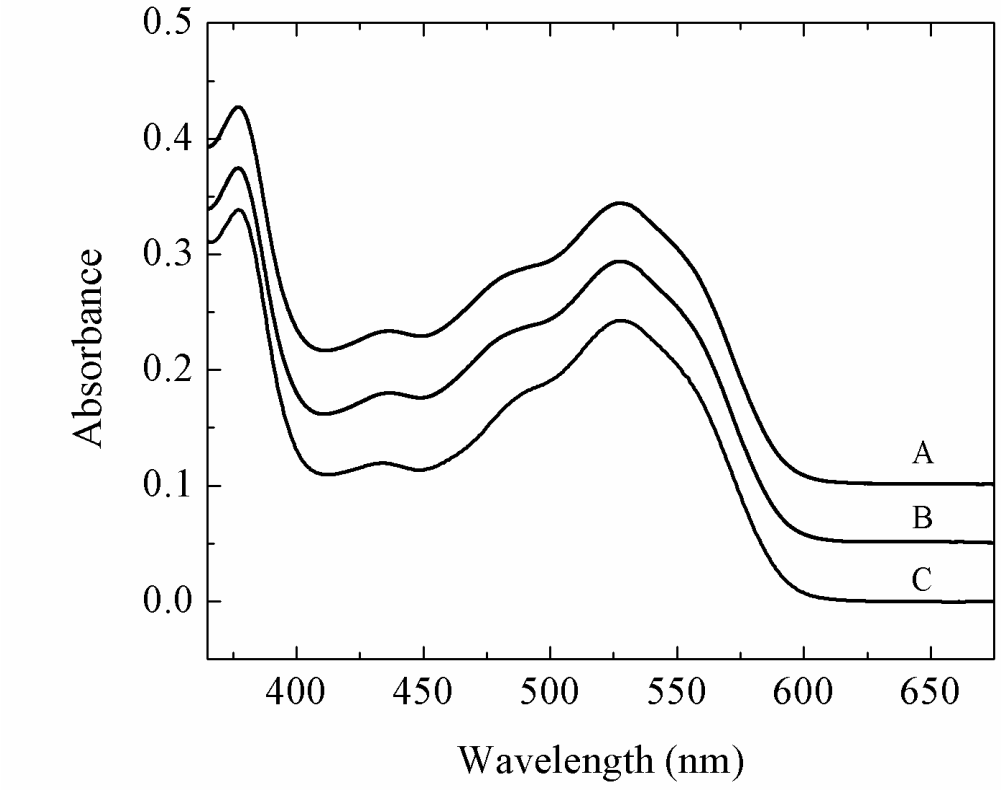

Figure 4.4. UV/visible absorption spectra of adenosylcobalamin in free solution, and in EAL in the holo-enzyme and ternary complex. The spectra were collected at 230 K for samples in the 50% dimethylsulfoxide/water cryosolvent system. (A) AdoCbl in solution. (B) AdoCbl in EAL (holoenzyme). (C) AdoCbl in EAL with bound (*S*)-2-amino-propanol substrate (ternary complex). Concentrations were as follows: 60 μM EAL, 30 μM AdoCbl, 5 mM (*S*)-2-amino-propanol.

4.3 UV/visible Transient Absorption Spectroscopy of Holoenzyme and Ternary Complex at 230 K

Quantum Yield of Cob(II)alamin Formation following Low Temperature Photolysis of AdoCbl in Solution, Holoenzyme and Ternary Complex

The quantum yield of AdoCbl photolysis at 240 K was measured on the 10^{-6} s time scale by using low, sub-saturating pulse energy ($\leq$ 3 mJ) excitation from the 532 nm output of the pulsed-Nd-YAG laser, and a continuous-wave probe for cob(II)alamin formation at 470 nm. The low energies were selected to prevent multiple photon absorption by AdoCbl. The ratio of the concentration of AdoCbl to EAL active sites was $\leq$ 0.5, to avoid possible interference from photolysis of free cofactor. The measured quantum yield at 10^{-6} s for AdoCbl photolysis in cryosolvent is $< 10^{-2}$, which is the detection limit of the instrument. The small quantum yield of AdoCbl photolysis in cryosolvent is consistent with the viscosity dependence of k_{gr} and k_{ce}.[126] The quantum yield was also $< 10^{-2}$ for AdoCbl in holo-EAL and in the ternary complex. Therefore, binding of the substrate does not enhance the quantum yield above the level of 10^{-2}.

Time Dependence of Photoproduct Cob(II)alamin Recombination Following Photolysis Under Saturating Pulsed-Laser Irradiation

Figure 4.5 shows the transient decay kinetics of cob(II)alamin at 240 K in the cryosolvent solution on the milliseconds time scale, following photolysis of AdoCbl in solution, in holo-EAL, in holo-EAL with the inhibitor (*S*)-1-amino-2-propanol bound, and in the ternary complex with (*S*)-2-amino-1-propanol bound. A relatively high laser

pulse energy of 10 mJ/pulse was used to enhance the population of cob(II)alamin, by photolyzing AdoCbl that had undergone geminate recombination on the timescale of the 10 ns laser pulse width. Measurements of the decay on shorter time scales of 1.0×10^{-7} s do not show additional kinetic transients. The kinetics in Figure 4.5 therefore represent the events that occur on the time scale of $\geq1.0\times10^{-7}$ s for each condition.

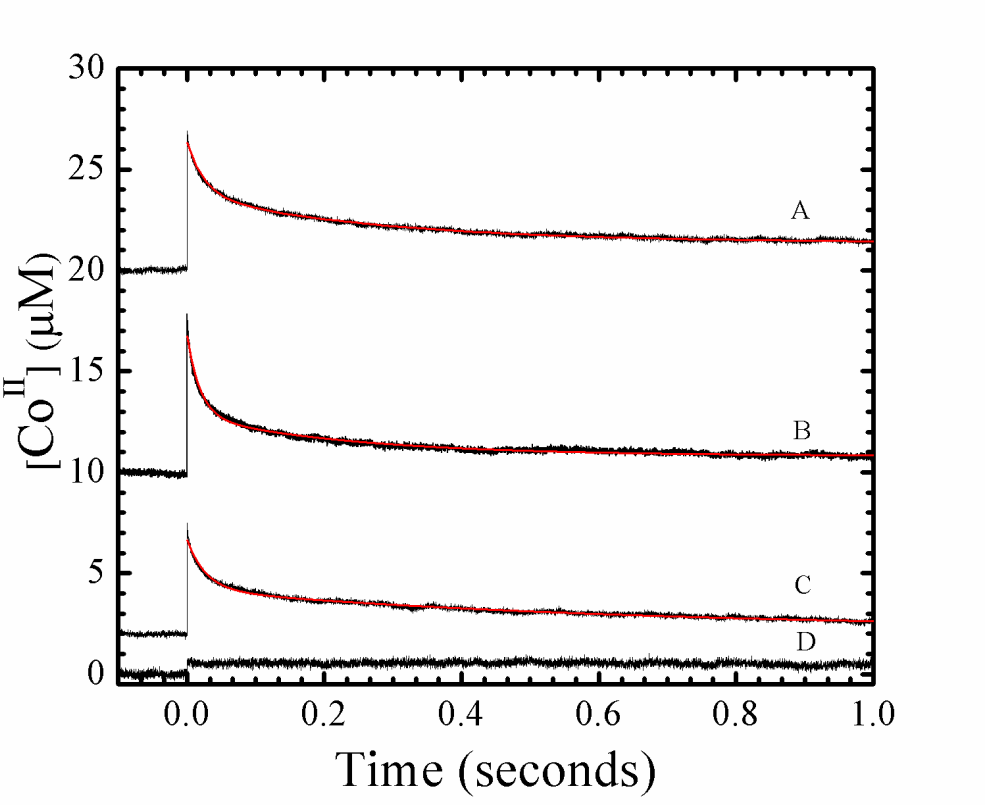

Figure 4.5. Time dependence of cob(II)alamin concentration following pulsed laser photolysis of adenosylcobalamin at 240 K, and overlaid best-fit biexponential plus constant decay functions (red, smooth curves). Fitting parameters are collected in Table 1. (A) Holo-EAL in aerobic solution. (B) Holo-EAL in aerobic solution, with bound (*S*)-2-amino-1-propanol bound (ternary complex). (C) Holo-EAL in aerobic solution, with bound (*S*)-1-amino-2-propanol bound (inhibitor complex). (D) Anaerobic solution. Concentrations were as follows: 60 μM EAL, 30 μM AdoCbl, 5 mM (*S*)-2-amino-propanol, 5 mM (*S*)-1-amino-2-propanol.

The transient decays for holo-EAL, ternary complex, and holo-EAL with inhibitor bound (Figure 4.5, A, B and C) were well fit by using a biexponential plus constant function. The biexponential and monoexponential plus constant functions did not provide satisfactory fits to the transient decays (Figure 4.6 and Figure 4.7). The results for holo-EAL in Table 1 show that the normalized relative amplitudes of the fast decay

population (P_f), the slow decay population (P_s), and the constant amplitude population (P_c) are 0.57, 0.33, and 0.11, respectively. Table 1 also shows that binding of the substrate or inhibitor to holo-EAL does not significantly alter the relative populations, or significantly influence the first-order rate constants for the fast (k_f) and slow (k_s) decay populations, relative to holo-EAL. Thus, the presence of the bound substrate or inhibitor does not significantly affect either the P_i or the $k_{decay,i}$ values, relative to holo-EAL.

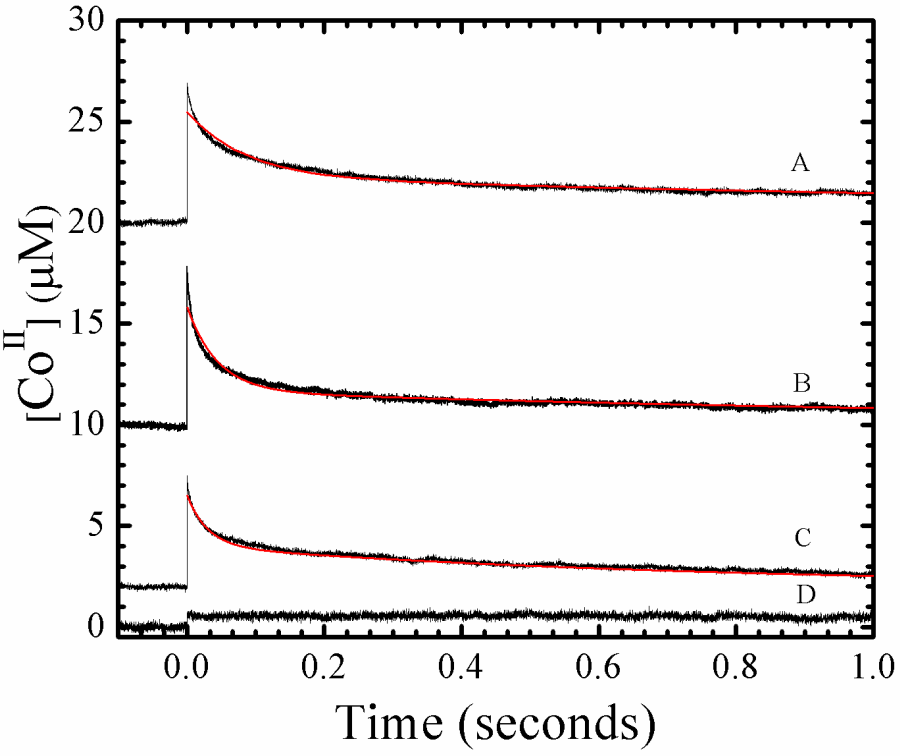

Figure 4.6. Time dependence of cob(II)alamin concentration following pulsed laser photolysis of adenosylcobalamin (AdoCbl) at 240 K, and overlaid best-fit bi-exponential decay functions (red). The cob(II)alamin concentration was obtained from the absorbance at 470 nm. (A) EAL in aerobic solution. (B) EAL in aerobic solution, with (*S*)-2-amino-1-propanol bound (ternary complex). (C) EAL in aerobic solution, with (*S*)-1-amino-2-propanol bound (inhibitor complex). (D) Anaerobic solution.

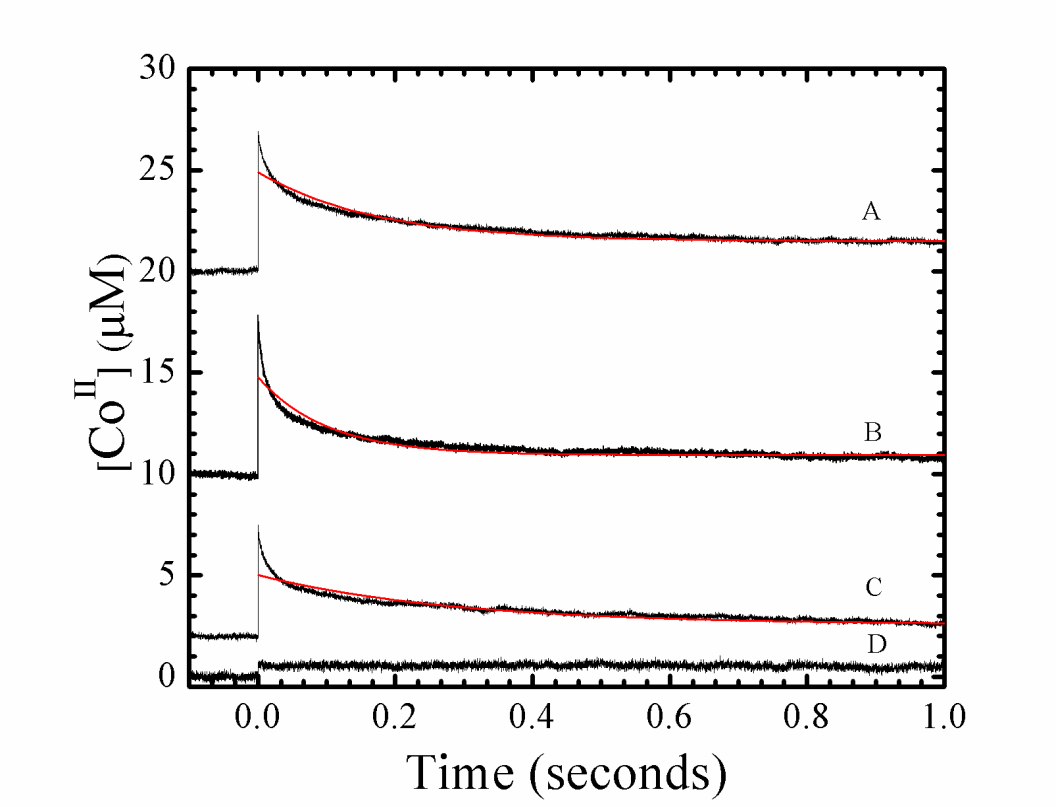

Figure 4.7. Time dependence of cob(II)alamin concentration following pulsed laser photolysis of adenosylcobalamin (AdoCbl) at 240 K, and overlaid best-fit monoexponential decay plus a constant functions (red). The cob(II)alamin concentration was obtained from the absorbance at 470 nm. (A) EAL in aerobic solution. (B) EAL in aerobic solution, with (*S*)-2-amino-1-propanol bound (ternary complex). (C) EAL in aerobic solution, with (*S*)-1-amino-2-propanol bound (inhibitor complex). (D) Anaerobic solution.

Table 1. Relative cob(II)alamin photoproduct amplitudes, limits on quantum yield and cage escape rate constant values, and observed recombination decay rate constants for cage escape populations at 240 K, following photolysis of AdoCbl with a saturating laser flash, in holo-EAL, holo-EAL with bound substrate, (*S*)-2-amino-propanol (ternary complex), and holo-EAL with bound substrate analog, (*S*)-1-amino-2-propanol. Standard deviations for determinations on at least three separate samples are shown in parentheses.

Condition	P_i	A_{rel} [a]	φ_i [b]	$k_{ce,i}$ [c] (s^{-1})	$k_{decay,i}$ (s^{-1})
EAL•AdoCbl	P_f	5.7 (1.1) $\times 10^{-1}$	$<6\times10^{-3}$	$<5.8\times10^{5}$	5.0 (1.4)
	P_s	3.3 (0.6) $\times 10^{-1}$	$<3\times10^{-3}$	$<2.9\times10^{5}$	4.3 (1.3)
	P_c	1.1 (0.7) $\times 10^{-1}$	$<1\times10^{-3}$	$<9.6\times10^{4}$	-
EAL•AdoCbl •Substrate	P_f	6.1 (0.5) $\times 10^{-1}$	$<6\times10^{-3}$	$<5.8\times10^{5}$	6.0 (1.4)
	P_s	3.0 (0.3) $\times 10^{-1}$	$<3\times10^{-3}$	$<2.9\times10^{5}$	4.9 (2.0)
	P_c	0.9 (0.5) $\times 10^{-1}$	$<1\times10^{-3}$	$<9.6\times10^{4}$	-
EAL•AdoCbl •Inhibitor	P_f	5.7 (0.4) $\times 10^{-1}$	$<6\times10^{-3}$	$<5.8\times10^{5}$	6.0 (2.1)
	P_s	3.4 (0.7) $\times 10^{-1}$	$<3\times10^{-3}$	$<2.9\times10^{5}$	4.0 (1.9)
	P_c	0.9 (0.5) $\times 10^{-1}$	$<1\times10^{-2}$	$<9.6\times10^{4}$	-

[a] Normalized relative amplitude at 10^{-6} s, obtained by using saturating laser flash (10 mJ).

[b] Upper limit on quantum yield, obtained from relative amplitude and upper limit on absolute quantum yield at 10^{-6} s of $<1\times10^{-2}$.

[c] Upper limit on cage escape rate constant, obtained by using $k_{gr}=9.5\times10^{7}$ s^{-1}.

Visible Light Irradiation of the EAL Ternary Complex Does Not Generate the Cob(II)alamin-Substrate Radical Pair

The ability of long-term irradiation to generate the cob(II)alamin-substrate radical pair was addressed by using EPR spectroscopy. Samples of holo-EAL and the ternary complex were irradiated for 1.5 min at 230 K by using the output of the pulsed-Nd-YAG laser at 532 nm. The relatively low temperature was chosen to suppress thermal radical pair formation, during the irradiation. The individual photoproduct spectra and the

difference spectrum for ternary complex minus holo-EAL are shown in Figure 4.8A-C. The cob(II)alamin-substrate radical pair spectrum, generated by the native, thermally activated pathway, by using (*S*)-2-aminopropanol substrate, is presented in Figure 4.8D. Comparison of the spectra in Figure 4.8 shows that irradiation does not generate a significant level of cob(II)alamin-substrate radical pair state. Therefore, light does not drive the productive formation of the ultimate product of the radical pair separation reaction.

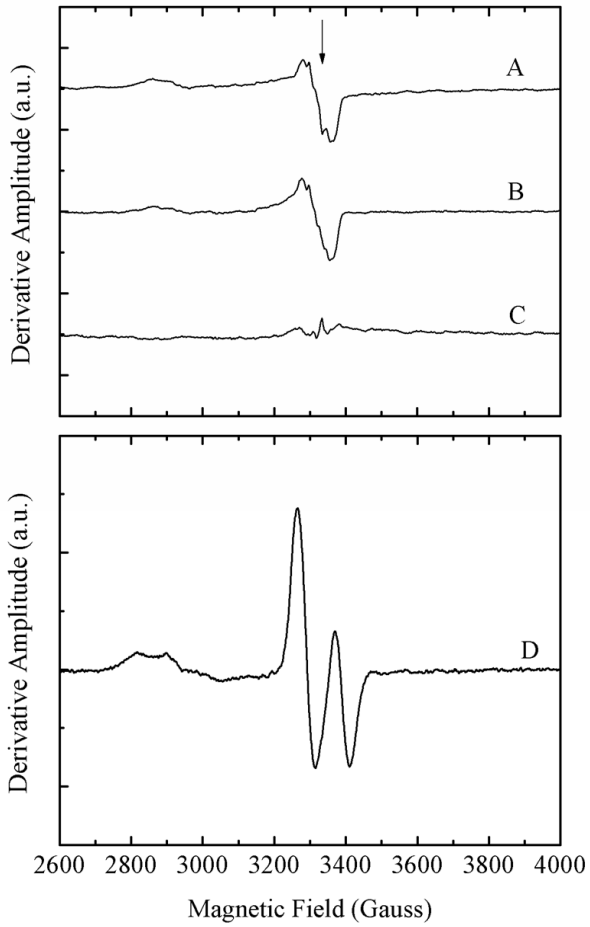

Figure 4.8. EPR spectra for EAL ternary complex, holo-EAL, and difference spectrum for ternary complex minus holo-EAL, following long-term photolysis, and control EPR spectrum of the (*S*)-2-amino-1-propanol-generated cob(II)alamin-substrate radical pair generated by the native, thermal reaction. Note that the ordinate scale in (A)-(C) is expanded by a factor of 80, relative to the scale for (D). (A) Holo-EAL. (B) EAL ternary complex. (C) Difference EPR spectrum; ternary complex (B) minus holo-EAL (A). (D) Cob(II)alamin-substrate radical pair EPR spectrum, following 15 min incubation at 275 K (EAL active site concentration, 150 mM; AdoCbl, 300 mM; (*S*)-2-amino-1-propanol, 10 mM). *Photolysis conditions*: EAL active sites, 120 μM; AdoCbl, 60 mM. Irradiation for 1.5 min with the 532 nm output of the pulsed Nd-YAG laser (10 Hz, 50 mJ/pulse) at 230 K. *EPR conditions*: Temperature, 120 K; microwave frequency, 9.436 GHz; microwave power, 20 mW; magnetic field modulation, 10 Gauss peak-peak; modulation frequency, 100 kHz; field sweep rate, 1.5 Gauss s^{-1}; time constant, 200 ms; average of 2 sweeps, minus average of 2 baseline spectra.

Effect of Photolysis on Thermally-Activated Cob(II)alamin-Substrate Radical Pair Formation

The EAL ternary complex was irradiated during the thermal cob(II)alamin-substrate radical pair formation reaction, at 246 K, in order to address effects of photolysis on the first-order rate constant for radical pair formation, and on the long-time equilibrium between the ternary complex and the radical pair states. The formation of the cob(II)alamin-substrate radical pair was detected by CW-EPR spectroscopy. The experiment was performed by using alternating light and dark time periods, that were applied during the rise of the radical pair, and following the establishment of equilibrium. This avoided uncertainties caused by comparison of different samples. The kinetics of cob(II)alamin-substrate radical formation obtained by using this protocol are shown in Figure 4.9. No distinguishable effect of continuous-wave visible irradiation was observed on the rate of cob(II)alamin-substrate radical pair formation. Irradiation also did not alter the long-time equilibrium populations of the ternary complex and the radical pair.

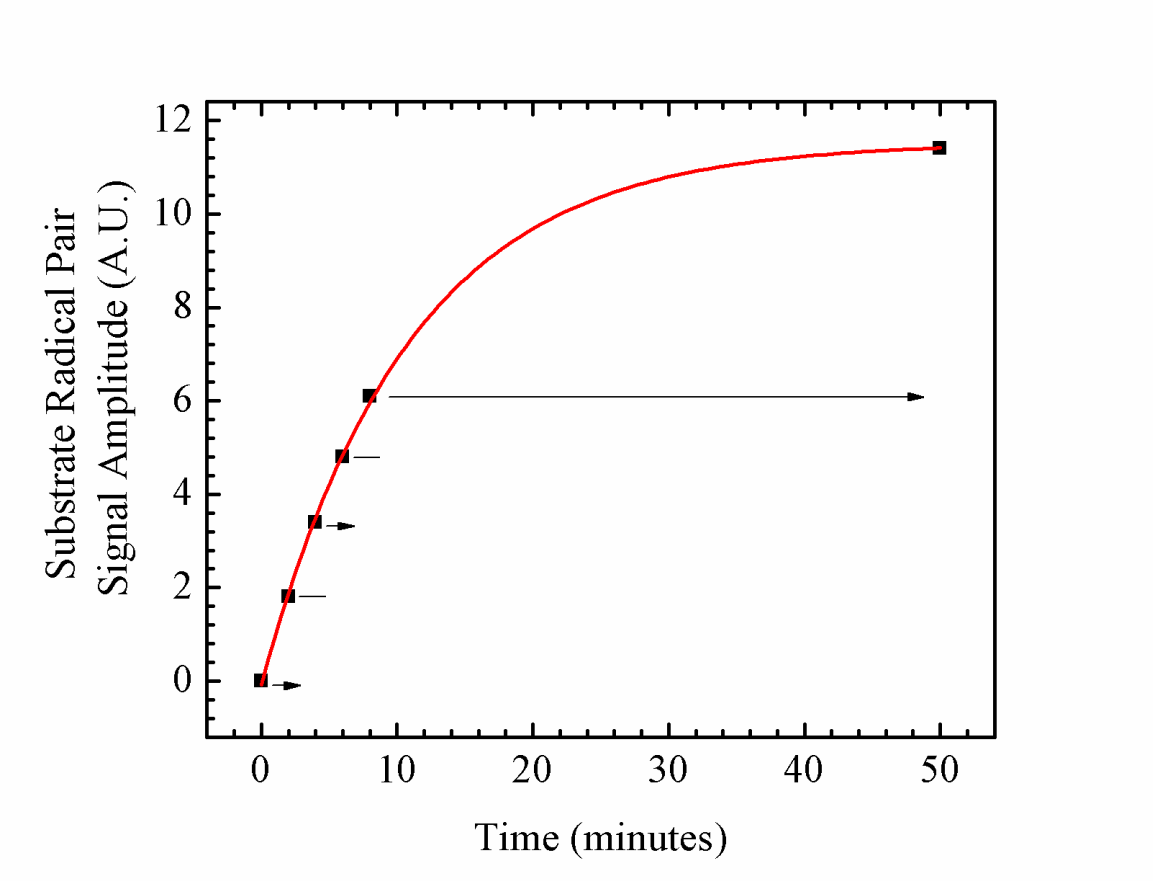

Figure 4.9. Time-dependence of the EPR amplitude of the cob(II)alamin-substrate radical pair state in EAL in the cryosolvent system at T=245 K, following temperature-step initiation of reaction. The amplitude is given by the difference between the first peak and second trough amplitudes, as shown in Figure 5B. The intermittent irradiation protocol is denoted, as follows: Arrows represent incubation periods under illumination, and lines represent dark incubation periods. The experimental data points are overlaid with the best-fit exponential growth function (solid curve; k_{obs}= 1.53×10^{-3} s^{-1}). EPR conditions are as described in the legend to Figure 4.8.

4.4 Discussion

Substrate Binding to Holo-EAL Does Not Activate the Co-C Bond for Cleavage by Distorting AdoCbl Structure

Brunold and coworkers have performed experimentally calibrated, time-domain density functional theory (TD-DFT) calculations, which predict significant spectral shifts of the α/β band maximum of AdoCbl, in response to relatively small changes in compression (approximately +15 nm/0.1 Å) or extension (approximately -15 nm/0.1 Å) of the Co-C bond length, and opposing shifts of comparable magnitude for changes in the Co-N_{axial} bond length.[33] The spectra in Figure 4.4 for holo-EAL and the ternary complex show that the presence of bound substrate does not induce significant shifts in the α/β band λ_{max}, or changes in the absorbance values, of other principal UV/visible absorption bands of the bound AdoCbl cofactor. Our results for the ternary complex are obtained under conditions in which the mechanisms that promote the thermal cleavage of the Co-C bond cleavage are poised.[35] Therefore, the EAL protein does not activate the Co-C bond for cleavage by significantly distorting the structure of the AdoCbl cofactor. This result is consistent with studies of other AdoCbl-dependent enzymes. Ultra-violet/visible absorption, magnetic circular dichroism (MCD) and resonance Raman studies showed that the protein in AdoCbl-dependent methylmalonyl-CoA mutase (MMCM) does not significantly distort AdoCbl in the holo-enzyme, or in holo-enzyme with bound substrate analogs.[33] An absence of Co-C bond length changes by the protein in MMCM was also concluded from infrared studies.[127] Picosecond optical studies suggested an absence of structural perturbations of the Co-C bond in glutamate mutase (GM).[75,97] Therefore, the

substrate trigger in AdoCbl-dependent enzymes does not appear to be mediated by protein-induced structural distortion of the cofactor.

Substrate Binding to Holo-EAL Does Not Elicit Prompt Stabilization of the Cob(II)alamin-Radical Pair Photoproduct

Table 4.1 shows the relative amplitudes of the cob(II)alamin-radical pair states on the 10^{-6} s time scale, following saturating laser pulse photolysis of the following enzyme states: holo-EAL, inhibitor-bound holo-EAL, and the EAL ternary complex. The relative amplitudes of each of the photoproduct populations, P_f, P_s, and P_c, are comparable for each enzyme state. The upper limits on the absolute quantum yields, φ_i, for each population, P_i, which are presented in Table 1, are also uniform and small for each enzyme state. In combination, these results suggest that the binding of substrate to holo-EAL does not induce, or "switch," the protein to a new state, in which a cob(II)alamin-5'-deoxyadenosyl radical pair in a configuration characteristic of the geminate radical pair photoproduct, is promptly stabilized. Therefore, a substrate binding-induced, protein-imposed barrier to recombination, a protein-mediated lowering of the free energy of the cob(II)alamin-radical pair state, or both, are not observed. Thus, the substrate does not induce protein-mediated mechanisms which promptly stabilize the photoproduct over Co(II)-C5' separation distances, r(Co C), in the range from >2.0 Å (greater than the Co-C bond length) to approximately 4 Å (the distance at which Co-C bond scission is >90% complete[94-96]).

Substrate Binding to Holo-EAL Does Not Significantly Influence Cage Escape of the Radical Pair

In solution, the existence of alkycobalamin radical pair photoproducts on the $\geq 10^{-6}$ s time scale requires escape from the geminate, caged radical pair state.[70,83] The cage escape yield is determined by competition between geminate recombination and cage escape processes, as described by the classical general description.[70,83-84] Our specific model for the EAL reaction, which is based on photolysis studies of holo-EAL and inhibitor-holo-EAL at 295 K,[125] is shown in Figure 4.10. The absence of a measurable quantum yield for photolysis at 240 K allows only limits to be placed on the values of the first-order rate constant for cage escape, $k_{ce,i}$, for the different P_i. An upper limit on the $k_{ce,i}$ value for each P_i in each EAL state is estimated by using the corresponding limiting ϕ_i values, and the following system of equations:[125]

$$\phi_i = \frac{k_{ce,i}}{k_{gr} + k_{ce,f} + k_{ce,s} + k_{ce,c}} \qquad (2)$$

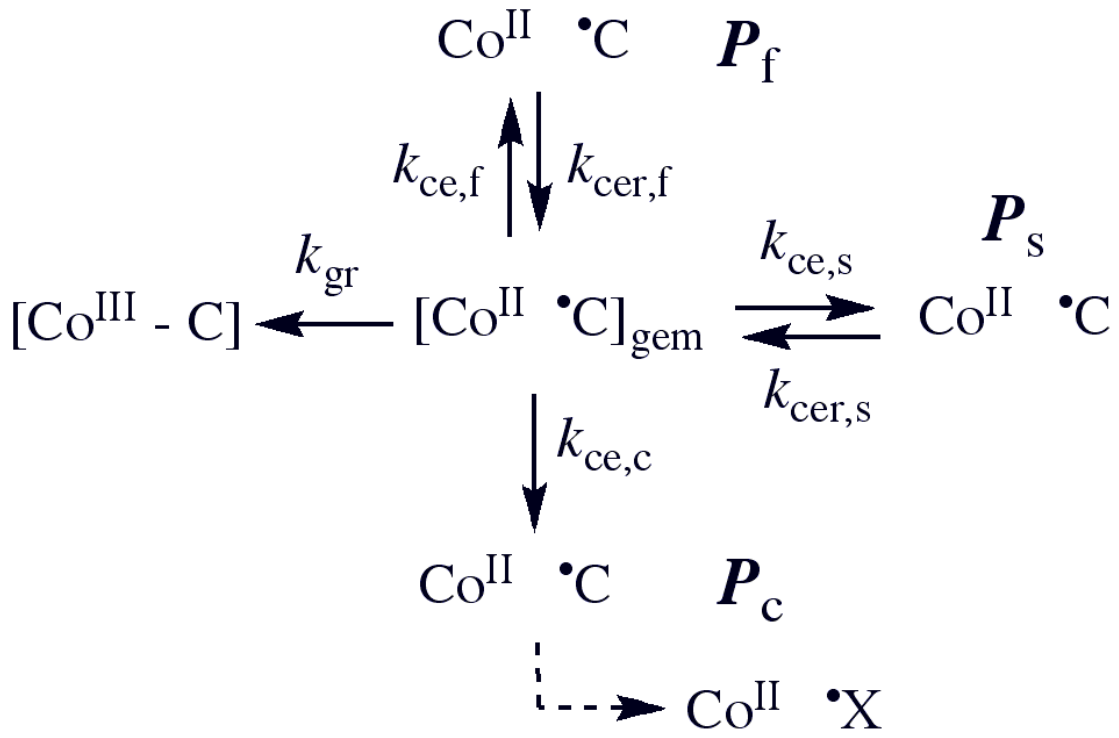

Figure 4.10. Proposed kinetic scheme for reactions of the cob(II)alamin-5'-deoxyadenosyl radical pair states following photolysis of adenosylcobalamin in EAL. First-order rate constants and different photoproduct populations are described in the text. X• indicates a secondary radical reaction product.

In Eq. 2, the index, *i*, corresponds to *f*, *s*, or *c*, and the quantum yield values for P_f, P_s, and P_c, are ϕ_f, ϕ_s, and ϕ_c, respectively. The geminate recombination rate constant in the EAL ternary complex at 240 K is estimated to be $k_{gr}=9.5\times10^7$ s^{-1}, based on extrapolation by using the Arrhenius relation [Eq. 1] and an activation energy of 5.2 kcal/mol, which corresponds to the rate of $k_{gr}=1.0\times10^9$ s^{-1} determined at 298 K.[79] The limiting values of the $k_{ce,i}$ are presented in Table 1. The $k_{ce,i}$ values for holo-EAL and inhibitor-bound holo-EAL do not differ significantly from the values for the ternary

complex. Therefore, substrate binding to holo-EAL does not significantly influence cage escape of the photoproduct radical pair.

The values of the activation energy for cage escape, $E_{a,ce}$, at 240 K are calculated to be 8 kcal/mol for each P_f and P_s, and 7-8 kcal/mol for each P_c. These $E_{a,ce}$ values for 240 K match the values reported for holo-EAL and inhibitor-bound holo-EAL at 298 K. This suggests that the mechanisms that govern cage escape at 240 and 298 K are the same.

Substrate Binding to Holo-EAL Does Not Significantly Alter Stabilization of the Cage-Escaped Cob(II)alamin-Radical Pair Photoproduct

Comparison of the observed cob(II)alamin photoproduct decay rate constants, $k_{decay,i}$, in Table 1 for the ternary complex, relative to holo-EAL and inhibitor-bound holo-EAL, provides an assessment of the microscopic effects of substrate binding on the protein that influence the stability of the cage-escaped radical pair states. The $k_{decay,i}$ values approximate well the values of the corresponding cage escape recombination rate constants, $k_{cer,i}$, which are defined in Figure 4.10 and Figure 4.11, because $k_{decay,i} << k_{gr}$. Table 1 shows that the $k_{decay,i} \approx k_{cer,i}$ values for the three populations, P_f, P_s, and P_c, for each EAL state are comparable. Therefore, the binding of substrate to holo-EAL does not cause significant changes in the active site structure, which influence the stability of cage-escaped cob(II)alamin-5'-deoxyadenosyl radical pairs. This includes any contribution to "trapping" of the radical pair state by reaction of the cob(II)alamin-5'-deoxyadensosyl radical pair with substrate to form the cob(II)alamin-substrate radical pair, because no detectable photo-induced cob(II)alamin-substrate radical pair formation

is observed by EPR spectroscopy. Over r_{CoC} values of approximately 4-6 Å, which correspond to the full extent of the radical pair separation coordinate,[23-26,37] the binding of substrate to holo-EAL does not induce factors that stabilize the photo-generated radical pair state.

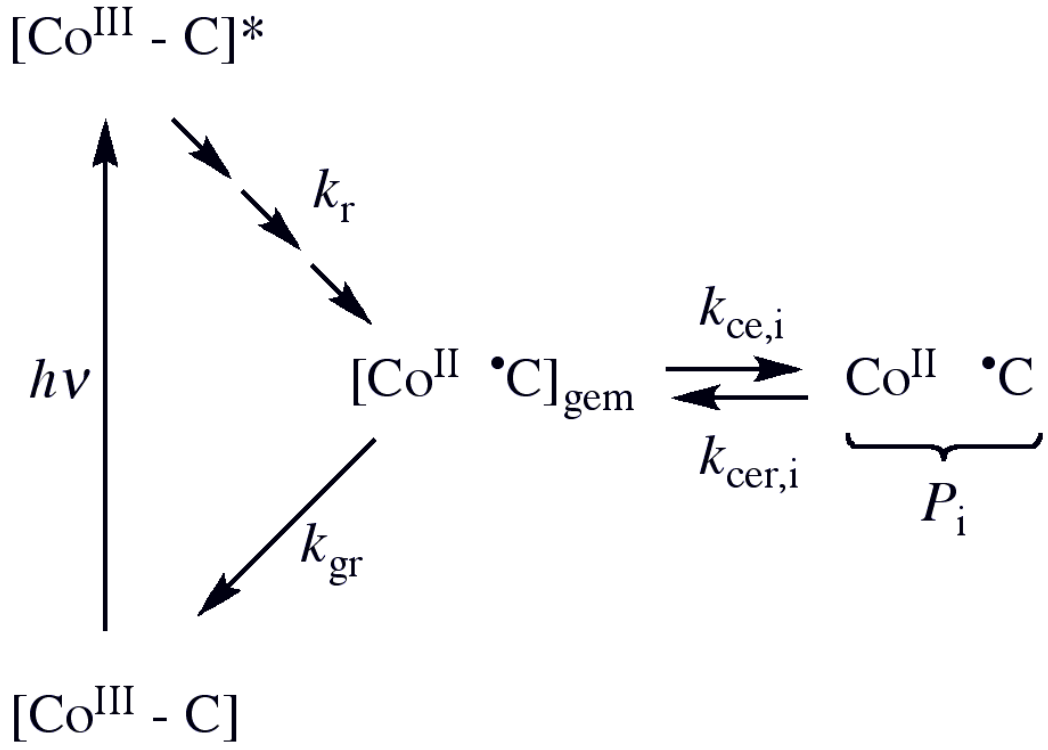

Figure 4.11. Simplified schematic diagram of the states and pathways of formation following photolysis of AdoCbl in solution and in holo-EAL. The cobalt in cobalamin and the C5'-methylene center in the 5'-deoxyadenosyl moiety are represented as follows: [Co^{III}-C], intact coenzyme; [Co^{III}-C]*, excited singlet state; [Co^{II} •C]$_{gem}$, geminate radical pair; Co^{II} •C, cage escaped radical pair. Intermediate excited and relaxed states,[70,82] which are not shown, are represented by the sequence of arrows leading from [Co^{III}-C]*. Rate constants are defined as follows: k_r, excited state to ground state relaxation; k_{gr}, geminate recombination; k_{ce}, cage escape; k_{cer}, reformation of geminate radical pair from cage escaped radical pair. The subscript, *i*, refers to three different cage escaped photoproduct radical pair species, P_i, that were identified in holo-EAL.[125]

Models for the Substrate-Initiated Co-C Bond Activation and Cleavage

Hypothetical free energy curves and pathways for the photolytic and thermal Co-C bond cleavage and radical pair separation are depicted on a 1-dimensional reaction coordinate in Figure 4.12. The curve for holo-EAL, which corresponds to the absence of substrate activation, and therefore, the uncatalyzed bond dissociation process, is modeled after calculated potential energy curves for complete Co-C bond homolysis in condensed phases.[94-96] The thermal free energy curve for the EAL ternary complex depicts a progressive lowering of the free energy, over the duration of the Co-C cleavage event. As shown in Figure 4.12, the contributions of the protein to Co-C bond cleavage catalysis must occur over relatively short r_{CoC} values, in the >2.0 - 4 Å range of early radical pair separation, because calculations show that the energy changes associated with Co-C separation are approximately 70% developed by 2.7-3.0 Å[93] and essentially complete at 4.0 Å.[94-96] As depicted in Figure 4.12, the photolysis results are consistent with a predominant decay channel of the photo-produced AdoCbl excited state that involves relaxation, through internal conversion and intersystem crossing, and eventual intersection with the uncatalyzed zero-order surface, leading to cob(II)alamin-radical pair recombination. Although the barrier region for the catalyzed zero-order surface is vertically aligned with Co-C separation distances achieved by photolysis in Figure 4.12, which should lead to a significant quantum yield for cob(II)alamain-radical pair formation, the catalyzed, zero-order surface is not accessed by the photogenerated radical pair in the EAL ternary complex.

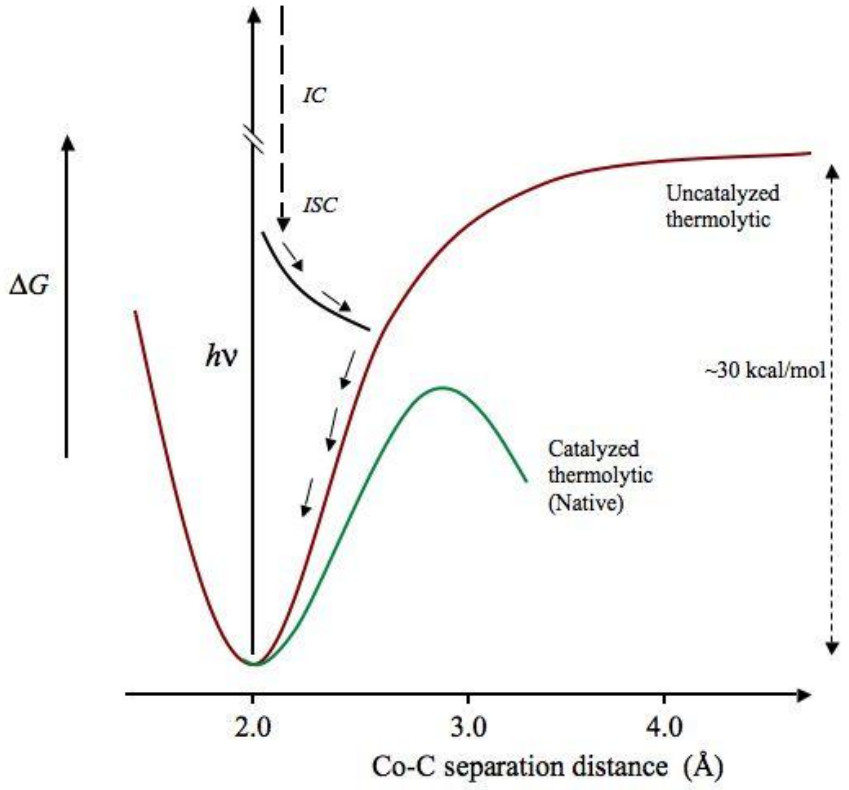

Figure 4.12. Free energy curves for Co-C bond cleavage that depict the uncatalyzed thermolytic and native catalyzed thermolytic conditions, and representative trajectory of the cob(II)alamin-5'-deoxyadenosyl radical pair photoproduct, in EAL. The uncatalyzed thermolytic curve is based on calculated energy curves for Co-C bond cleavage for AdoCbl in solution and in proteins,[94-96] and the native catalyzed thermolytic curve is based on the limit on the maximum of the free energy barrier of -15 kcal/mol.[35] The representative photoproduct trajectory is based on calculations.[93] Internal conversion of the AdoCbl excited state is represented by the arrow labeled IC and intersystem crossing by the arrow labeled ISC.

The interpretation of the EAL photolysis results requires the explicit introduction of protein structural changes, as an orthogonal coordinate, to the representative chemical reaction coordinate, which tracks the Co-C bond cleavage. A two-dimensional free

energy surface is shown in Figure 4.13A and 4.13B, in perspective and projection forms, respectively. Path 1 on the free energy surface in Figure 4.13B depicts the light-induced, essentially non-adiabatic switch of the bound cofactor from AdoCbl to the cob(II)alamin-5'-deoxyadenosyl radical pair. The protein is not in a configuration that can stabilize the nascent radical pair, which leads to rapid recombination. Path 2 represents the native, thermally-activated path, which involves the adjustment of the protein to accommodate the formation of the cob(II)alamin-5'-deoxyadenosyl radical pair, with a concomitant lowering of the free energy as Co-C bond cleavage occurs, which facilitates transition to the stable cob(II)alamin-radical pair state. Path 3 represents the structural change of the protein, in the absence of Co-C bond cleavage, which also leads to rapid decay back to the minimum of the AdoCbl state.

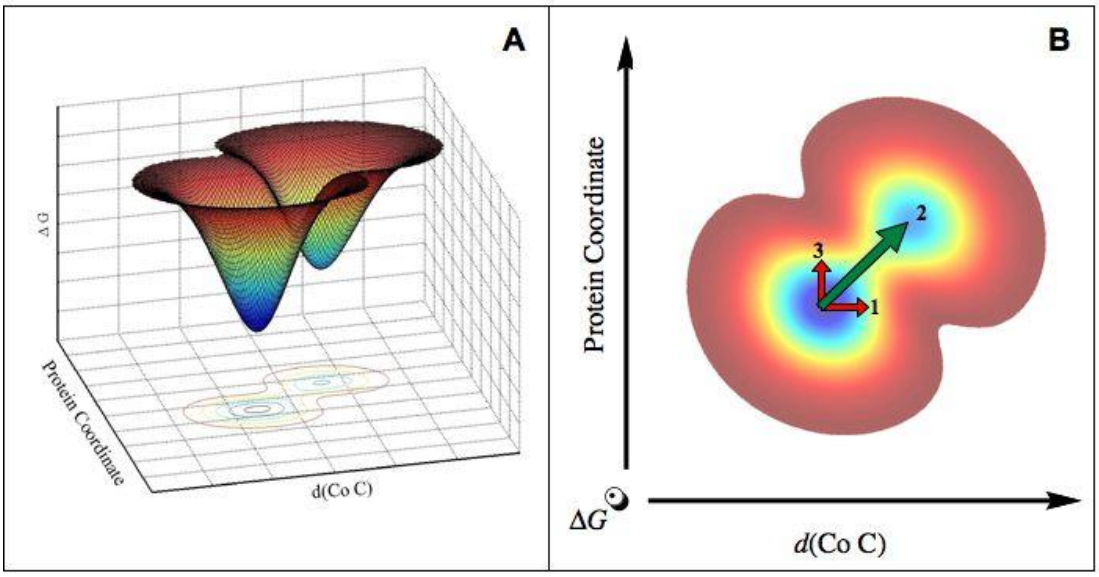

Figure 4.13. Two-dimensional representations of the ground state free energy surface for radical pair formation and separation in EAL as a function of collective protein structural and chemical (Co-C bond cleavage) coordinates. (*A*) Perspective view. Two minima, which represent the ternary complex and the cob(II)alamin-5'-deoxyadenosyl radical pair states, are shown. (*B*) Projection view. The one-dimensional trajectories for photolysis (Path 1) and protein structural change (Path 3) are represented by red arrows. The two-dimensional trajectory for the native thermal Co-C bond cleavage is represented by the green arrow (Path 2).

Figure 4.13 is a minimal, coarse-grained free energy surface, with two minima that represent the two canonical EAL ternary complex states. In finer detail, the many degrees of freedom in the protein will lead to a free energy landscape that is rich in local minima.[58] Shallow local minima at r_{CoC} values of 2.6-3.0 Å may capture the

cob(II)alamin-5'-deoxyadenosyl radical pair photoproduct, leading to the observed P_i states. States of this type may be similar to those found for the 4'-5'-dehydroadenosylcobalamin cofactor in AdoCbl-dependent diol dehydratase, which traps (by internal allyl radical stabilization) the 4'-5'-dehydroadenosyl radical thermal cleavage product.[128] If the P_i states lie along or near Path 2, they would decay forward with finite probability, to form long-time stable radical pairs, including the cob(II)alamin-substrate radical pair. This is not observed. Therefore, we propose that the P_i states are not on the native path of Co-C bond cleavage, and therefore, represent local minima near Path 1.

In principle, the nascent cob(II)alamin-5'-deoxyadenosyl radical pair formed by photolysis on Path 1 in Figure 4.13B, could execute a Brownian or biased walk over the free energy surface to the region of Path 2, and thus react to form a stable cob(II)alamin-5'-deoxyadenosyl radical pair. A trajectory of the photolyzed cob(II)alamin-5'-deoxyadenosyl radical pair towards the thermal reaction path requires a structural change along the protein coordinate, that occurs on a time-scale comparable to, or faster than, the time scale of geminate recombination, or $\leq 10^{-8}$ s. The undetectable photolysis quantum yield values indicate that the thermal fluctuations in the protein, that would drive the trajectory from Path 1 to the native thermal Path 2, occur on time scales at least 10-fold longer than t_{gr}, which corresponds to $>10^{-7}$ s. This limit is consistent with the characteristic time of thermal cob(II)alamin-substrate radical pair formation at 240 K of 9.1×10^{2} s.[35]

4.5 Conclusions

The substrate-protein interactions in the EAL ternary complex do not activate the Co-C bond for cleavage by inducing significant distortion of the structure of the AdoCbl cofactor, relative to holo-EAL. Photolysis of AdoCbl in the EAL ternary complex overcomes the demanding microscopic event of Co-C bond homolysis (bond dissociation energy in solution, ~30 kcal/mol [92]) in the process of radical pair separation, and presents the protein with a cob(II)alamin-5'-deoxyadenosyl radical pair configuration that putatively mimics an early thermal cleavage state. The results indicate that substrate binding to EAL does not "switch" the protein to a new static structural state, which stabilizes this cob(II)alamin-5'-deoxyadenosyl radical pair, either through increased barriers to recombination, decreased barriers to forward radical pair separation, or through lowering of the free energy of the radical pair state, or a combination of these effects. Rather, the results suggest that the protein interacts with the cofactor, and contiguously guides the cleavage of the Co-C bond, at every microscopic step along the cleavage coordinate. The Co-C bond is never "free" in the EAL ternary complex, compared to in solution. This situation is represented in Figure 4.13 by the diagonal trajectory across the free energy landscape, which requires progress along coupled chemical and protein coordinates. Protein involvement in rapid stabilization of the nascent radical pair has been proposed, based on magnetic field effects on the radical pair yield.[129-130] Mechanisms that involve the development of favorable cofactor-protein interactions as Co-C bond cleavage proceeds, have been proposed for EAL[37] and other AdoCbl-dependent enzymes.[131] In the photolysis experiment, fluctuations in the protein structure (conformational sampling),[58] that might allow the non-native photoproduct state

to access the native Co-C bond cleavage trajectory occur on time scales of $>10^{-7}$ s, and are thus too slow to compete with geminate recombination. The results suggest that future application of the AdoCbl photolysis approach to the elucidation of the structural and dynamical bases of the native radical pair creation and separation in EAL and other AdoCbl-dependent enzymes must involve a concomitant perturbation of the protein coordinate.

Chapter 5: Developing a Biologically-Inspired Molecular Solar Energy Conversion Device: Reaction of Solution and Protein-Bound Cobalamin Cofactors with Carbon Dioxide and Halo-Organic Compounds

Synopsis

The efficient capture, conversion and storage of solar energy are challenges that have been confronted by photosynthetic organisms for billions of years. Bacteria and green plants store solar energy through conversion to chemical energy by the fixation of carbon dioxide (CO_2). Though over 3.5 billion years of evolution have occurred since the appearance of the first photosynthetic organism[132], the photosynthetic efficiency of modern plants is just 3% to 6%[133], as compared to over 30% in commercially available solar cells. A number of inherent limitations on the efficiency of energy storage are present in "natural photosynthesis", which are derived from the need to incorporate photosynthesis into the limited pH and solvent conditions of the cellular environment, as well as the overall metabolic scheme of the organism. This has imposed the evolution of "natural photosynthesis" to occur over a large range in time, from 10^{-9} to 10^{0} s, and on spatial scales from 10^{-11} to 10^{-6} m. The cellular environment must accommodate innately fast processes, such as photon absorption and capture, and effectively integrate them with slower and spatially separated processes such as energy transduction and CO_2 fixation. In a cell-free system, *in vitro*, the constraint of integrating efficient free energy capture and storage into the overall metabolic scheme of the organism is absent. It is hypothesized that light can be used to reduce CO_2 in a single protein structure, under "biological conditions" (aqueous solution, pH 6-8, physiological temperature, $T \approx 300$ K, and a partial pressure of CO_2 of $P_{CO2} \approx 1$ atm), which will compress the broad time and spatial scales of natural photosynthesis, and thus increase the efficiency of the process.

5.1 Introduction

Compressed Photosynthesis Construct

Our aim is to design and construct a protein-based artificial photosynthetic system that reduces carbon dioxide (CO_2) and toxic halo-organic compounds within a single protein structure, the robust and adaptable $(\beta\alpha)_8$, triose phosphate isomerase (TIM)-barrel protein structure.[134] The EutB subunit of the coenzyme B_{12} (adenosylcobalamin)-dependent enzyme, ethanolamine ammonia-lyase (EAL), from *Salmonella typhimurium*[1,10,13], was selected as the protein template and is shown in Figure 5.1. The native function of the EutB subunit of EAL is to bind the radical generating B_{12} cofactor and substrate and further act as a scaffold for high energy radical mediated reactions to occur. The TIM-barrel structure is comprised of a cylindrical β-barrel composed of eight β-strands surrounded by eight α-helices that protect and stabilize the interior. The active site of EAL is equipped with amino acids that bind substrate and cofactor and can be easily changed through mutations without destabilizing the protein structure. This has allowed the $(\beta\alpha)_8$, TIM-barrel protein structure the capacity to catalyze a wide variety of reactions.[3,15,135-138] It is estimated that the $(\beta\alpha)_8$, TIM-barrel is present in more than 10% of all proteins of known structure.[14] The stability of TIM–barrel proteins also makes the fold a good choice as a scaffold for a compressed photosynthesis unit. The EAL TIM-barrel protein, has for example, been shown to have the ability to function in over a wide range of pH conditions, at least 50% activity from 5.8 - 9.2 pH.[15-16] The EutB subunit of EAL is also equipped with residues that facilitate the insertion and binding of the AdoCbl cofactor in the protein's active site. The cofactor will be used to store light energy, by

the photo-induced reduction to the Co^{I} state, as well as elicit binding of the CO_2 molecule in the active site. The Co^{I} state of the cobalt ion, of the AdoCbl cofactor, has the available electrons as well as a reduction potential low enough to catalyze the two electron reduction of CO_2.

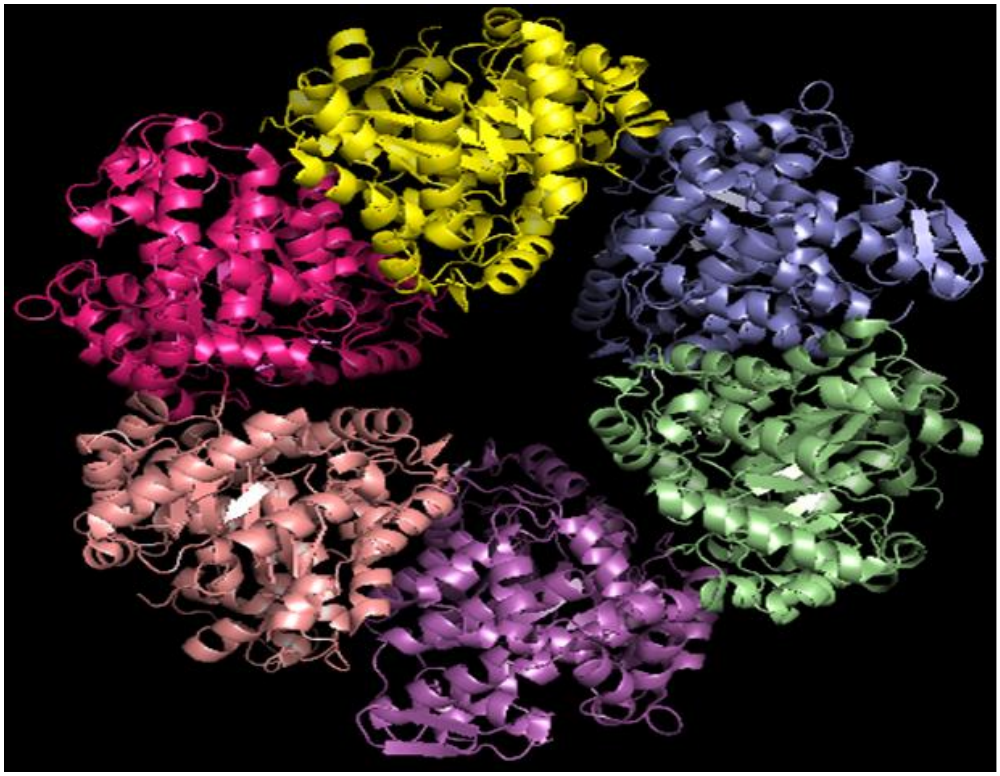

Figure 5.1. The crystallized hexamer of EutB subunit of EAL in *L. monocytogenes.*[139]

CO_2 is a very stable molecule that requires high overpotentials, potentials above the thermodynamically determined reduction potential, for reduction by electrolysis, as shown by the electrochemical potentials for reduction in Table 5.1. A single one electron reduction to form CO_2^{-} requires an overpotential of -1.9 V, but can be lowered

significantly when a two electron reduction mechanism is used, as is the case for formate production, $E°$ = -0.61 V (versus normal hydrogen electrode (NHE) pH = 7.0 in aqueous solution) or carbon monoxide/water with an electrochemical potential of $E°$ = -0.53 V (versus NHE, under standard conditions).[140-141]

Table 5.1. The Electrochemical Potentials for Reduction of CO_2.[140-141]

Reaction	Electrochemical Potential*
$CO_2 + 2H^+ + 2e^- \rightarrow CO + H_2O$	E = -0.53 V
$CO_2 + 2H^+ + 2e^- \rightarrow HCO_2H$	E = -0.61 V
$CO_2 + 4H^+ + 4e^- \rightarrow HCHO + H_2O$	E = -0.48 V
$CO_2 + 6H^+ + 6e^- \rightarrow CH_3OH + H_2O$	E = -0.38 V
$CO_2 + 8H^+ + 8e^- \rightarrow CH_4 + 2H_2O$	E = -0.24 V
$CO_2 + e^- \rightarrow CO_2^-$	E = -1.90 V

* $E°$ referenced to NHE, pH 7 in aqueous solution, 25 °C, 1 atm pressure, and 1 M for other solutes.

The reduction of CO_2 has been shown to be catalysized by electron rich metal ions[142-147] including cobalt containing macrocycles.[142,148-151] The fully-reduced, Co^I, forms of the native cobalamin (Cbl) cofactor and a derivative, cobinamide (Cbi), formed by the removal of the α-axial dimethylbenzimidazole (DMBz) ligand of the cobalamin, possess relatively low redox potentials that are commensurate with reduction of CO_2 and halo-organic compounds. We propose to use the Cbl cofactor, as well as the Cbi derivative, to function as the catalyst for the reduction reaction of CO_2 and halo-organic compounds inside the active site of EutB.

The cofactor structure and function in the native EAL system is described in detail in Chapter 1. The structure of the native cofactor of the EAL enzyme system, adenosylcobalamin (AdoCbl), and derivatives are shown in Figure 5.2, and methylcobinamide is shown in Figure 5.3. The cobalamin cofactor contains a cobalt ion centered in a corrin ring. The cobalt ion in cobalamin nominally exists with hexa-coordinate ligation in the cob(III)alamin state, penta-coordinate ligation in the cob(II)alamin state and tetra-coordinate ligation when in the cob(I)alamin oxidation state.[152] The "upper" β-axial, ligand varies according to the cob(III)alamin compound; adenosylcobalamin, deoxyadenosyl; aquocobalamin (AquoCbl); water at pH < pKa = 7.8; hydroxocobalamin, hydroxyl at pH > pKa ~ 7.8[153], methylcobalamin (MeCbl), a methyl group; cyanocobalamin, cyanide. Nitrogen atoms from the corrin ring make up four of the ligands for the cobalt atom with the DMBz providing the "lower" α-axial ligand. The reduction potentials of selected cobalamin and cobinamide compounds are shown in Table 5.2. The cob(II)alamin/cob(I)alamin electrochemical midpoint potential (-0.95 V), is within the range of CO_2 electrochemical midpoint potentials (E_m, versus saturated calomel electrode, SCE; where E_m(SCE) = E_m(NHE) – 0.24 V).[153] The dissociation of the DMBz ligand from the cobalt ion is associated with the formation of cob(I)alamin, and has been shown to contribute significantly to the E_m of the molecule. The removal of the DMBz ligand, to form cobinamide, results in a Co^I E_m value higher than that of cob(I)alamin, but within the range of CO_2 reduction. The cob(II)inamide/cob(I)inamide couple has an E_m value of -0.74 V, versus saturated calomel electrode (SCE).[153] The α-axial position, which is occupied by the DMBz ligand in cobalamin, is replaced by a solvent water molecule in the cobinamide compound.

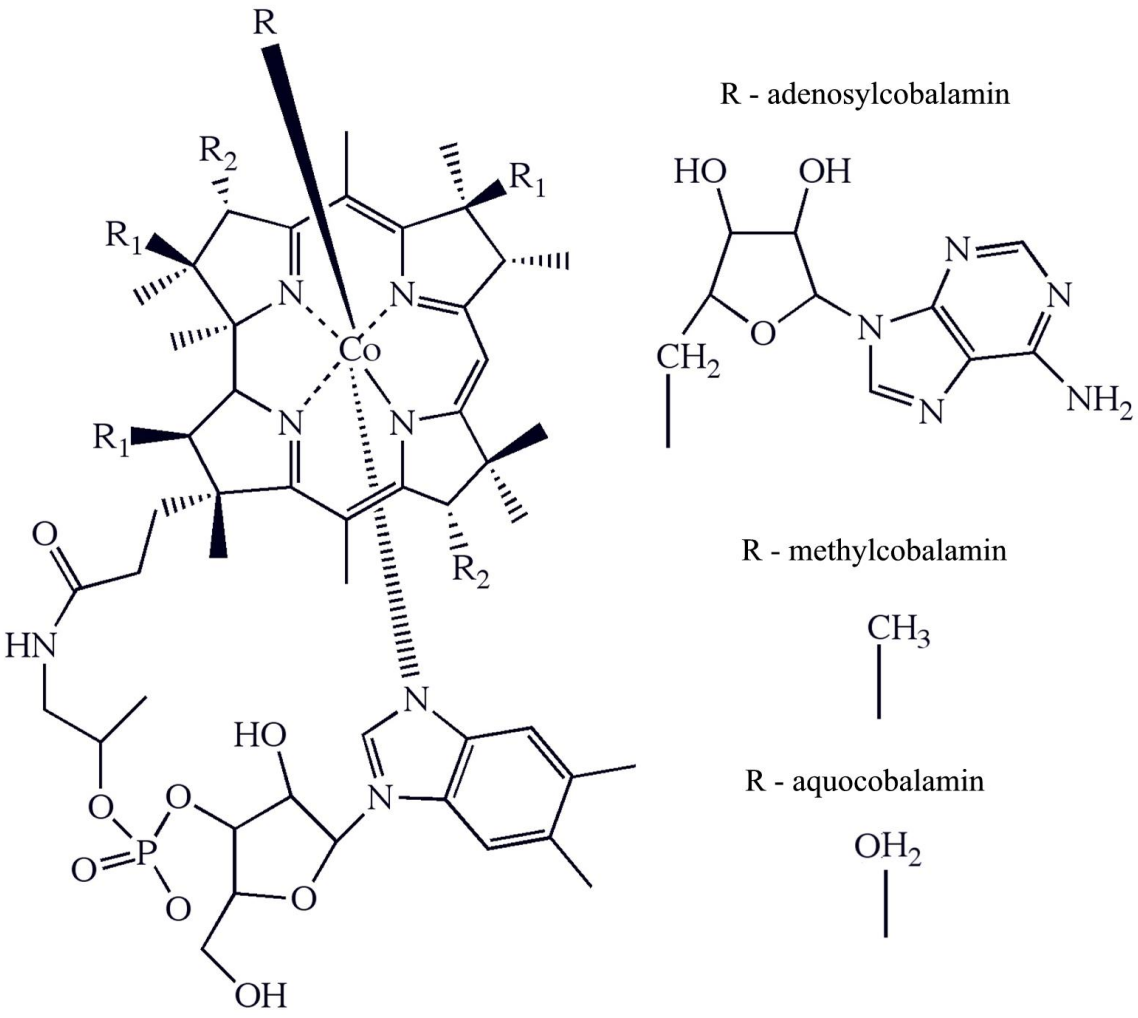

Figure 5.2. The native cobalamin cofactor of the EAL enzyme system and β-axial ligands; adenosylcobalamin (AdoCbl), aquocobalamin (AquoCbl), and methylcobalamin (MeCbl).

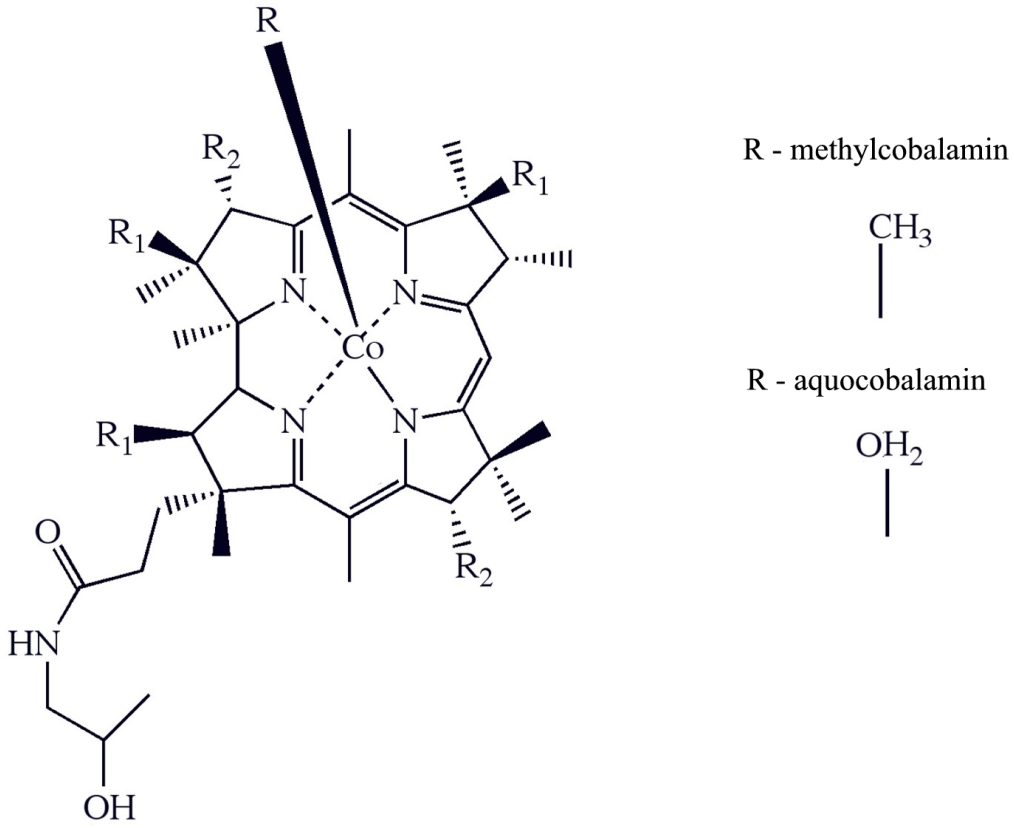

Figure 5.3. The methylcobinamide (MeCbi) cofactor derived by the cleavage of the DMBz axial ligand of methylcobalamin.

Table 5.2. Redox Potentials for Cobalamin Compounds versus SCE.[153]

	Cobalamin (DMB base-on)		Cobalamin (DMB base-off)[a]	
redox couple	$AquoCo^{III}/Co^{II}$	Co^{II}/Co^{I}	$AquoCo^{III}/Co^{II}$	Co^{II}/Co^{I}
E° (V)	-0.042	-0.953	0.27	-0.74

[a]Values for base-off cobalamin are assumed to represent cobinamide

Reactions of Metal Complexes with CO_2 and Halo-Organics

The use of metal centers to catalyze the reduction of CO_2 as been studied in detail in non-aqueous solutions,[142-147] while the even more difficult challenge of studying the reduction of CO_2 under biological conditions has been an addressed to a much lesser extent.[142,154-155] Numerous studies have characterized the reaction of CO_2 with transition metals complexes containing Co^{II} and Ni^{II} ligated in large cyclic molecules, which are generally referred to as macrocycles.[142,148-151] Electrochemical studies, in organic solvents, utilizing large over potentials, are typically used to characterize the ability of the metal center to reduce CO_2. The ligation of the metal center has a direct affect on the reduction potential of the catalyst as well as the rate of reduction of the molecule. The weak electrophilic carbon atom in CO_2 readily binds to metal centers with high electron density, as is the case when the metals exist in a low oxidation state.[156] The orientation and coordination of CO_2 when bound to metal centers has also been examined,[156-157] and structurally characterized as a η^1-C binding mode with a bent CO_2 bound to a redox center[156] as shown in Figure 5.4.

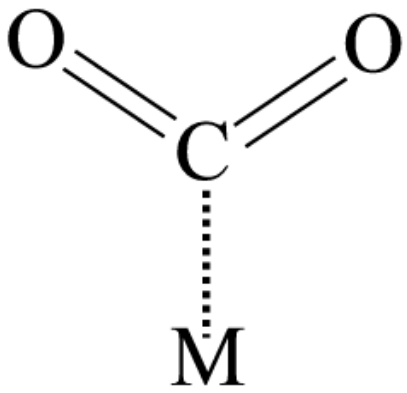

Figure 5.4. Binding, η^1-C mode, of CO_2 to a metal redox center (M).

The first macrocycles used to study the catalyzed reduction of CO_2 were substituted 1,4,5,8-tetrazacyclotetradecane (cyclam) compounds which were shown to react to form carbon monoxide (CO) and hydrogen (H_2).[148,150-151,158] The reduction of CO_2 occurred at potentials of -1.3 to -1.5 V, versus SCE in aqueous acetonitrile/water or water and required a source of protons. Recent studies have shown that the cobalt-containing macrocycle complexes generate hydrogen gas.[155] These studies did, however, required low pH values of the solvent and utilized macrocycles with low solubility in water.

The detection of products formed from photo-initiated reduction reactions is experimentally difficult, due to the inability to enhance the reaction rate by applying an over-potential as is the case with electrolysis experiments. The same cobalt containing cyclam macrocycles discussed above, reduced to Co^{II} and Co^{I}, from photo-initiated reduction by the excited state of phenazine, were shown to react with CO_2 to primarily form formate (HCO_2^-) and small amounts of CO and H_2.[149-150] The first step in the reaction was shown to be the protonation of the Co^{I} state of the catalyst, which illustrates the effect of the solvent on the overall reaction.

The use of cobalt corrinoid cofactors as a reductant for toxic halo-organic molecules has also been studied.[159-161] The degradation of halo-organics can be accomplished with low redox potential metal center macrocycles by the direct transfer of electrons to the molecule, or by the binding of intermediates to the reduced cofactor.[162-164] The reaction of chloroacetonitrile with cobalamin, using electrolysis, has been studied in detail in 70/30 water-ethanol solution.[161] Following reduction of the cofactor to Co^{II}, then to Co^{I}, the chlorine atom of chloroacetonitrile is displaced by Co^{I}, which then forms a Co^{III}-CH_2CN complex. The Co^{III} is then re-reduced to release the product and reform Co^{I} and react again. This reaction could in principle be initiated by photo-induced reduction for the efficient reduction of toxic chlorinated compounds and readily integrated into a protein construct.

5.2 Materials and Methods

Sample Preparation

The chemicals trifluoromethanesulfonic acid (triflic acid), titanium(III) chloride ($TiCl_3$), AdoCbl, and MeCbl were purchased from Sigma-Aldrich (St. Louis, MO). Isotopically labeled chloroacetonitrile, $^{13}C_2H_2Cl^{15}N$, was purchased from Isotec (Champaign, Illinois). Dry nitrogen gas, liquid nitrogen, and CO_2 were purchased from nexAir (Suwanee, GA). Solutions under spectroscopic analysis were contained in a 3 mL anaerobic quartz cuvette. Samples prepared for cobalamin and cobinamide reduction experiments were prepared in 10 mM potassium phosphate buffer adjusted to pH 7.5. The samples were made anaerobic as described later in this section. The addition of Ti(III) citrate was achieved by anaerobic injection to the sample through a septum on an anaerobic cuvette. Samples used for the photo reduction of cobalamin and cobinamide were prepared in 10 mM potassium phosphate buffer, 1 mM EDTA and 10 - 35 μM 5-DRF with the pH adjusted to 7.5.

Chloroacetonitril samples and controls were prepared in anaerobic 400 MHz NMR tubes and exposed to a 150 W Hg lamp for 6 hours. Nuclear magnetic resonance spectroscopy (NMR), using an Inova 400 MHz spectrometer, of ^{13}C, ^{1}H, ^{15}N nuclei, was performed on both isotopically labeled and unlabeled CO_2 and chloroacetonitrile before and after reduction. All experiments were performed in 10 mM potassium phosphate, 100 mM EDTA, 10 μM 5'-deazariboflavin and 50 μM cobinamide in deuterated water, which was adjusted to pH 7.5.

EAL was purified from the *Escherichia coli* overexpression strain incorporating the cloned *S. typhimurium* EAL coding sequence[165] essentially as described previously,[166] the exception being that the enzyme was dialyzed against buffer containing 100 mM HEPES (pH 7.5), 10 mM potassium chloride, 5 mM dithiothreitol, 10 mM urea, and 10%

glycerol.[167] Enzyme activity was determined as described previously[168] by using the coupled assay with alcohol dehydrogenase/NADH. The specific activity of the purified enzyme with aminoethanol as the substrate was 35-45 μmol min^{-1} mg^{-1}.

EutB protein was grown, in a 10 L fermentor, from *Escherichia coli* over expression strain incorporating the cloned *S. typhimurium* EAL coding sequence[165] essentially as described previously,[166] with the exception that the Shine-Dalgarno binding region and the start codon of the EutC subunit was removed from the *S. typhimurium* plasmid, resulting in the over expression of only the EutB subunit. The purification procedure was the same as described with the exception of the centrifugation following dialysis. The higher solubility of EutB as compared to EAL resulted in >90% of the protein remaining in solution after the final centrifugation step. Gel electrophoresis indicated high purity, (> 90 %), of the protein following dialysis and dehydration. Therefore, the solution was used as the EutB protein stock.

Preparation of pH controlled MeCbi Samples

A 0.5 M MES (2-(*N*-morpholino)ethanesulfonic acid) solution was prepared as the buffering agent for the experiments. MES has a pK_a of 6.15, and a buffer range of pH 5.5 to pH 6.7. From a 0.5 M buffer solution, stock solutions of pH 6.0 100 mM MES and 10 mM ethylenediaminetetraacetic acid (EDTA) were made. EDTA was added to serve as the sacrificial electron donor for the 5-DRF molecule following loss of an electron. MeCbi was added to the buffer at a concentration of 50 μM from synthesized MeCbi stock. The sample was made anaerobic by bubbling with water-saturated nitrogen gas. Bicarbonate solution was injected, through a teflon coated septum via a syringe, to the

solution while it was kept under positive nitrogen gas pressure. Both the syringe and nitrogen gas were removed following injection, and the sample was left under positive pressure. A 0.5 M stock solution of sodium bicarbonate was used for the 10 mM bicarbonate sample.

The pH of the buffered solution was adjusted so that buffered solution with bicarbonate added was at a final pH of 6.0 for the 20 mM and 50 mM bicarbonate solutions. A 1 M stock solution of sodium bicarbonate was made for the 20 mM bicarbonate samples. A 1:3 solution of HCl/water was diluted 10 times. The diluted HCl was then added, via syringe to the sample, in a volume of 15 µL for every 20 µL of 1 M bicarbonate solution. The 15 µL of HCl lowered the pH by 0.3, while the 20 µL of 1 M bicarbonate solution raised it by 0.3, resulting in a final pH value of 6.0. A 1 M stock of bicarbonate was used for the 50 mM bicarbonate sample and the volume of solution added via syringe was increased by 2.5 times. For the 50 mM sample, 65 µL of 10-fold diluted 1:3 HCl/water solution was added for every 50 µL of 1 M bicarbonate solution added to the solution. This resulted in a final pH that returned to 6.0.

MeCbi was added to a 100 mM MES/1 mM EDTA buffered solution into a 4 mL anaerobic cuvette and made anaerobic by the nitrogen gas bubbling method for 15 minutes. The spectrum was taken of the Co^{III} state of MeCbi in solution, before being exposed to a 300 W xenon lamp for 15 seconds. A spectrum was then collected of the cob(II)inamide created by photolysis. This was repeated for an aerobic MeCbi solution, resulting in the generation of AquoCbi. Cob(I)inamide was generated in an anaerobic solution of MeCbi in the 100 mM MES/1 mM EDTA buffer solution. 5'-Deazariboflavin, 5'DRF, 5 µM, was used to reduce the MeCbi to the Co^{I} state. The

concentration and molar extinction coefficients of the solutions were calculated by comparing the spectra of methylcob(III)inamide at pH of 7.5 to the same concentration at pH of 6.0. The extinction coefficent for methylcob(III)inamide, at each pH value, was shown to be the same within error and the value for methylcob(III)inamide at 6.0 was used to determine extinction coefficients for the remaining cobinamide oxidation states at pH 6.0, which were shown to be similar to the pH 7.5 counterparts.

Anaerobic Techniques

Deoxygenation of the solutions was achieved by using two techniques. In the first method, a solution was sealed in a glass flask with an elastic septum coated with a teflon surface. A needle connected to a dry nitrogen gas flow line was inserted through the septum. Nitrogen was saturated with water vapor by being bubbled through distilled water before being bubbled through the solution for at least 30 minutes. The gas was allowed to exit the sample through a needle inserted through the septum.

The freeze/pump-thaw method (FPT) was also used to degas protein containing samples. The solution placed in a glass test tube with a tubing connector on the side. The top of the test tube was sealed with a rubber stopper. A gas line that could be alternated between dry nitrogen and a vacuum pump was attached to the test tube tubing connector. The tube was backfilled with nitrogen, then was frozen under nitrogen. The tube was then removed from the liquid nitrogen, and a vacuum (from a 10^{-3} torr pump) was applied to the sample. Gas from the melting sample was collected by the vacuum line. The sample was allowed to melt completely before the vacuum line was switched

off, and then a positive nitrogen gas pressure was applied inside the container. The freeze/pump-thaw cycle was then repeated for a total of 3 to 5 times.

Titanium(III) Citrate Preparation

Titanium (III) citrate was prepared by the method described by Zehnder and Wuhrmann.[169] Dry nitrogen gas bubbling was used to make an anaerobic solution of 25 mL of 200 mM sodium citrate in 10 mM KP_i buffer. Under an argon atmosphere, inside a glove box, $TiCl_3$ (0.359 g) was added and stirred in the anaerobic buffer. The pH of the solution was adjusted to 7.5.

Nuclear Magnetic Resonance (NMR) Product Analysis

NMR of ^{13}C, ^{1}H, and ^{15}N were performed, using an Inova 400 MHz spectrometer, on both isotopically labeled and unlabeled CO_2 and chloroacetonitrile before and after reduction. All experiments where performed in 10 mM potassium phosphate, 100 mM EDTA, 10 μM 5'-deazariboflavin and 50 μM cobinamide in deuterated water that was adjusted to pH 7.5.

UV/Visible Absorption Spectroscopy

A Shimadzu UV 1601 spectrophotometer with 0.5 nm wavelength resolution was used to measure absorption in the ultraviolet and visible range. A scattering baseline of the protein was collected for each protein sample before addition of the cofactor, and was

later subtracted. The oxidation state of the central cobalt atom of Cbl and Cbi was monitored by the UV/visible spectra. Beer's Law, as described in Chapter 2.1, was used to calculate the concentrations of the cobalt oxidation states.[109]

Synthesis of Methylcobinamide (MeCbi)

The synthesis of MeCbi was based on the method described by Zou.[170] A powder sample of 50 mg of MeCbl was dried inside a vacuum decanter, at 10^{-3} torr, over phosphorus pentoxide, P_2O_5, for 12 h. The anhydrous MeCbl was then dissolved in 0.6 mL of anhydrous trifluoromethanesulfonic acid after being anaerobically being transferred to a 1 atm argon glove box. The mixture was stirred for 24 h. The solution was added to 100 mL of 1 M dibasic potassium phosphate (K_2HPO_4). An Amberlite XAD-2 column was used to remove the cleaved nucleotide. Mixtures of water and 10% water/acetonitrile were used for washing. The MeCbi was subsequently eluted and collected with 50% aqueous acetonitrile.

Molar extinction coefficients for MeCbi stock solution in aqueous solution were obtained by conversion of a small amount of the compound to dicyanocobinamide ($(CN)_2$Cbi). MeCbi was photolyzed aerobically in solution in the presence of 0.5 M potassium cyanide (KCN), converting it to $(CN)_2$Cbi. The literature molar extinction coefficient of $(CN)_2$Cbi at 368 nm is 30,400 $M^{-1}cm^{-1}$.[171] All MeCbi was assumed to have been converted to $(CN)_2$Cbi. From this assay, Figure 5.5, and the spectra in Figure 5.6, molar extinction coefficients for MeCbi, cob(II)inamide, and d cob(I)inamide were calculated at 465 nm and 387 nm by using Beer's Law. The values are presented in Table 5.3.

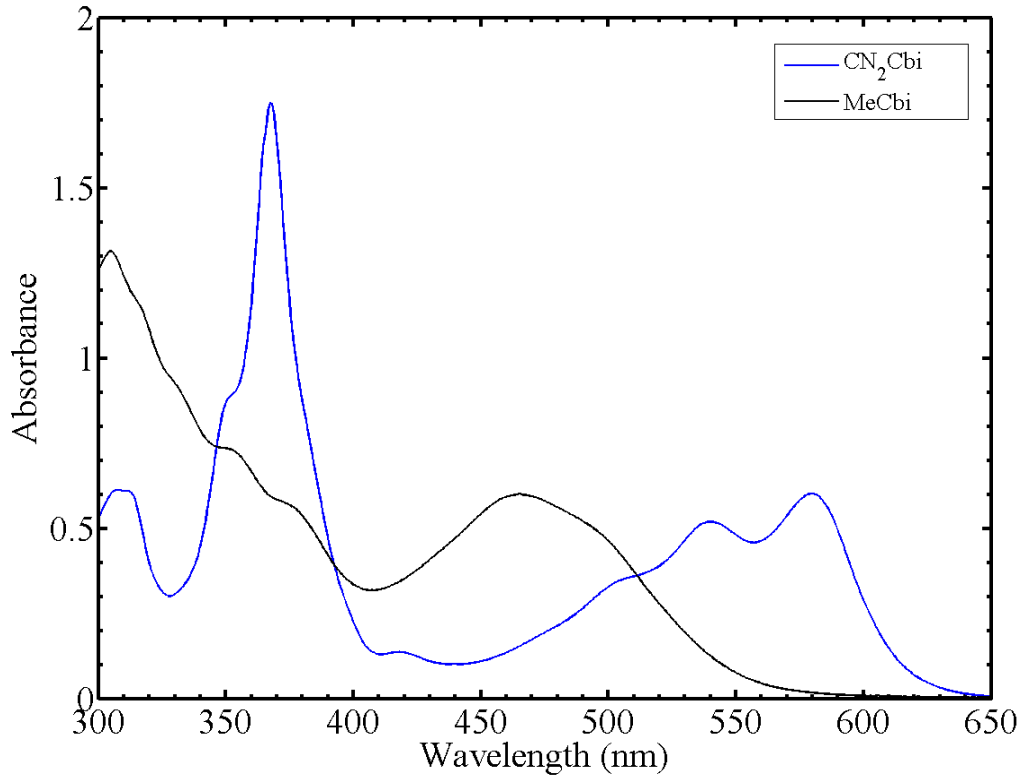

Figure 5.5. Ultraviolet/visible absorption spectra of MeCbi and $(CN)_2$Cbi compound created for determination of MeCbi stock following synthesis and purification. MeCbi (57.8 μM), in 0.5 M KCN in aqueous solution, pH adjusted to 7.5, 295 K. Photolysis was performed with a 300 watt Xenon lamp for 30 s.

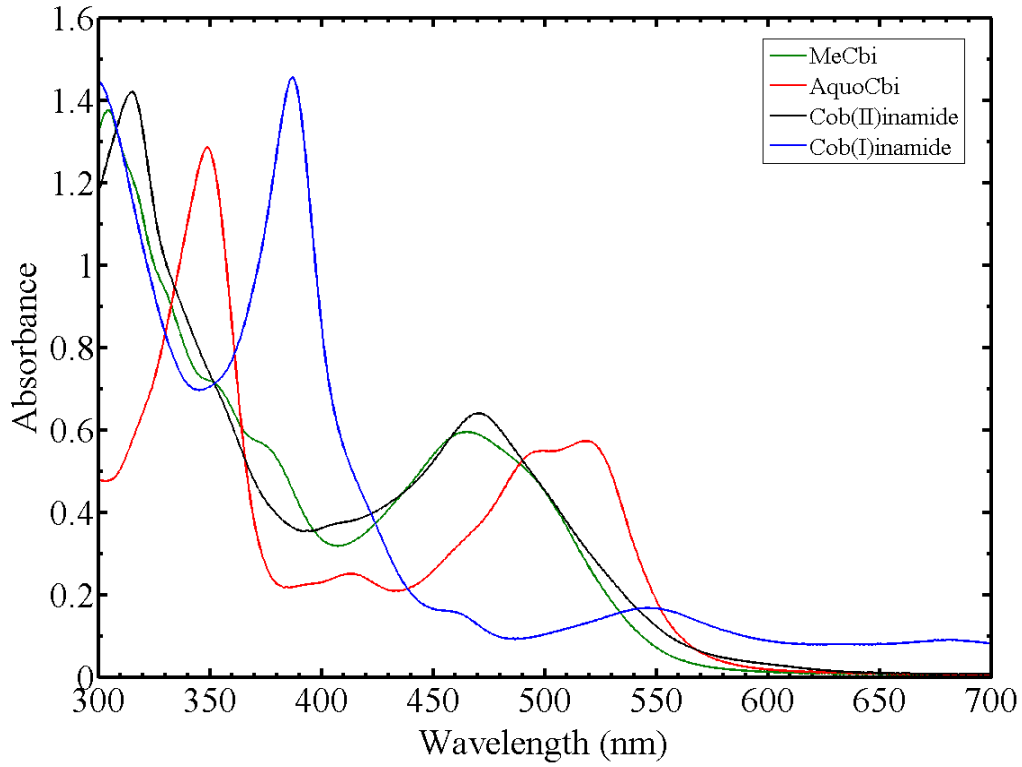

Figure 5.6. Ultraviolet/visible absorption spectra of cobinamide compounds in 10 mM KP_i at pH 7.5. MeCbi (54.0 μM) was photolyzed anaerobically to produce cob(II)inamide. Cob(II)inamide was then photolyzed aerobically to produce AquoCbi. Photo-activated 5'-DRF (10 μM) was used to reduce MeCbi to cob(I)inamide anaerobically in 1 mM EDTA and 10 mM KP_i at pH 7.5. The cob(I)inamide spectra have been scaled by a factor of 1.07 to match its concentration to the rest of the spectra.

Table 5.3. Molar Extinction Coefficients for Cobinamide Compounds.

	ε_λ ($M^{-1}cm^{-1}$)		
λ (nm)	MeCbi	cob(II)inamide	cob(I)inamide
465	10400	11100	2560
387	7990	6390	25400

5.3 Reduction of Cobalamin and Cobinamide

Production of low redox state cobalamins and cobinamide require the use of a reducing agent with an electrochemical potential lower than that of the state of interest. The chemical reductant, titanium(III) citrate was used to generate the cob(I)alamin and cob(I)inamide states for reactivity studies. Additionally, the low excited state reduction potential of the photo-excitable reducing agent, 5'-deazariboflavin (5'-DRF) was used to photo-initiate reduction of the cofactor.[172] 5'-DRF was used in concert with the electron donor, EDTA, to re-reduce the ground state of the molecule following photo-oxidation of 5'-DRF. The 5'-DRF provides a method to create reduced states of the cofactors, and monitor oxidation of the cofactors, without competing chemical reduction reactions taking place, as is the case with reduction by the addition of high concentrations of Ti(III) citrate. The photo-activation and subsequent reduction steps of 5-DRF photo-activation take place in less than 10^{-8} s and can be used as a probe of slow diffusion and reduction processes involved in the cofactor and protein system.

UV/visible spectroscopy was used to identify the oxidation state of the cobalamin and cobinamide cofactors as well as to characterize the redox reactions.[74] The extinction coefficients for each compound were used to calculate the concentrations of the cobalamin or cobinamide redox species present in the solution.

Reduction of Cobalamin

The ultraviolet/visible spectra of the four cobalamin compounds, AdoCbl, cob(II)alamin, AquoCbl, and cob(I)alamin are shown in Figure 5.7. Solution samples of

AdoCbl in 10 mM KP_i at 7.5 pH were made anaerobic by the freeze/pump-thaw method. A 300 W xenon lamp was used to photolyze AdoCbl to cob(II)alamin. The solution was then exposed to air with atmospheric oxygen concentration to convert cob(II)alamin to AquoCbl. The spectra of AdoCbl, cob(II)alamin, and AquoCbl and shown in Figure 5.7 were derived from the same sample and have the same concentration, of approximately 49 μM. The literature molar extinction coefficient for AdoCbl at 526 nm was used to calculate the sample concentration. Cob(I)alamin was prepared by the anaerobic reduction of AquoCbl by using added Ti(III). Baseline spectra of Ti(III) citrate in buffer were subtracted from the spectrum of cob(I)alamin mixed with Ti(III) citrate. A scaling factor was added to the cob(I)alamin spectrum to match the concentration of the other cobalamin spectra shown in Figure 5.7. The addition of Ti(III) citrate to solutions of AdoCbl and MeCbl did not result in the reduction to either cob(II)alamin or cob(I)alamin. All cobalamin compounds in the presence of 5'-DRF and light were reduced to cob(II)alamin but not cob(I)alamin.

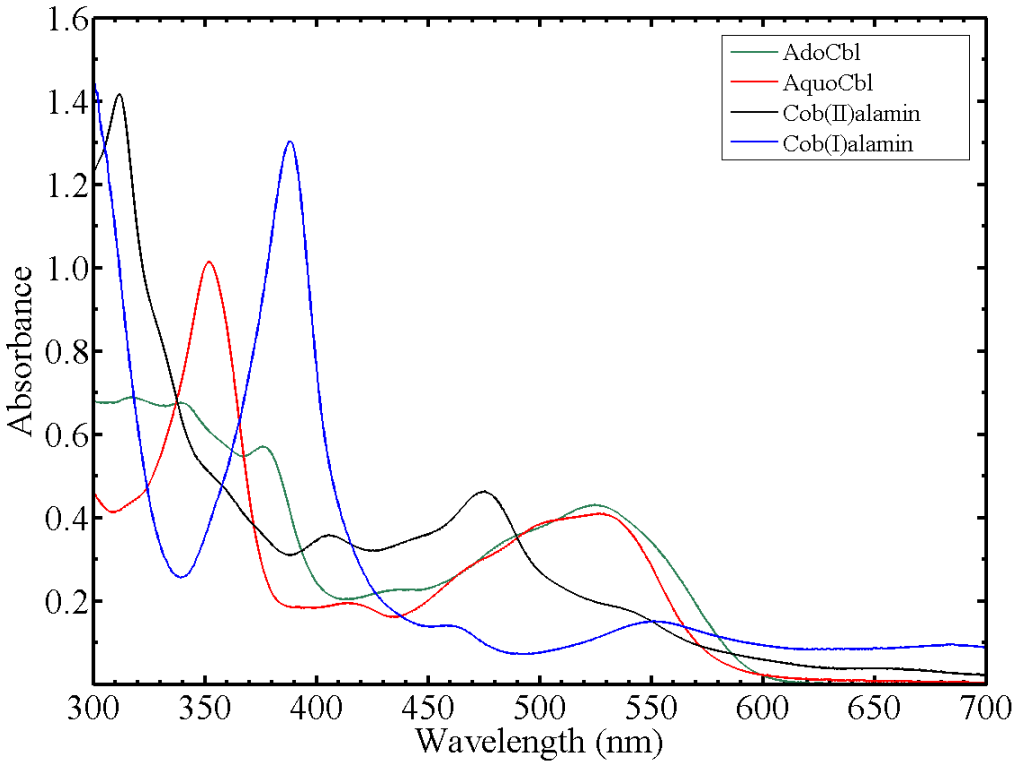

Figure 5.7: Ultraviolet/visible absorption spectra of cobalamin compounds in 10 mM KPi at pH 7.5. AdoCbl (49 μM) was photolyzed anaerobically to produce cob(II)alamin. Cob(II)allamin was photolyzed aerobically to produce AquoCbl. Ti(III) citrate (10 mM) was used to reduce AquoCbl to cob(I)alamin anaerobically. A baseline spectrum of Ti(III) citrate was subtracted from the final spectrum. A scaling factor of 1.12 was added to the cob(I)alamin spectra to match the concentration of the other spectra in the figure.

Cobinamide

The ultraviolet/visible absorbance spectra of MeCbi, AquoCbi, cob(II)inamide, and cob(I)inamide are shown in Figure 5.6. MeCbi, cob(II)inamide, and AquoCbi were derived from the same sample. MeCbi (57 μM) was photolyzed to cob(II)inamide and then oxidized to form AquoCbi by exposure to air. Cob(II)inamide in the presence of O_2, converts slowly, on a greater than hours timescale, to AquoCbi. In the presence of O_2

and light, cob(II)inamide is immediately converted to AquoCbi. Cob(I)inamide was derived from the photoreduction of MeCbi by 10 μM 5'-DRF, and its spectrum was scaled to the concentration of the other cobinamide spectra.

Comparison of Cobalamin and Cobinamide Reduction

In the presence of Ti(III) citrate, the cobalt ion of both cobalamin and cobinamide, is reduced to the +2 oxidation state on a timescale that is faster than the mixing time of the experiment. The reduction of the Co^{II} state to the Co^{I} state by Ti(III) citrate takes place on a minute's timescale, and can be time-resolved by using UV/visible absorption spectroscopy. The rate of increase of Co^{I} concentration, which is measured from the change in absorbance at 387 nm, was used to measure the rate constants, k_{obs}, for the reduction reaction. The reduction of Co^{III} to Co^{I}, following the addition of 250 μM Ti(III) citrate, for AquoCbl and AquoCbi is shown in Figure 5.8 For the redox reaction between 77 μM AquoCbl and 250 μM Ti(III) citrate, $k_{obs,Cbl}$ is 0.0013 s^{-1}, and $k_{obs,Cbi}$ for the reaction between 77 μM AquoCbi and 250 μM Ti(III) citrate is 0.060 s^{-1}. These rate constants were obtained from monoexponential fits of the data shown in Figure 5.8. The results show that the rate of AquoCbi reduction to the Co^{I} state, by 250 μM Ti(III) citrate, is 46 times faster than the reduction of AquoCbl.

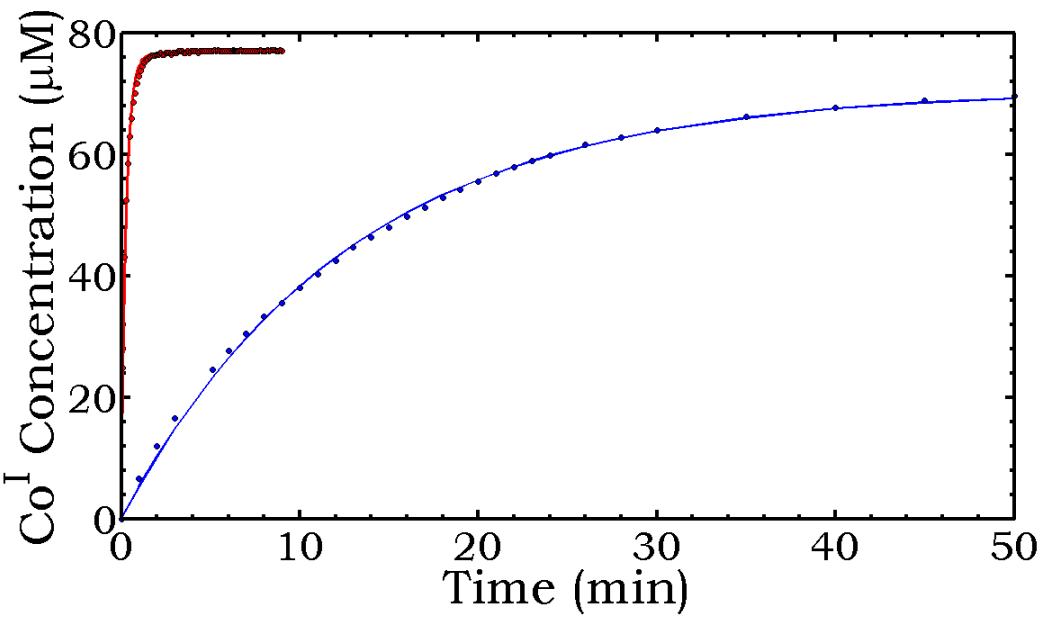

Figure 5.8: Time dependence of the reduction of AquoCbl and AquoCbi by 1 mM Ti(III) citrate in anaerobic 10 mM KP_i at pH 7.5 (points) and fits of a monoexponential growth function (solid curves). The rate of reduction of cobinamide ($k_{obs,Cbi}$ = 0.060 s^{-1}) was 46 times faster than the rate of cobalamin reduction ($k_{obs,Cbl}$ = 0.0013 s^{-1}) by the same concentration of Ti(III) citrate. Co^{I} concentrations were calculated from ultraviolet/visible absorbance at 387 nm. Data was collected at 298 K.

The rate of reduction of the Co^{III} state in AquoCbl and AquoCbi as a function of Ti(III) citrate concentration is shown in Figure 5.9. At high concentrations of Ti(III) citrate, the reaction rate for reduction approaches a constant value, therefore we assume the mechanism for reduction shown in scheme 5.1.

$$A + B \leftrightarrow AB \rightarrow C \qquad \text{(Scheme 5.1)}$$

The cobalamin (A) and Ti(III) citrate (B), forms a reversible complex (AB) which can then form the reduced cob(I)alamin (C) irreversibly. The rate of cob(I)alamin formation is given by equation 5.1.

$$k_{obs} = \frac{k_2[A_0][B_0]}{[B] + \frac{k_{-1} + k_2}{k_1}} \tag{5.1}$$

The rate k_1 and k_{-1} represent the forward and reverse rate constants for complex AB formation, respectively. The rate k_2 represents the rate constant for formation of cob(I)alamin (C). At high concentrations of Ti(III) citrate (B) the rate, ν_{max}, of cob(I)alamin formation is given by equation 5.2.

$$\nu_{max} = k_2[A_0] \tag{5.2}$$

A Lineweaver-Burke plot, $1/k_{obs}$ versus the inverse of Ti(III) concentration, with a linear fit to the data points is shown in Figure 5.10. The rate, k_2, of cob(I)alamin reaction with Ti(III) citrate can be calculated given the concentration of cobalamin, which is constant (77 μM), and ν_{max}, which is 1/(y-intercept), to be 162 M s^{-1}.

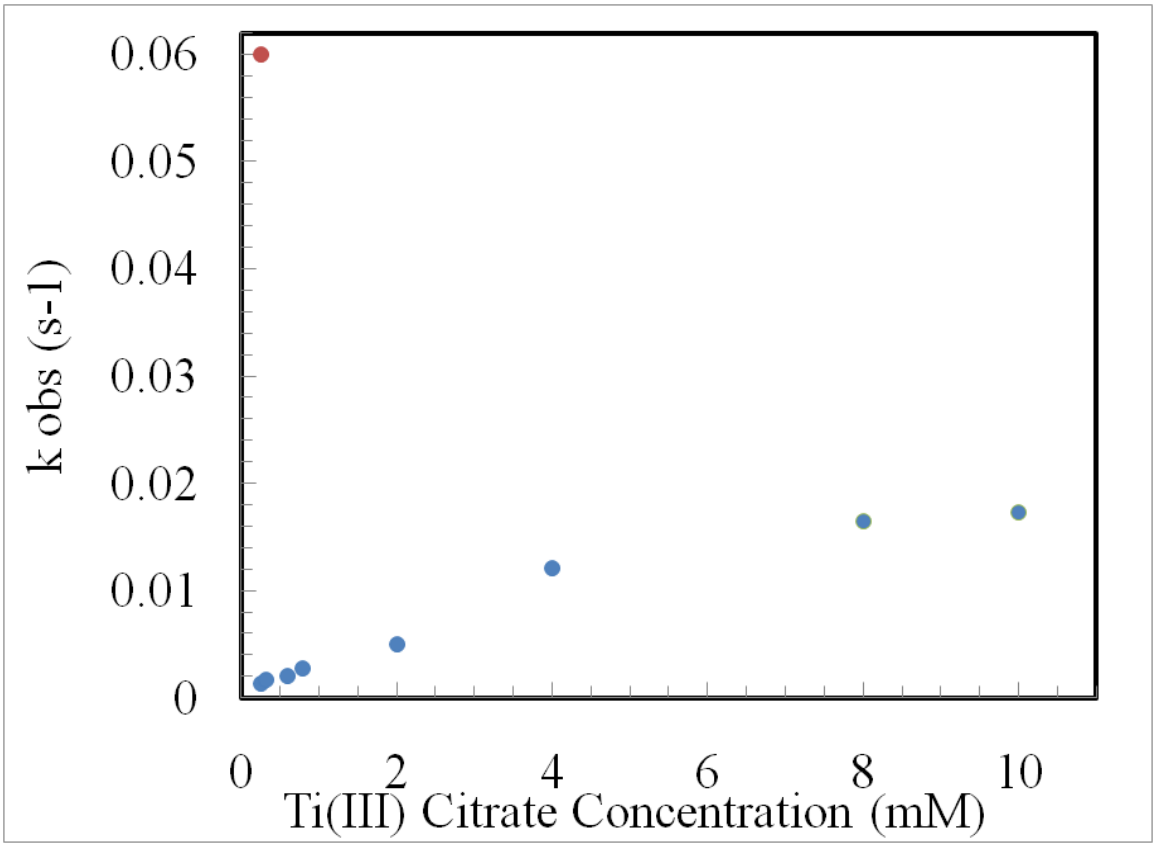

Figure 5.9. (Right) Plot of observed rate constant of Co^{II} reduction to Co^{I} (k_{obs}) against Ti(III) citrate concentration. The cobalamin data shows that the rate is dependent upon Ti(III) concentration. The blue point represents the reduction rate of cob(II)inamide, which is 46.0 times the reduction rate of cob(II)alamin at the same Ti(III) citrate concentration. Rate constants for reduction were calculated from the increase in Co^{I} concentration measured from the absorbance change at 387 nm and using the associated difference extinction coefficient.

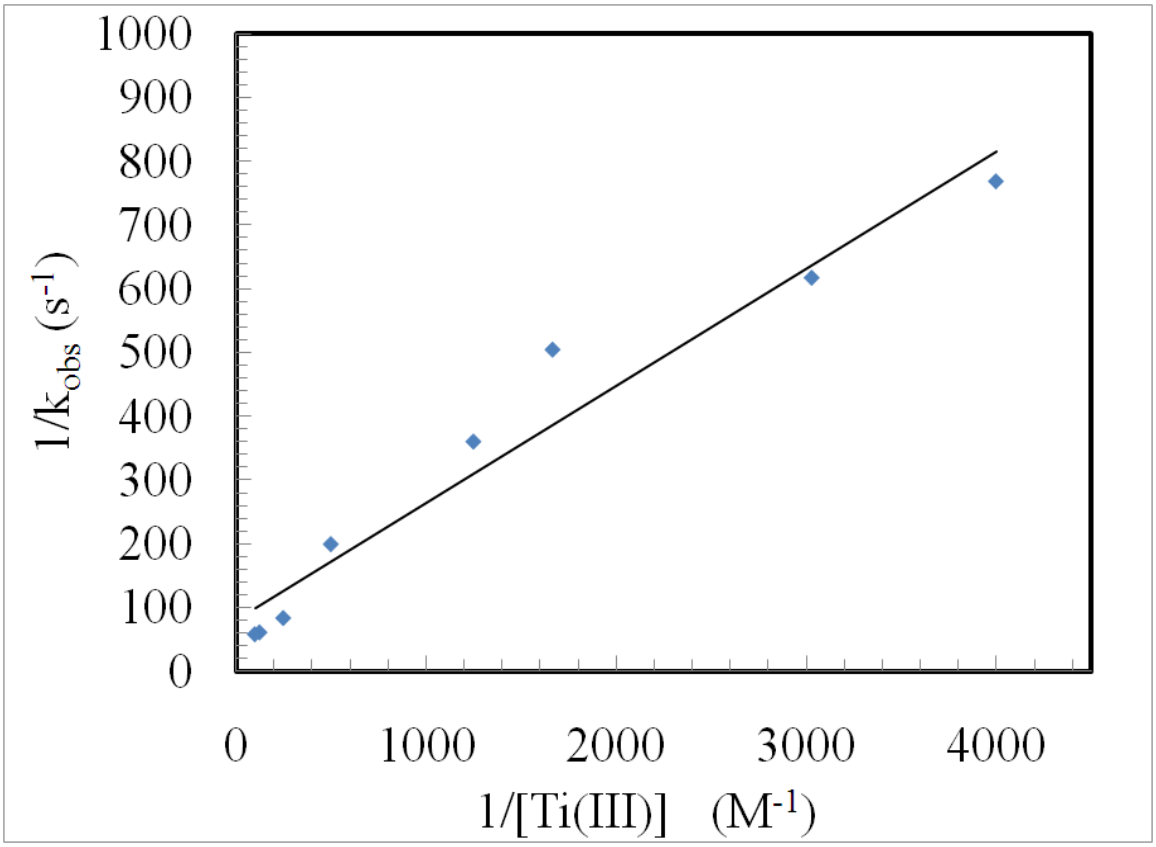

Figure 5.10. Lineweaver-Burke plot of the rate of reduction of the Co^{III} state in AquoCbl and AquoCbi as a function of Ti(III) citrate concentration. The equation for the linear fit shown is $y = 0.183830x + 80.193$, $R^2 = 0.9528$.

Conclusion

The native forms of the B_{12} cofactor, AdoCbl and MeCbl, were not reduced by Ti(III) citrate. Both cofactors have steric hindrances, caused by the α and β-axial ligands, which limit access to the cobalt ion. AquoCbl, whose cobalt ion has access to the solvent, is reduced by Ti(III) citrate, illustrating the necessity of the catalytic center of the compressed photosynthesis construct to be free of a strongly covalently bonded β-axial ligand. Cobinamide reduction by 250 μM Ti(III) citrate is enhanced relative to

cobalamin reduction by a factor of 46. The axial ligation to the DMBz group has been shown to be strengthened upon reduction of AdoCbl to cob(II)alamin.[152] The cob(II)alamin state is stabilized by the DMBz ligand, which increases the activation energy barrier to formation of cob(I)alamin and therefore, decreases the rate for the reduction of cob(II)alamin to cob(I)alamin. The absence of a lower α-axial DMBz ligand in cobinamide destabilizes the +3 and +2 cobalt oxidation states[152], making reduction more feasible. There is, however, no DMBz ligand in either the cob(I)alamin and cob(I)inamide, which results in the free energy of each state being essentially the same. The oxygen ligand, contributed by water, at the axial position reduces the stability of cob(II)inamide as compared to the stronger nitrogen ligand, from the DMBz group, of the cob(II)alamin. This results in the activation energy for the cob(II)inamide reduction to cob(I)inamide being less than that of cob(II)alamin conversion to cob(I)alamin. The lowered activation energy increases the reduction rate of cobinamide, as was demonstrated in the Ti(III) citrate reduction described in Figure 5.8.

Cobinamide and cobalamin compounds are reduced in two one-electron steps by Ti(III) citrate and 5'-DRF. This is evident following the use of Ti(III) citrate as the reducing agent, which resulted in slow reduction time and the observation of two states following Co^{III}. The one-electron reduction step of AquoCbl and AquoCbi to the Co^{II} state occurs on a timescale that is faster than the mixing time. The second one-electron reduction to Co^{I} state takes place on the minute's timescale. The reduction by 5'-DRF also involves two one-electron reductions, which are both fast on the timescale of the experiment, < 15 s, and cannot be resolved in time. Since photolysis converts MeCbi to cob(II)inamide and cob(II)inamide is reduced to cob(I)inamide, a single-electron transfer

reaction is the most likely mechanism for the reduction of cob(II)inamide by photoexcited 5'-DRF. Photo-reduction to Co^{I} was made possible by the removal of the lower α-axial ligand of cobalamin, possibly due to the short lifetime of the excited state of the 5'-DRF, as compared to the time for the removal of the DMBz axial ligand from the cobalamin.

The result illustrates the need for a modified cofactor for compressed photosynthesis whose reduction to an oxidation state, used for the catalysis of reduction of CO_2 or halo-organics, is not limited by steric hindrances in its α and β-ligands. We conclude that the replacement of the α ligand with H_2O, and the removal of the β-ligand of cobalamin, forming AquoCbi, leads to a suitable cofactor for compressed photosynthesis due to the cofactor's ability to be readily reduced to cob(I)inamide, and, that it retains the necessary reduction potential and oxidation state to perform the two electron reduction of CO_2. Further studies will be described in Section 5.5 that describe the ability of the reduced cofactor to bind to the EutB subunit.

5.4 Oxidation of Cob(I)alamin and Cob(I)inamide in the Presence of CO_2.

The decay of the chemically or photo-generated Co^{I} oxidation state of the cobalamin and cobinamide cofactors was monitored by using UV/visible spectroscopy. The extinction coefficients for each compound were used to calculate and monitor the concentrations of cobalamin or cobinamide species. The decay of the Co^{I} state of the cofactors was monitored in the presence of CO_2, as well as in the presence of N_2 gas, as a control.

Experiments were performed using a partial pressure of CO_2 gas of approximately 1 atm, which resulted in a decrease in pH to 5.5, of samples in 10 mM KP_i buffer at pH 7.5, by the mechanism depicted in Figure 5.11. The oxygen atoms in CO_2 are electronegative and withdraw electron density from the carbon atom causing the carbon to become a Lewis acid. The CO_2 and water therefore react to produce carbonic acid, which comes into equilibrium with bicarbonate (HCO_3^-)and carbonate (CO_3^{2-}). Calculations of the solubility of CO_2 in water at 25°C at 1 atm partial pressure led to a value of 33 mM.[173] The calculated equilibrium distribution of CO_2 species in solution at 1 atm partial pressure is shown in Figure 5.12, and illustrates the need for pH values of approximately 6.0 to ensure the presence of substantial amounts of CO_2 in solution. Photo-initiated reduction of cobinamide and its reaction with CO_2 was performed using bicarbonate solutions with pH values adjusted to 6.0.

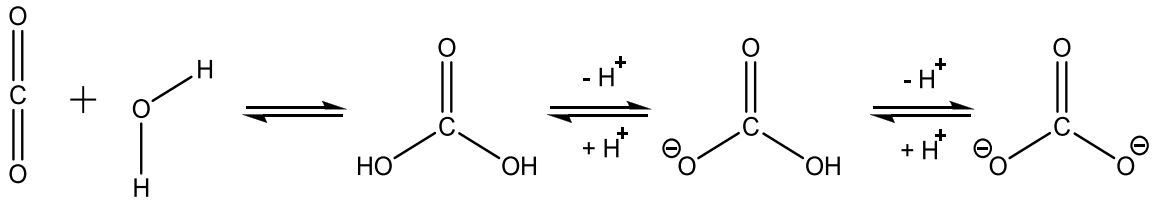

Figure 5.11. Formation of carbonic acid from CO_2 in aqueous solution.

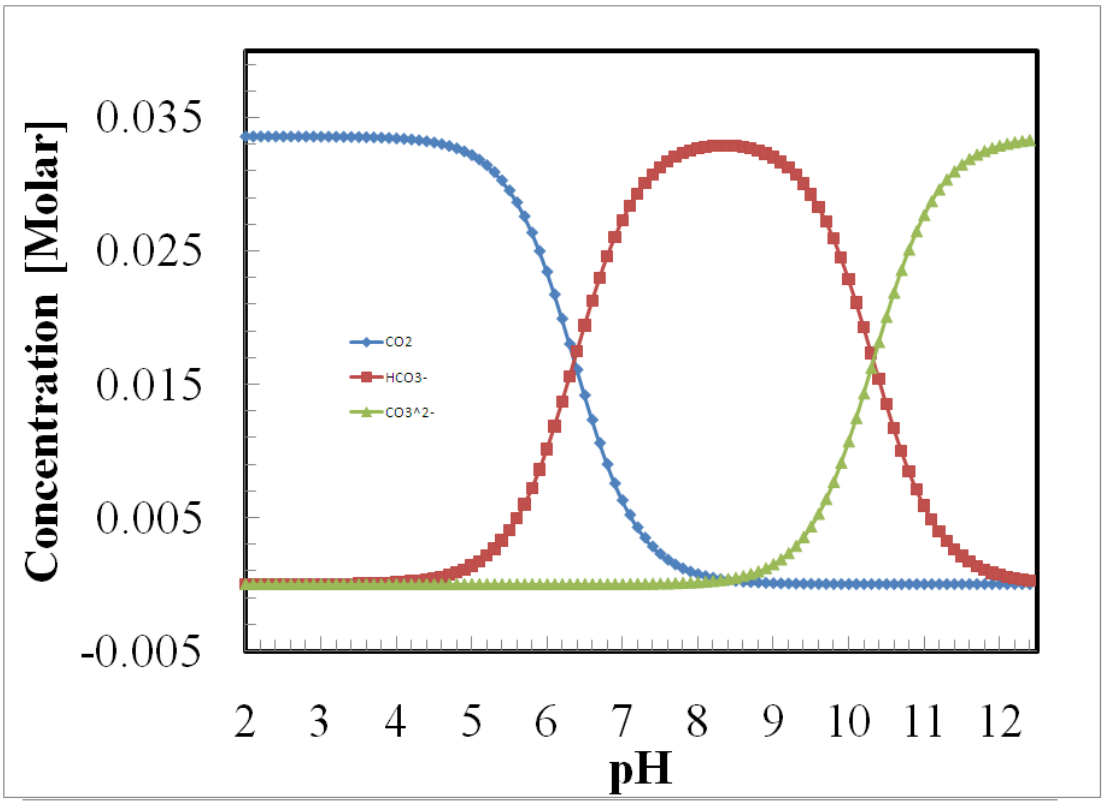

Figure 5.12. Concentrations of CO_2 equilibrium products under 1 atm (positive 5psi) partial pressure in aqueous solution. Assumption: $[CO_2]$ is $[CO_2] + [HCO_3^-]$, $[HCO_3^-] = 10^{\wedge-3} * [CO_2]$.[174]

Reaction of Cob(I)inamide in Aqueous Solution at pH 6.0

The oxidation of cob(I)inamide in anaerobic aqueous solution at pH 6.0 was used as a control for the reaction of cob(I)inamide with CO_2 in solution and is shown in Figure 5.13. The pH of 6.0 (rather than 7.5) was chosen to increase the CO_2 concentration because it increases with decreasing pH. Water was added anaerobically (80 µL) by using a syringe, after the sample was made anaerobic by N_2 bubbling, and before photolysis. Absorption spectra were collected before and during the decay, and at the end

of the experiment. Separate experiments were performed which monitored the time course of the decay of the cob(I)inamide species by single wavelength detection of the 387 nm peak of cob(I)inamide. No Co^{III}-cobinamide species were detected. This confirmed that the decrease in cob(I)inamide was associated with the production of cob(II)inamide.

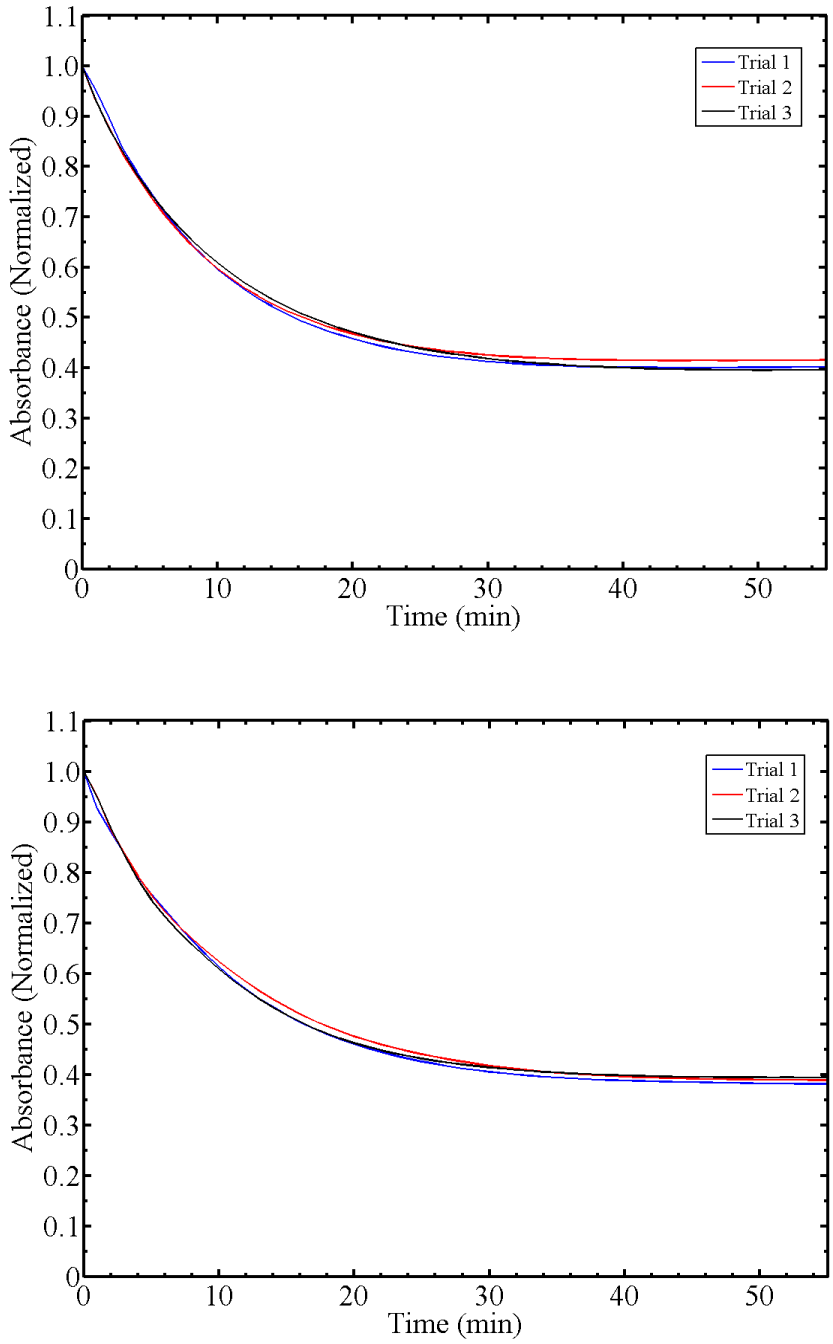

Figure 5.13. Reaction of photo-generated cob(I)inamide in aqueous solution at pH 6.0. Top: Water was added to the sample, as a control for the addition of bicarbonate solution. Bottom: No additions to the sample. The absorbance was detected at 387 nm, which corresponds to the UV absorption peak of cob(I)inamide.

The decay of cob(I)inamide was fitted to a single exponential plus constant function. The averaged fitting parameters for the decay amplitude, the decay time constant, and the amplitude of the constant factor are presented in Table 5.4. The time constants of the decay for the water-added (9.1 ±0.6 min) and no-addition (10.1 ±0.5 min) samples were the same, to within the standard deviations. The results indicate that cob(I)inamide decays on the approximately 10 min time scale in the absence of any added reactant. This background reaction will compete with the reaction of cob(I)inamide with CO_2.

Table 5.4. Monoexponential fitting parameters of the cob(I)inamide decay reactions shown in Figure 5.13 and 5.14.

Treatment	A	τ (s)	$A_{constant}$	R
Nothing Added	7.76 (±0.05) x 10^{-1}	1.01 (±0.05) x 10^{1}	4.83 (±0.13) x 10^{-1}	0.9998
Water Added	7.29 (±0.27) x 10^{-1}	9.09 (±0.63) x 10^{0}	4.83 (±0.04) x 10^{-1}	0.9998
Bicarb 10 mM	7.46 (±0.36) x 10^{-1}	1.34 (±0.20) x 10^{1}	4.95 (±0.15) x 10^{-1}	0.9999
Bicarb 20 mM	7.45 (±0.73) x 10^{-1}	1.27 (±0.17) x 10^{1}	4.94 (±0.24) x 10^{-1}	0.9999
Bicarb 50 mM	6.27 (±0.54) x 10^{-1}	1.35 (±0.02) x 10^{1}	4.87 (±0.11) x 10^{-1}	0.9997

Reaction of cob(I)inamide with CO_2 in aqueous solution at pH 6.0

In order to more precisly control the pH and CO_2 concentration in solution, MeCbi/CO_2 samples were prepared as described in Section 5.2. The oxidation of cob(I)inamide in anaerobic solution with CO_2 present at pH 6.0 was monitored for solutions containing different bicarbonate concentrations. As stated above, the pH of 6.0 was chosen to increase the CO_2 concentration in the sample, relative to pH 7.5. The decay of cob(I)inamide in the presence of bicarbonate, at final concentrations of 10 mM, 20 mM, and 50 mM is shown in Figure 5.14. The 10 mM and 20 mM bicarbonate trials both had the same volume of bicarbonate (80 µL) added, while the volume added for the 50 mM trials increased by 2.5-fold, due to the solubility limit of sodium bicarbonate. The UV/visible spectra obtained following the decay of the samples showed that the reaction product was cob(II)inamide. No Co^{III} species were detected.

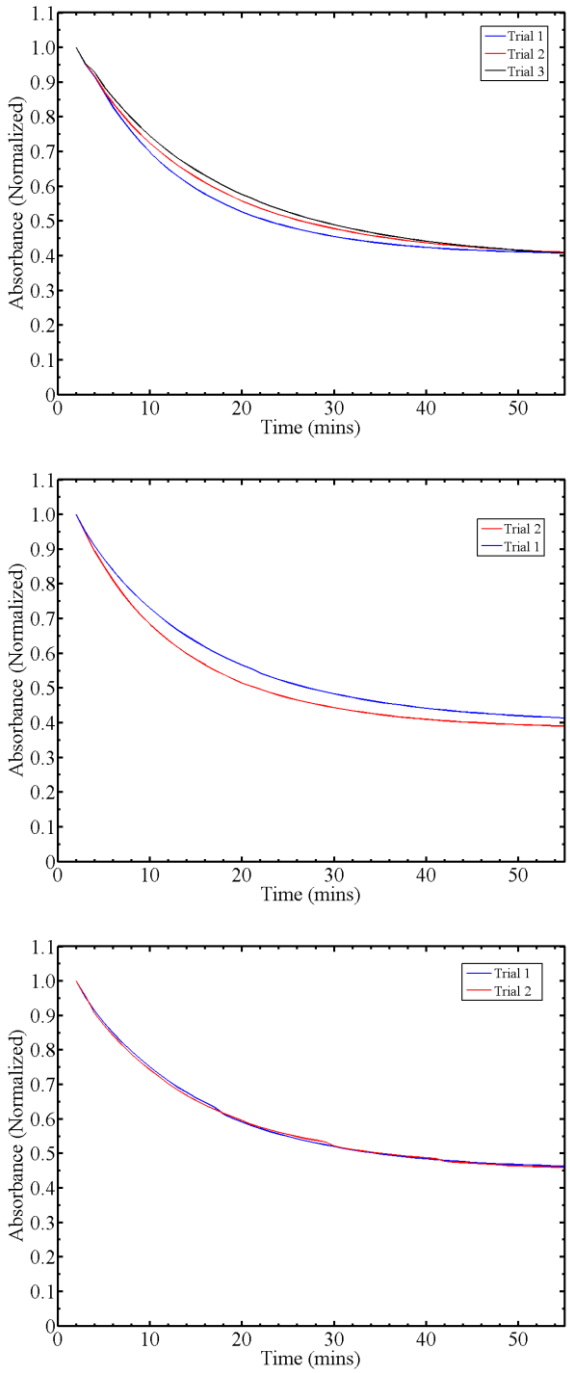

Figure 5.14. Reaction of photo-generated cob(I)inamide in aqueous solution at pH 6.0 in the presence of different concentrations of bicarbonate. Top: 10 mM Bicarbonate added. Middle: 20 mM Bicarbonate added. Bottom: 50 mM Bicarbonate added. The normalized absorbance was detected at 387 nm, which corresponds to the UV absorption peak of cob(I)inamide.

The cob(I)inamide decay in the presence of various bicarbonate (CO_2) concentrations, shown in Figures 5.14, was fit well by a single exponential plus constant function. Fitting parameters for the cob(I)inamide decay are shown in Table 5.4. The average time constant values are 13.4 ±2.0, 12.7 ±1.7, and 13.5 ±0.2 min for the 10 mM, 20 mM and 50 mM bicarbonate samples, respectively. These values are all significantly larger than the time constants for the control decays of 9.1 ±0.6 min (water added) and 10.1 ±0.5 (no-addition) (Table 5.4), indicating that CO_2 decreases rather than increases the rate of oxidation of cob(I)inamide. These results suggest that CO_2 interacts weakly with the cob(I)inamide, to produce the longer decay time constant of the reaction.

5.5 Reaction of Cobinamide with Chloroacetonitrile in Aqueous Solution at pH 7.5

The starting material, Figure 5.15, and products, Figure 5.16, of de-halogenation of chloroacetonitrile ($ClCH_2CN$) catalyzed by cob(I)inamide were monitored by using ^{13}C,^{15}N-labelled reactants and ^{13}C-NMR. The starting material spectra is characterized by a peak at 26 ppm from the carbon-13 attached to the chlorine, and two hydrogen atoms. The peak displays splitting due to coupling to the cyanide ^{13}C as well as a small split from the remote ^{15}N. A second peak from chloroacetonitrile is shown at 118 ppm due to the ^{13}C of the cyanide group. This peak also displays two splitting from the ^{13}C of the ^{13}C-Cl, and the ^{15}N of the cyanide. Peaks at 57 and 52 ppm are from EDTA in solution.

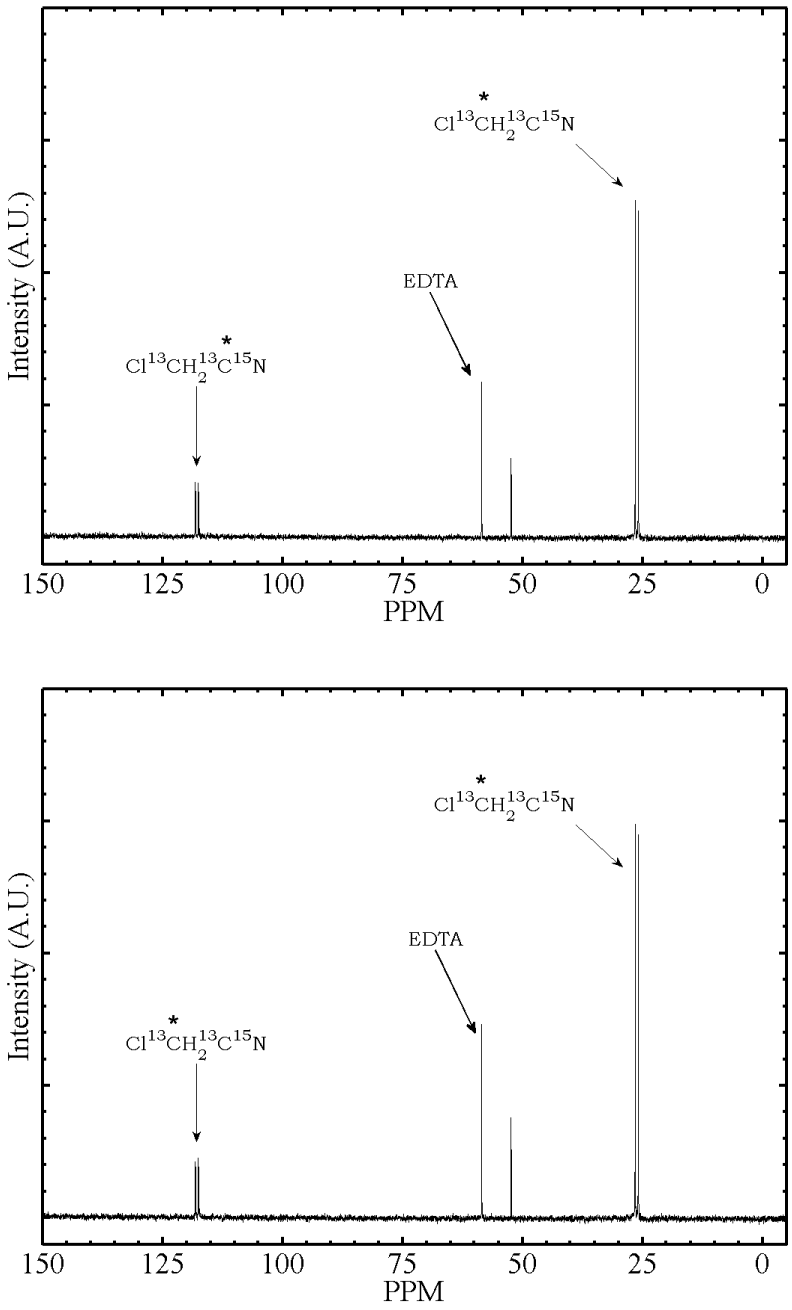

Figure 5.15. ^{13}C NMR before photoreduction of chloroacetonitrile ($^{13}CH_3{}^{13}C^{15}N$). Top: No MeCbi added. Bottom: 50 μM MeCbi added. Sample solution contain 100 mM chloroacetonitrile, 100 mM EDTA, 10 mM KP_i, and 10 μM 5'-deazariboflavin.

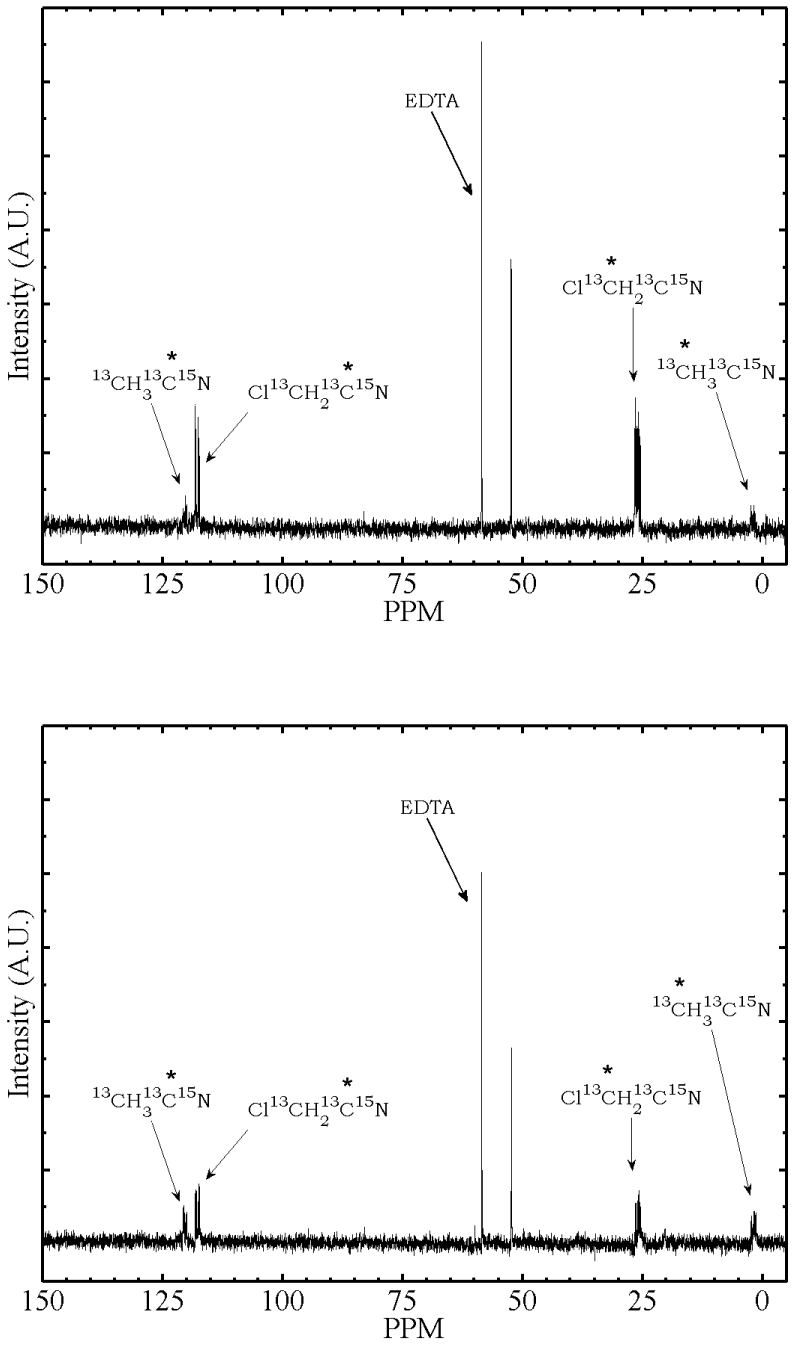

Figure 5.16. ^{13}C NMR following photoreduction (150 W Hg Lamp, 3 hours) of chloroacetonitrile ($^{13}CH_3{}^{13}C^{15}N$). Top: No MeCbi added. Bottom: 50 μM MeCbi added. Cobinamide causes a 2 fold increase in the reduction to acetonitrile. Solution contained 100 mM chloroacetonitrile, 100 mM EDTA, 10 mM KP_i, 50 μM cobinamide and 10 μM 5'-DRF.

The results, following 3 hours of irradiation by the full bandwidth of a 150 W Hg lamp, are shown in Figure 5.16. A triplet spitting of the ^{13}C atom attached to the chlorine, for both starting and product material, was observed following photolysis, suggesting deuteration from the solvent of the original hydrogens. Exchange of hydrogen with solvent deuterium was only observed following irradiation. The irradiation of chloroacetonitrile, in the presence of MeCbi, 5'-DRF and EDTA, resulted in the loss of the chlorine from the molecule as shown by the 1.75 ppm peak for the carbon of the newly produced $^{13}CH_3$ group of $^{13}CH_3{}^{13}C^{15}N$. The ^{13}C of the cyanide group was also detected at 121 ppm.

The results show that the chlorine of the halo-organic compound was removed and replaced with a deuterium atom from solution. Deuteration of the hydrogen atoms was also observed. The degradation of chloracetonitrile, with and without MeCbi present, is proposed to be due to electron transfer from cob(I)inamide or 5'DRF to chloracetonitrile, which results in the loss of a chlorine ion.[175] Integration of the starting material and product peaks was performed using the 57 ppm peak from EDTA as a reference. Samples without MeCbi showed a decrease in the area of the 118 ppm chloracetonitrile peak of 11%, as compared to 20% with MeCbi present. The 26 ppm peak of the chloroacetonitrile showed a decrease of 60 % without MeCbi present and 83% with MeCbi present. The 26 ppm peak, from the ^{13}C attached to the chlorine, is not as reliable an indicator of product degradation as the 118 ppm. The 26 ppm peak is more strongly affected by changes in the nuclear Overhauser contributions due to the ^{13}C having two bonded hydrogen atoms. Dueteration of the hydrogen atoms decreases the intensity of the peak without the removal of the chlorine atom. Therefore, the 118 ppm

peak is used to quantify the degradation of the starting material. Using cobinamide as a reduction catalyst provided a nearly 2-fold increase in the reduction to acetonitrile as compared to the same sample conditions without cobinamide present. Integration of the 122 ppm peak, from the ^{13}C of cyanide, of the product, $^{13}CH_3{}^{13}C^{15}N$, also showed a 2 fold increase for samples containing MeCbi.

Electrochemical studies have shown that the cob(I)inamide complex binds chloractonitrile, displacing a chlorine ion to form an alkyl-cob(III)inamide complex, in 70/30 water-ethanol mixtures[161]. The formation and release of acetonitrile takes place during the re-reduction of the alkyl-cob(III)inamide to cob(I)inamide. This process requires two electrons from the electrodes to reduce the cobalt atom and two protons from solution. Our results show that the dehalogenation reaction does occur when the constant source of reduction electrons from an electrode, as previously reported[161], is replaced with those from a photo-generated, short-lived, excited state, such as 5'-DRF. These results the ability of the cobinamide cofactor to catalyse the photo-induced dehalogenation of toxic halo-organic compounds.

5.6 Discussion

Dihydrogen formation

The lowering of the rate of oxidation of cobinamide due to the presence of CO_2, is shown in Figure 5.13, 5.14 and summarized in Table 5.4. We propose that CO_2 competes with a reaction of the cob(I)inamide state in aqueous solution. The protonation of Co^I in

macrocyclic cobalt complexes and subsequent dihydrogen (H_2) formation has been observed in aqueous solution, and has been described by the following reactions.[155,176-177]

$$[Co^{II}]^{2+} + e^- \rightarrow [Co^{I}]^{+} \quad (5.3)$$

$$[Co^{I}]^{+} + H_2O \rightarrow [Co^{I}]^{+} + H^+ + OH^- \quad (5.4)$$

$$[Co^{I}]^{+} + H^+ \rightarrow [H^-Co^{III}]^{2+} \quad (5.5)$$

$$[H^-Co^{III}]^{2+} + H^+ \rightarrow [Co^{III}]^{3+} + H_2 \quad (5.6)$$

$$2[H^-Co^{III}]^{2+} \rightarrow 2[Co^{II}]^{2+} + H_2 \quad (5.7)$$

The cob(I)inamide reacts with protons in solution to form the $[H^-Co^{III}]$, Co^{III}-hydride. The Co^{III}-hydride complex can react with an additional proton in solution to form H_2 gas and the Co^{III} state, as shown in equation 5.6. Alternatively, the hydride complex can react with another hydride complex in solution, as show in equation 5.7, to eliminate H_2, which results in the formation of $2Co^{II}$.[177] Spectra following the decay of the cob(I)inamide state showed only the presence of cob(II)inamide. The observed decay to cob(II)inamide is consistent with the reaction mechanism described in equation 5.7. A sacrificial electron donor, EDTA, is used to provide the electrons for the initial reduction to cob(I)inamide.

Typically CO_2 reduction experiments are performed in aprotic organic solvents which are absent of protons to compete with CO_2 binding and reduction by the catalyst. Ogata et al. did however, report on the interaction of CO_2 with Co^I macrocycles, in the protic solvent mixture of acetonitrile/methanol, and observed an increase in the rate of decay of the Co^I complex to the Co^{II} state in the presence of CO_2.[176] The increase in the decay rate of Co^I was also shown to be linearly proportional to the concentration of CO_2. The results illustrated that, in acetonitrile/methanol, the reaction rate of the macrocycle with CO_2 was faster than the reaction rate of the macrocycle with protons, ~ 2 s.

CO_2 Binding Interaction with Cob(I)inamide

We propose that the decrease in the decay rate of cob(I)inamide to cob(II)inamide, in the presence of CO_2, is caused by the binding of CO_2 to cob(I)inamide. We propose the binding of CO_2 to cob(I)inamide competes with the reduction reaction with protons from solution, and that the reduction of CO_2 by cob(I)inamide is much slower than that of the proton reaction. The two electronegative oxygen atoms in CO_2 result in a slight positive charge on the carbon located in the center. The electrophilicity of the carbon atom in CO_2 promotes binding of the molecule to accessible high electron density metal centers. The most likely orientation of a CO_2 molecule bound to a single metal center ligated by a tetracoordinate ring is η^1.[144] The η^1 mode describes the electronegative metal center binding with the π^* molecular orbital of CO_2, resulting in the bending of the oxygens of the CO_2 molecule away from the metal center. The proposed cob(I)inamide and CO_2 complex is shown in Figure 5.4 and is consistent in explaining the results that the increased CO_2 concentration results in a slower decay rate. The

mechanism, illustrated in Figure 5.4, is that the CO_2 molecule binds to one or both axial-ligand positions and prevents solvent molecules from entering the region, lowering the transfer of a proton to the complex, which has been shown to be the main oxidative reaction for the complex in aqueous solution.[155,177-178]

$$[Co^{I}]^{+} + CO_2 \rightarrow [Co^{I}CO_2]^{+} \quad (5.8)$$

$$[CO^{I}CO_2]^{+} \rightarrow [Co^{III}CO_2{}^{2-}]^{+} \quad (5.9)$$

$$[Co^{III}CO_2{}^{2-}]^{+} + H^{+} \rightarrow [Co^{III}CO_2{}^{-}H]^{2+} \quad (5.10)$$

$$[Co^{III}CO_2{}^{-}H]^{2+} + e^{-} \rightarrow [Co^{II}]^{2+} + CO + OH^{-} \quad (5.11)$$

The proposed reaction mechanism is shown in Equation 5.8-5.11, in which a cob(I)inamide bound CO_2 molecule is reduced to carbon monoxide (CO). The cofactor, in a reduced Co^{I} state, binds CO_2 from solution to form a $[Co^{I}CO_2]^{+}$ complex. The cobalt center is then oxidized to Co^{III}, transferring two electrons to CO_2. The complex is then reduced to form Co^{II}, CO and OH^{-}. Other mechanisms are possible for the reaction of cob(I)inamide with CO_2 that result in the production of formate. The Co^{I} state is first protonated to form $[Co^{III}H^{-}]^{2+}$ followed by the insertion of CO_2 to form $[Co^{III}O_2CH]^{2+}$. With the addition of an electron from a donor, the $[Co^{III}O_2CH]^{2+}$ complex forms and releases HCO_2^{-} and is left in the $[Co^{II}]^{2+}$ state.

The rate of decay of cob(I)inamide, in the presence of 10 mM, 20 mM and 50 mM CO_2, were the same within the standard deviations of the measurements. Further experiments with higher stability and sensitivity are needed in the range between 0 and 10 mM of bicarbonate. A CO_2 binding mechanism, as proposed in equations 5.9-5.12, would result in a hyperbolic curve in the decay time as a function of the concentration of bicarbonate. This is a result of an increase in the amount of bound CO_2, which would lower k_{on} and increasing time constant, as illustrated in equation 5.12.

$$K_{diss} = \frac{k_{on}[CO_2]}{k_{off}} \tag{5.12}$$

5.7 Reduction of Cobalamin and Cobinamide Cofactors Bound to EAL and EutB Protein

The characterization of the assembly of the photosynthesis construct is a fundamental requirement for further protein engineering and rate enhancement of the reaction. The EutB subunit natively binds the cobalamin cofactor in the Co^{III} state, which exists in the Co^{II} state on short time scales less than 0.02 s, during native enzyme turnover on the natural substrate, aminoethanol. Experiments carried out and described in Chapter 3 showed that photolysis of the AdoCbl cofactor results in the cob(II)alamin state, bound to the EAL protein, on timescales longer than 1 hour. However, we seek to examine the ability to reduce the cobalamin and cobinamide cofactors to the tetra-coordinate ligated, highly reactive, Co^{I} state while bound to EAL and the EutB protein alone.

All samples were prepared by binding cobalamin or cobinamide to EAL or EutB in 10 mM KP_i at 7.5 pH. Samples were made anaerobic by the FPT method. A 300 W Xe lamp was used to photolyze the sample for 30 seconds, to produce protein bound cob(II)alamin or cob(II)inamide. Further reduction of the bound Co^{II} states to EAL or EutB was performed by either Ti(III) citrate or light activated 5'-DRF.

Reduction of Cobalamin Bound to EAL and EutB

The absorption spectra of AdoCbl bound to EAL, following photolysis, and the addition of Ti(III) citrate, is shown in Figure 5.17. The baseline spectrum of EAL was subtracted from the spectra of AdoCbl bound to EAL. Cob(II)alamin state was observed following the photolysis of the cofactor, bound to EAL. Following the addition of Ti(III) citrate, no cob(I)alamin species was detected for up to 45 min.

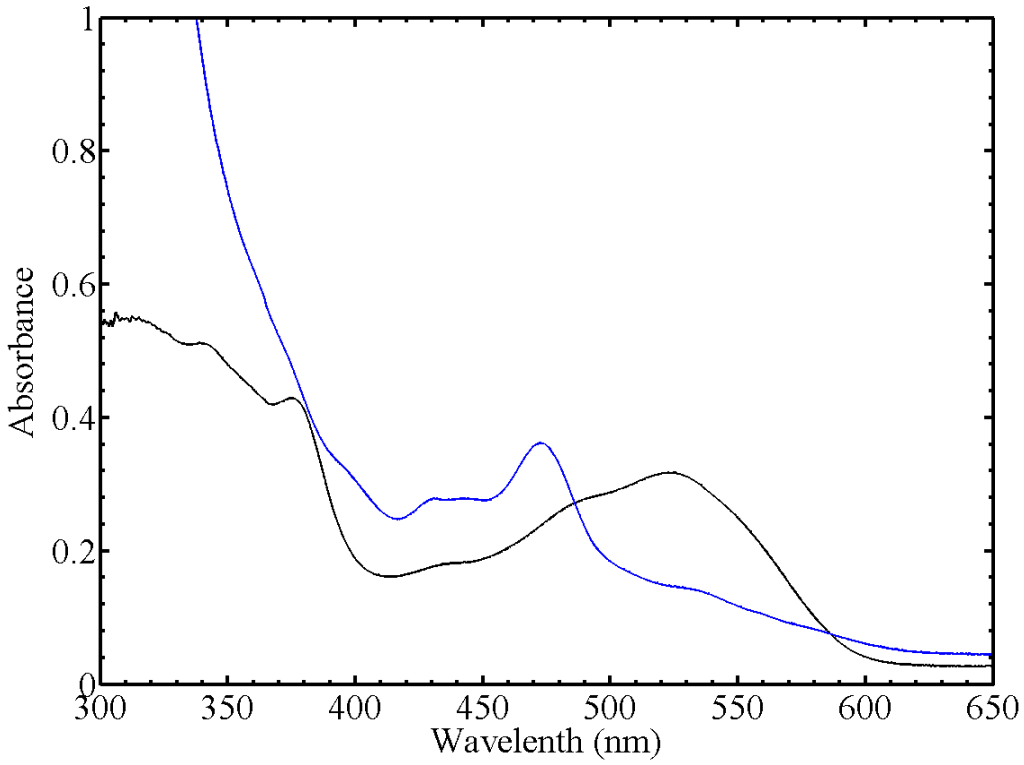

Figure 5.17. Absorption spectra of AdoCbl bound to EAL (black) in 10 mM KP_i at pH 7.5, and following photolysis and the addition of Ti(III) citrate (blue). AdoCbl (37 μM) bound to EAl (60 μM) was photolyzed anaerobically to produce cob(II)alamin. Ti(III) citrate (1 mM) was added to the solution anaerobically in an attempt to produce cob(I)alamin. A baseline spectrum of EAL was subtracted from the final spectra displayed.

The experiment was repeated with the AdoCbl cofactor bound to the EutB protein. The absorption spectra of AdoCbl bound to EutB, following photolysis, and the addition of Ti(III) citrate, are shown in Figure 5.18. The baseline spectrum of EutB was subtracted from both spectra. Cob(II)alamin was observed following the photolysis of AdoCbl bound to EutB, as was the case for AdoCbl bound to EAL. The formation of cob(II)alamin in EutB, however, was dependent on the presence of O_2 in solution. In an

aerobic environment, the photolysis of EutB bound AdoCbl results in the formation of AquoCbl, indicating the shielding of the cob(II)alamin cofactor from oxygen in EAL is partially dependent on the EutC subunit.

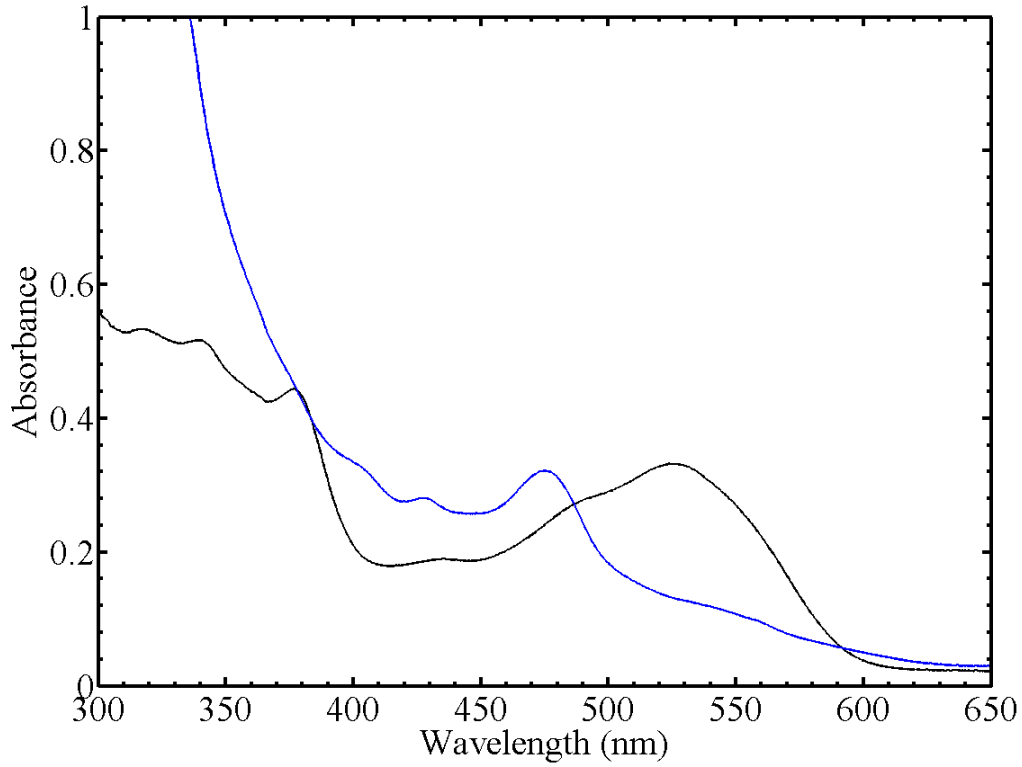

Figure 5.18. Absorption spectra of AdoCbl bound to EutB (black) in 10 mM KP_i at pH 7.5, and following photolysis and the addition of Ti(III) citrate (blue). AdoCbl (38 μM) bound to EutB (60 μM) was photolyzed anaerobically to produce cob(II)alamin. Ti(III) citrate (1 mM) was added to the solution anaerobically in an attempt to produce cob(I)alamin. A baseline spectrum of EutB was subtracted from the final spectra displayed.

The addition of Ti(III) citrate to EutB bound cob(II)alamin did not result in the formation of cob(I)alamin, for up to 45 min. These results indicate that the cobalamin

cofactor is not capable of being reduced, on a less than 45 mins time scale, to the cob(I)alamin state when bound to EutB.

Reduction of Cobinamide Bound to EAL and EutB

The absorption spectra of MeCbi bound to EAL, following photolysis, and the addition of Ti(III) citrate, is shown in Figure 5.19. The baseline spectrum of EAL was subtracted from both spectra. Photolysis of the MeCbi cofactor, bound to EAL, resulted in the formation of cob(II)inamide. Following the addition of Ti(III) citrate, an increase in absorption at 387 nm, commensurate with the cob(I)inamide species, was detected. The conversion of cob(II)inamide to cob(I)inamide in the sample was calculated to be complete within 10 mins.

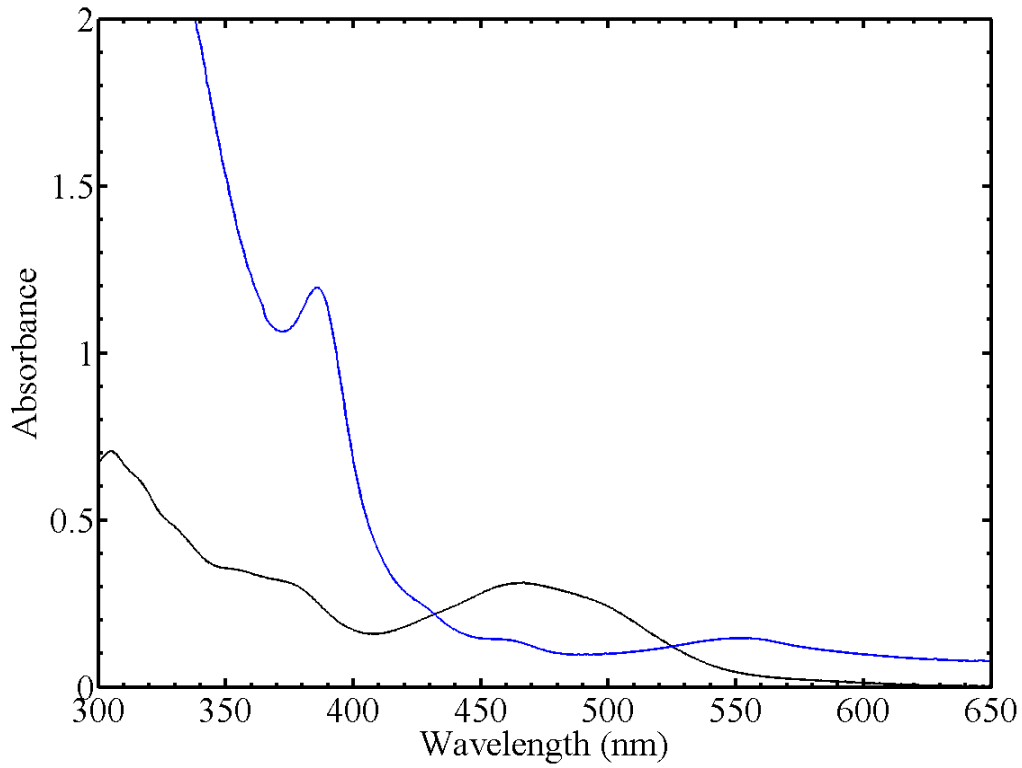

Figure 5.19. Absorption spectra of MeCbi bound to EAL (black) in 10 mM KP_i at pH 7.5, and following photolysis and the addition of Ti(III) citrate (blue). MeCbi (30 μM) bound to EAL (60 μM) was photolyzed anaerobically to produce cob(II)inamide. Ti(III) citrate (1 mM) was added to the solution anaerobically to produce cob(I)inamide. A baseline spectrum of EAL was subtracted from the final spectra displayed.

The reduction of EutB bound MeCbi was characterized by the same methods. The absorption spectra of MeCbi bound to EutB, following photolysis, and the addition of Ti(III) citrate, is shown in Figure 5.20. Cob(II)inamide was observed following photolysis of the cofactor bound to EutB. An increase in the 387 nm peak was immediately observed following the addition of Ti(III) citrate, indicating that the cobinamide cofactor was readily reduced when bound to EutB.

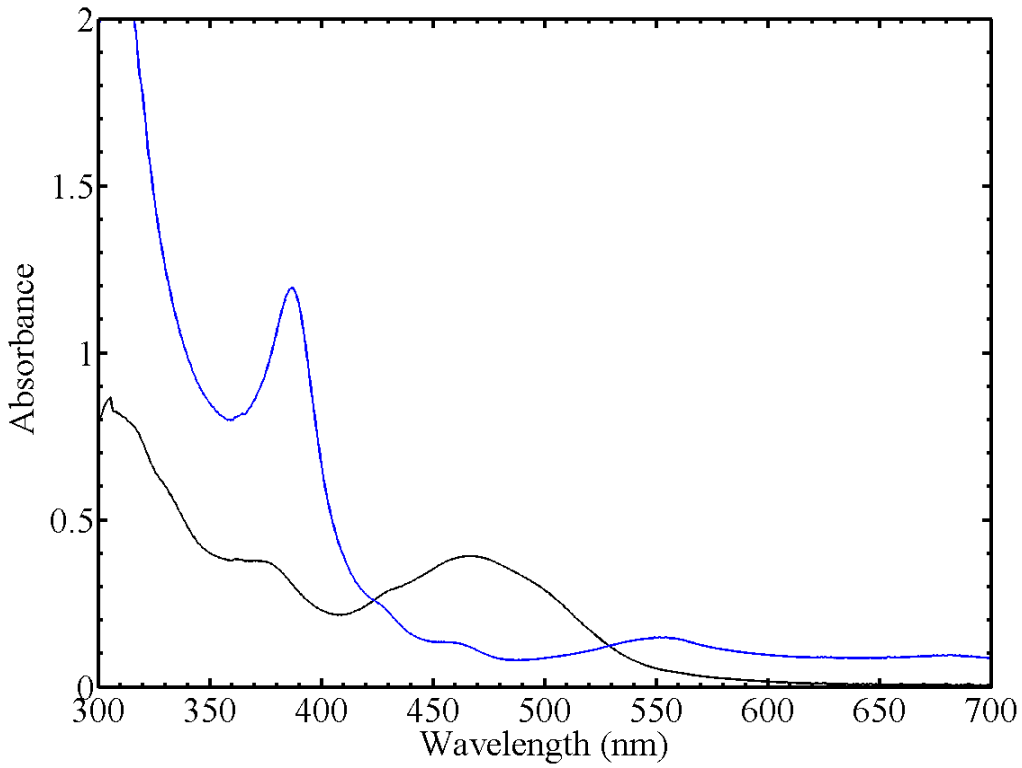

Figure 5.20. Absorption spectra of MeCbi bound to EutB (black) in 10 mM KP_i at pH 7.5, and following photolysis and the addition of Ti(III) citrate (blue). MeCbi (38 μM) bound to EutB (60 μM) was photolyzed anaerobically to produce cob(II)inamide. Ti(III) citrate (1 mM) was added to the solution anaerobically to produce cob(I)inamide. A baseline spectrum of EutB was subtracted from the final spectra displayed.

The photo-initiated reduction of the cobinamide cofactor by 5'-DRF is shown in Figure 5.21. Reduction of the cofactor to cob(II)inamide was observed, but further reduction of the cofactor to cob(I)inamide did not occur. Solution reduction of MeCbi to cob(I)inamide by 5'-DRF was demonstrated in Section 5.3. The inability to reduce MeCbi, by 5'DRF, in the presence of EutB indicates that the cofactor is bound to the protein and does not allow access to the cofactor by the 5'-DRF.

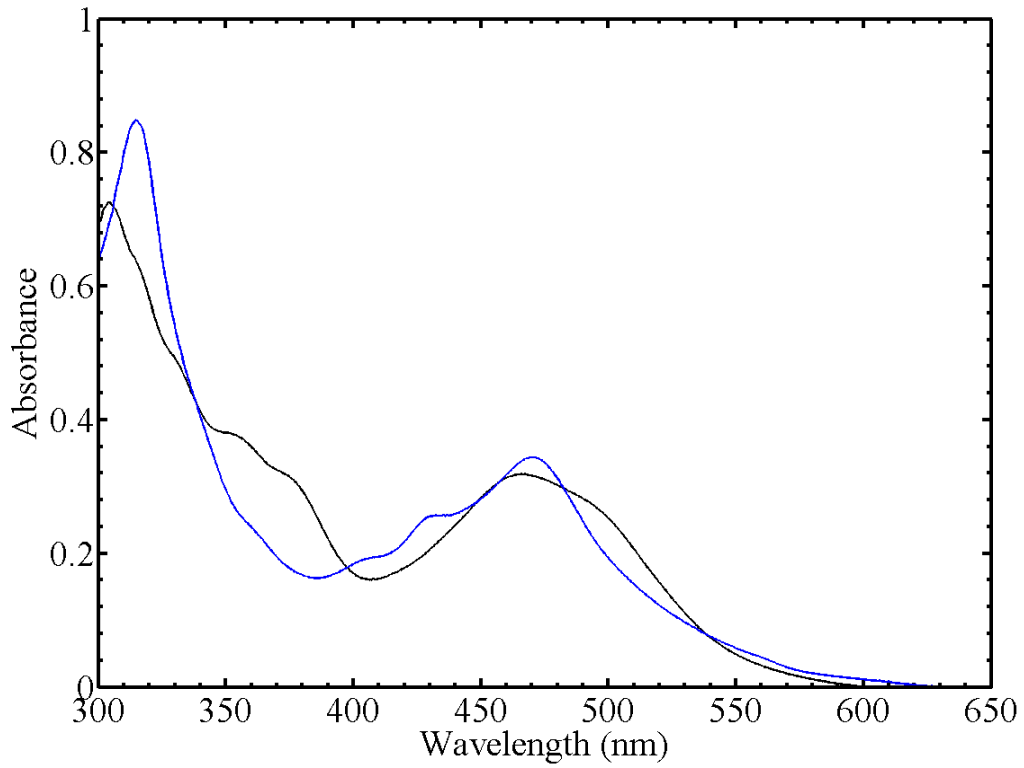

Figure 5.21. Absorption spectra of MeCbi bound to EutB (black) in 10 mM KP_i, 1 mM EDTA, 5'-DRF (10 μM), at pH 7.5, and following irradiation (30 s, 300 W xenon lamp) (blue). MeCbi (31 μM) bound to EutB (60 μM) was photolyzed anaerobically in the presence of 5'DRF in an attempt to produce cob(I)inamide. Cob(II)inamide was observed. A baseline spectrum of EAL was subtracted from the final spectra displayed.

Conclusion

A summary of the results of the reduction of the protein bound cofactors is presented in Table 5.5. The headings indicate the cobalt oxidation state that was achieved by the combination of protein, cofactor, and reducing agent, and "Yes" and "No" specify whether the oxidation state was observed. The labeled, "n.p.", indicates that the experiments were not performed. The results indicate that the removal of the

DMBz ligand from the Co atom, which is necessary for Co^{I} formation, is made more difficult following binding to the EAL protein. It is proposed that the EutC subunit sterically hinders the DMBz ligand removal resulting in no formation of the Co^{I} state by Ti(III) citrate. It is possible, in the case of EAL bound cobalamin, that the cobalamin is not accessible to the Ti(III) citrate and is completely covered by the EutC subunit, although crystallographic studies indicate large cavity, 5 Å by 15 Å[13], between the EutB and EutC subunits that may provide access.

Table 5.5. Summary of reduction of cobalamin and cobinamide bound to EAL and EutB. The n.p. represents "not performed".

Protein	Cofactor	Reduction by Ti(III)[a]		Reduction by 5'-DRF[a]	
		Co^{II}	Co^{I}	Co^{II}	Co^{I}
EAL	Cobalamin	Yes	No	n.p.	n.p.
	Cobinamide	Yes	Yes	n.p.	n.p.
EutB	Cobalamin	Yes	No	n.p	n.p
	Cobinamide	Yes	Yes	Yes	No

[a] Samples containing 5'-DRF were photolyzed with a 300 W xenon lamp for 30 s.

The removal of the DMBz ligand of the cobalamin, to form cobinamide, resulted in the ability of the cofactor to be reduced to the Co^{I} state when bound to both EAL and EutB. These results indicate that the Ti(III) citrate reductant does have access to the binding site, implying that the DMBz ligand is the rate limiting factor for reduction. The reduction of EutB bound cob(III)inamide to cob(I)inamide, by 5'-DRF, was not observed. We hypothesize that the binding site of the protein shields the cofactor and does not allow access of the 5'-DRF to the cofactor. The short excited state lifetime of the 5'-

DRF, less than 10 nanoseconds, as well as the increased size of the reductant, as compared to Ti(III), may not be commensurate with diffusion into a sterically restricted binding site.

In order to initiate photo-initiated reduction of the EutB bound cofactor, experiments are ongoing to synthesize the molecule shown in Figure 5.22. It is hypothesized that 5'-DRF access to the cofactor, limited by the protein binding site, will not be an issue following the attachment of 5'-DRF directly to the α-axial ligand of the B_{12} cofactor allowing the reduction of cob(III)inamide to the cob(I)inamide state while bound to EutB.

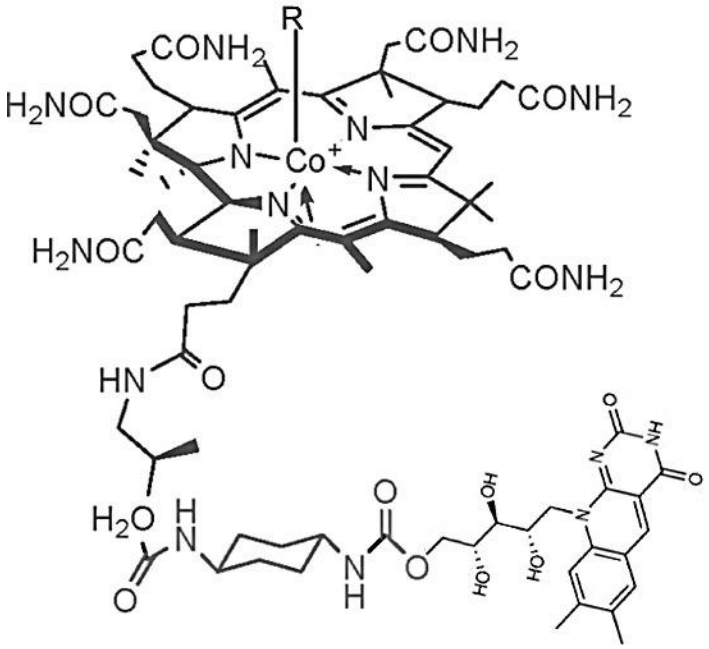

Figure 5.22. Proposed structure of cobinamide compound with 5'-DRF attached to act as the photo-initiated reducing agent of the cofactor when bound to EutB.

With the method developed here to readily produce the cob(I)inamide state bound to the EutB protein with Ti(III) citrate, the focus of this work can now shift to mutations of the protein active site of the EutB protein. The protein environment will be mutated to have a high binding affinity for CO_2. The active site will also be optimized to reduce access of oxygen and protons from the reduced cofactor, in order to minimize competing reduction reactions. The protein will then be mutated to enhance the rate of CO_2 or toxic halo-organic compounds. The results present solutions to the difficult challenge of using low redox state metal centers for catalysis in aqueous solution.

Appendix

Appendix 1.

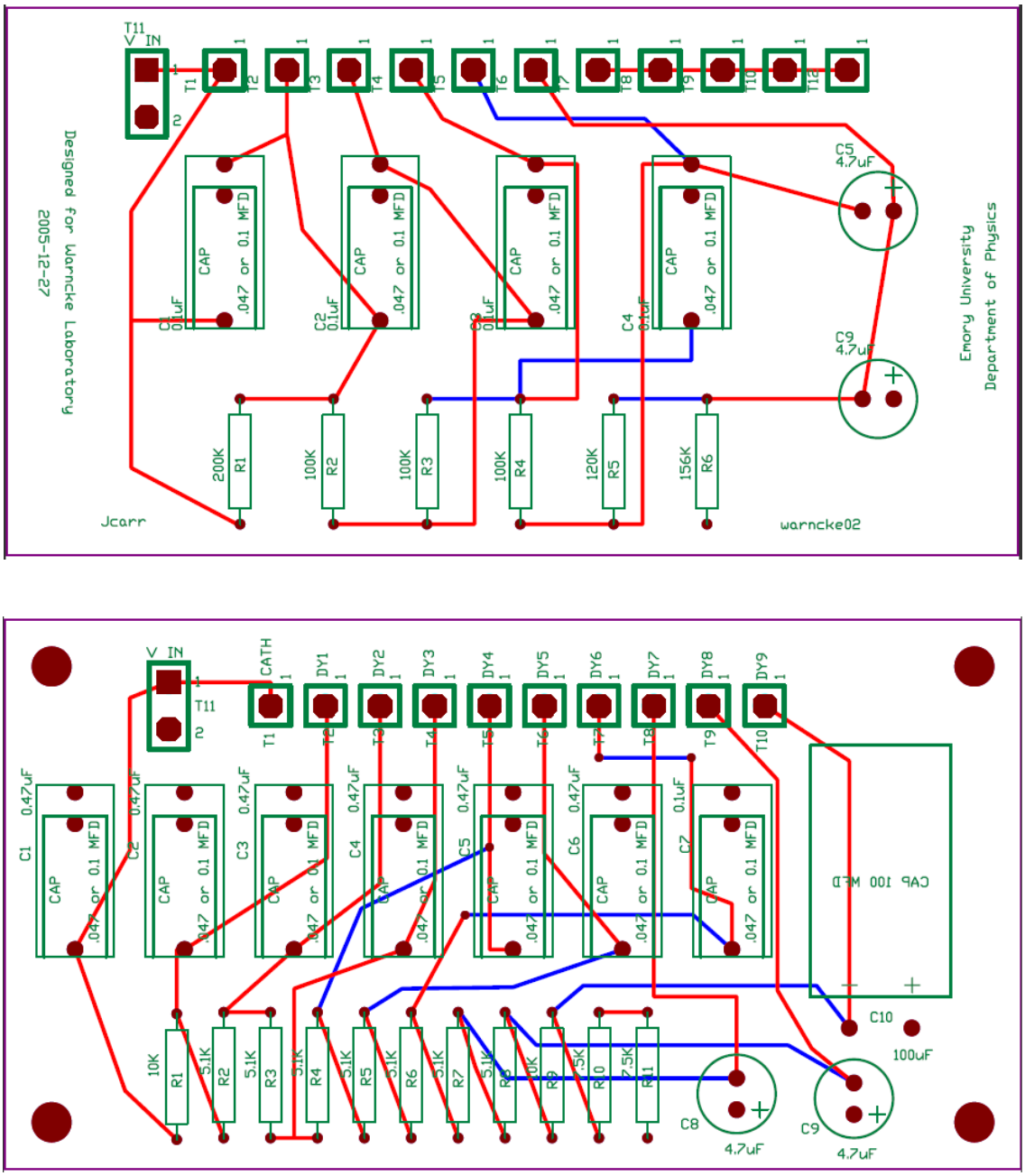

Figure A.1. Integrated circuit design for high current PMT detection circuit. 5 stage dynode design (top) and 9 stage dynode design (bottom).

Appendix 2.

Labview 4.0 Control Program for the Transient Absorption Spectrometer

Program name: NewTASMultishot,nobacknoshut15k

GPIB Command Flow

" " = SubVI

[] = Variable Inputs

[Input1] = Probe Beam Baseline Guess (mv)

[Input2] = Total time to record (ms)

[Input3] = Voltage per division for TAS recording (mv)

[Input4] = Stir time (seconds)

[Input5] = Time between shots (seconds)

[Input6] = Number of iterations

() = Values

Lines 1 through 22 describe setting the spectrometer to measure and record the voltage due to the probe beam. The recorded probe beam baseline voltage is used to optimization of voltage resolution of the oscilloscope, and therefore, the resolution of the change in absorption when performing transient measurements.

1. Cl; TM1; TL .2; TS 1->Send to 15 *%Clears SRS DG535, Sets trigger to external, trigger level to 0.2Volts and trigger slope to rising edge.*

2. "Reset TDS" == *RST ->Send to 2, *CLS->Send to 2 %*Clears and resets TDS oscilloscope*

3. "Wait" → Inside while loop, Busy?->Send to 2, Receive (A) if (A) not = 0 then repeat, if (A) = 0 then continue. *% Asks TDS Oscilloscope if it is busy and waits until the oscilloscope has finished processing commands.*

4. "HORZ SET TDS" == 0.25 -> HOR:MAI:SEC ->Send to 2 *% Sets Horizonatal scale to measure DC offset on PMT due to probe beam.*

5. "Wait"

6. "TDS TRIG SET 2" == TRIG:MAI LEV 1.50; MOD NORM -> Send to 2 *%Sets trigger level of TDS to 1.50 and sets Trigger mode to Normal.*

7. "Wait"

8. CH1:SCAL -> [Input1] (From baseline guess) x .0002 -> Send to 2 *%Sets TDS Ch1 voltage scale to be in range of baseline, [Input1] is the estimate of the dc level..*

9. "Wait"

10. CH1:POS -> 3-> Send to 2 *%Sets TDS Ch1 voltage position to 3, i.e. moves 0 volt level 3 units up.*

11. "Wait"

12. Wait 15000 milliseconds *%Wait command allows time for PMT stabilization.*

13. TRIG FORC -> Send to 2 *%Forces triggering of TDS oscilloscope to record probe beam level.*

14. "Wait"

15. Wait 2000 milliseconds

16. :MEASU:IMM:SOURCE CH1;->Send to 2

17. :MEASU:IMM:TYP LOW;->Send to 2

18. :MEASU:IMM:VAL?->Send to 2 *% Commands 16, 17, 18 tells TDS to measure DC offset on PMT. This is measuring the probe beam baseline.*

19. Receive → (Ch1Baseline) *% Receive and creates value "Ch1Baseline", this is the DC offset of the PMT caused by the probe beam.*

20. "Wait"

21. CL;TM2;->Send to 15 *%Clears SRS DG535 and sets trigger mode to external.*

Lines 22 through 67 sets the parameters for data acquisition.

Below is inside for loop with input [Number of Runs]

22. "Reset TDS" == *RST ->Send to 2, *CLS->Send to 2 *%Clears and resets TDS oscilloscope*

23. "Wait"

24. HOR:RECO 15000->Send to 2 *% Sets the number of data points that are acquired for each record for the TDS Oscilloscope.*

25. "Wait"
26. "HORZ SET TDS" == ([Input2] / 300) x 10000 -> HOR:MAI:SEC ->Send to 2 *% Sets total "horizonatal" time that will be recorded and saved by the TDS oscilloscope. [Input2] is entered in milliseconds.*

27. "Wait"

28. "TDS Delay Mod" ==HOR:MOD DELAYE -> Send to 2 *%Sets TDS Oscilloscope horizontal axis to delay mode.*

29. HOR:MAI?->Send to 2 *% Asks TDS Oscilloscope to measure what the horizontal time scale is set to on the scope, secs/division. This is done to avoid having someone put in a total record time that does not equate to standard time per division. For example, if a time per division ended up being .532 secs/division, the scope would automatically set the value to 0.5 secs and this command would then measure 0.5.*

30. "Wait"

31. Receive → (time/division) *% Receive and creates value (time/division), which is the time per division scale the TDS oscilloscope is set to.*

32. HOR:DEL:TIM:RUNSA -> (time/division) x 120 -> Send to 2 *% This sets the delay time for the TDS oscilloscope to wait after the main trigger before the delayed time base begins. This is necessary because what points the TDS record is dependent on its time away from the main trigger.*

33. [Input3] x 0.001 -> CH1:SCAL -> Send to 2 *% Sets the voltage scale, and thus resolution of the TDS oscilloscope.*

34. “Wait”

35. HOR:DEL? -> Send to 2 *% Tells TDS to measure horizontal time delay setting.*

36. Receive -> (horzdelay) *% Receives and creates value for horizontal delay time.*

37. “Wait”

38. HOR:DEL:SEC -> (time/division) -> Send to 2 % *This sets the time per division for the delay time base of the TDS oscilloscope.*

39. “Wait”

40. HOR:POS -> 25 -> Send to 2 *% Sets horizontal time position of TDS Oscilloscope.*

41. “Wait”
42. “SRS A DELAY” == [Input4] -> DT 2,1, -> Send to 15 *% Sets the ttl output for the SRS DG535. Sets delay time of channel A output to [input4] relative to T0. This sets the stir time of sample stirrer.*

43. “SRS B DELAY” == [Input5] + 0.055 + 0.035 + 1 -> DT 3,1, -> Send to 15 *% Sets the ttl output for the SRS DG535. Sets delay time of channel B output to [input5] + delays relative to T0. This sets the time between excitation pulses.*

44. “SRS C DELAY” == [Input5] + 0.055 + 0.035 -> DT 5,1, -> Send to 15 *% Sets the ttl output for the SRS DG535. Sets delay time of channel C output to [input5] + delays relative to T0.*

45. “SRS D DELAY” == [Input5] + 0.055 -> DT 6,1, -> Send to 15 *% Sets the ttl output for the SRS DG535. Sets delay time of channel D output to [input5] + delays relative to T0.*

46. CH1:SCAL? -> Send to 2 *% Tells TDS to measure channel 1 voltage scale of TDS oscilloscope.*

47. Receive -> (voltscale) *% Receives and creates value for channel 1 volts per division.*

48. “Wait”

49. CH1:OFFS -> (voltscale) x 3.0 x [Input6] + (Ch1Baseline) -> Send to 2 *% Sets vertical offset of Channel one considering the probe beam so that the trace is displayed and recorded on the TDS oscilloscope. This allows the voltage resolution to be maximized. If [Input6] is set to 0 the trace is centered on the screen, -1 and 1 move the trace up or down 3 units.*

50. "Wait"

51. "TDS RUN STOP" == ACQ:STOPA SEQ -> Send to 2 *% Sets TDS Oscilloscope to stop taking acquisitions after a "sequence" is complete. The sequence is defined by the conditions set in the acquisition mode of the TDS.*

52. "Wait"

53. ACQ:MOD SAM; -> Send to 2 *% Sets TDS Oscilloscope to sample mode rather than average.*

54. "Wait"

55. {TDS TRIG SET 2}

56. == TRIG:MAI LEV 1.50; MOD NORM -> Send to 2 *%Sets trigger level of TDS to 1.50 and sets Trigger mode to Normal.*

57. "Wait"

58. "TDS TRIG SET" == TRIG:MAI:EDG:COUP DC; SOU AuX; SLO RIS; -> Send to 2 *%Sets trigger of TDS to DC coupling, the source of the trigger to the Aux input and the slope to rise..*
59. "Wait"

60. TRIG:MAI:LEV 0.150 -> Send to 2 *%Sets Trigger level of TDS Oscilloscope to 0.150 volts. This voltage is provided by photodiode inside sample compartment.*

61. Wait _>2000 milliseconds

62. TM 1;TL0.15; TS 1 ->Send to 15 *%Sets trigger mode of SRS DG535 to external, trigger level to 0.15 volts (provided by Q-switch output form Nd-YAG laser) and the trigger slope to rising edge.*

63. Wait [Input5] x 1100 milliseconds *%Sets wait time based on delay between shots to allow SRS DG535 to be set.*

64. CL;TM2 -> Send to 15 *% Clears SRS DG 535 and sets trigger mode to single shot. Since SRS DG 535 controls laser shutter this ensures only one shot is allowed through as data collection and transfer is happening.*

65. *WAI;
    DAT:SOU CH1;
    :DAT:ENC ASCI
    :DAT:WID 2;
    :DAT:STAR 0;
    :DAT:STOP 15000
    :WFMP?;
    :CURV?;
    :HEAD ON;
    VERB OFF
    ->Send to 2 *% Sets the format and location of the waveform data that is transferred with the CURV command.*

66. Receive -> (DATA) *%% Receives and creates value for settings of scope and data in waveform. Information is in ASCI format..*

67. [Input6] - > for loop % *Repeats lines 22 through 66 for [Input6] number of iterations.*

Data extraction, sorting and creation of saved file.

68. Labview pattern matching function is used to extract data shown in the following description from the data set (DATA)

69. (FinalData) = [(:CURV) + (YOFFSET x -1)] x (YSCALE) + (Ch1Baseline) *% Converts data to voltage units, inverts data and accounts for y offset.*

70. A matrix of the 1 through the number of data points is multipled by (XSCALE) factor to create time data.

71. Time data is combined with (FinalData) and 2 x 2 matrix is saved for each individual laser shot and collection.

Bibliography

(1) Toraya, T. *Chemical Reviews* **2003**, *103*, 2095.

(2) Banerjee, R.; Ragsdale, S. W. *Annual Review of Biochemistry* **2003**, *72*, 209.

(3) Brown, K. L. *Chem. Rev.* **2005**, *105*, 2075.

(4) Hay, B. P.; Finke, R. G. *Inorg. Chem.* **1984**, *23*, 3041.

(5) Halpern, J.; Kim, S. H.; Leung, T. W. *Journal of the American Chemical Society* **1984**, *106*, 8317.

(6) Hay, B. P.; Finke, R. G. *Polyhedron* **1988**, *7*, 1469.

(7) Marsh, E. N.; Harding, S. E. *Biochemical Journal* **1993**, *290*, 551.

(8) Hubbard, B. K.; Gulick, A. M.; Babbitt, P. C.; Rayment, I.; Gerlt, J. A. *Faseb Journal* **1999**, *13*, A1446.

(9) Sun, L.; Warncke, K. *Proteins-Structure Function and Bioinformatics* **2006**, *64*, 308.

(10) Bandarian, V.; Reed, G. H. In *Chemistry and Biochemistry of B12*; Banerjee, R., Ed.; John Wiley and Sons: New York, 1999, p 811.

(11) Bradbeer, C. *J Biol Chem* **1965**, *240*, 4669.

(12) Genomics, J. C. f. S. 2007.

(13) Shibata, N.; Tamagaki, H.; Hieda, N.; Akita, K.; Komori, H.; Shomura, Y.; Terawaki, S.; Mori, K.; Yasuoka, N.; Higuchi, Y.; Toraya, T. *Journal of Biological Chemistry* **2010**, *285*, 26484.

(14) Gerlt, J. A.; Raushel, F. M. *Curr. Op. Chem. Biol.* **2003**, *7*.

(15) Banerjee, R. *Chemistry and Biochemistry of B12*; Wiley New York, 1999.

(16) *In B12*; Babior, B. M., Ed.; Wiley:: New York, 1982; Vol. Vol. 2,.

(17) Kratky, C.; Farber, G.; Gruber, K.; Wilson, K.; Dauter, Z.; Nolting, H. F.; Konrat, R.; Krautler, B. *Journal of the American Chemical Society* **1995**, *117*, 4654.

(18) Ke, S. C.; Torrent, M.; Museav, D. G.; Morokuma, K.; Warncke, K. *Biochemistry* **1999**, *38*, 12681.

(19) Abend, A.; Bandarian, V.; Nitsche, R.; Stupperich, E.; Retey, J.; Reed, G. H. *Archives of Biochemistry and Biophysics* **1999**, *370*, 138.

(20) Babior, B. M.; Moss, T. H.; Ormejohn.Wh; Beinert, H. *Journal of Biological Chemistry* **1974**, *249*, 4537.

(21) Carty, T. J.; Babior, B. M.; Abeles, R. H. *Journal of Biological Chemistry* **1971**, *246*, 6313.

(22) Graves, S. W.; Fox, J. A.; Babior, B. M. *Biochemistry* **1980**, *19*, 3630.

(23) Warncke, K.; Utada, A. S. *Journal of the American Chemical Society* **2001**, *123*, 8564.

(24) Canfield, J. M.; Warncke, K. *Journal of Physical Chemistry B* **2002**, *106*, 8831.

(25) Bandarian, V.; Reed, G. H. *Biochemistry-Us* **2002**, *41*, 8580.

(26) LoBrutto, R.; Bandarian, V.; Magnusson, O. T.; Chen, X.; Schramm, V. L.; Reed, G. H. *Biochemistry-Us* **2001**, *40*, 9.

(27) Canfield, J. M.; Warncke, K. *Journal of Physical Chemistry B* **2005**, *109*, 3053.
(28) Warncke, K.; Schmidt, J. C.; Ke, S. C. *J. Am. Chem. Soc.* **2008**, *130*, 6055.
(29) Bender, G.; Poyner, R. R.; Reed, G. H. *Biochemistry* **2008**, *47*, 11360.
(30) Bandarian, V. R., G. H.; Banerjee, R., Ed.; Ed.; Wiley and Sons: New York, 1999, p 811.
(31) Halpern, J.; Kim, S.-H.; Leung, T. W. *J. Am. Chem. Soc.* **1984**, *106*, 8317.
(32) Hay, B. P.; Finke, R. G. *Polyhedron* **1988**, *7*, 1469.
(33) Brooks, A. J.; Vlasie, M.; Banerjee, R.; Brunold, T. C. *J. Am. Chem. Soc.* **2004**, *126*, 8167.
(34) Brooks, A. J.; Vlasie, M.; Banerjee, R.; Brunold, T. C. *J. Am. Chem. Soc.* **2005**, *127*, 16522.
(35) Wang, M.; Warncke, K. *J. Am. Chem. Soc.* **2008**, *130*, 4846.
(36) Brown, K. *Chem. Rev.* **2005**, *105*, 2075.
(37) Shibata, N.; Tamagaki, H.; Hieda, N.; Akita, K.; Komori, H.; Shomura, Y.; Terawaki, S.-I.; Mori, K.; Yasuoka, N.; Higuchi, Y.; Toraya, T. *J Biol Chem* **2010**, *JBC Papers in Press: Manuscript M110.125112 (June 1, 2010): .*
(38) Finke, R. G.; Hay, B. P. *Inorganic Chemistry* **1984**, *23*, 3041.
(39) Hay, B. P.; Finke, R. G. *Journal of the American Chemical Society* **1986**, *108*, 4820.
(40) Geno, M. K.; Halpern, J. *Journal of the Chemical Society-Chemical Communications* **1987**, 1052.
(41) Halpern, J. *Science* **1985**, *227*, 869.
(42) Hill, H. A. O.; Pratt, J. M.; Williams, R. J. P. *Chem Brit* **1969**, *5*, 156.
(43) Tsou, T. T.; Loots, M.; Halpern, J. *Journal of the American Chemical Society* **1982**, *104*, 623.
(44) Ng, F. T. T.; Rempel, G. L.; Halpern, J. *Inorg Chim a-Lett* **1983**, *77*, L165.
(45) Halpern, J.; Ng, F. T. T.; Rempel, G. L. *Journal of the American Chemical Society* **1979**, *101*, 7124.
(46) Stich, T. A.; Brooks, A. J.; Buan, N. R.; Brunold, T. C. *Journal of the American Chemical Society* **2003**, *125*, 5897.
(47) Mayer, I. *Chemical Physics Letters* **1983**, *97*, 270.
(48) Mayer, I. *Int J Quantum Chem* **1984**, *26*, 151.
(49) Mayer, I. *Theor Chim Acta* **1985**, *67*, 315.
(50) Puckett, J. M.; Mitchell, M. B.; Hirota, S.; Marzilli, L. G. *Inorganic Chemistry* **1996**, *35*, 4656.
(51) Marzilli, L. G.; Brescianipahor, N.; Randaccio, L.; Zangrando, E.; Finke, R. G.; Myers, S. A. *Inorg Chim a-Bioinor* **1985**, *107*, 139.
(52) Dong, S. L.; Padmakumar, R.; Banerjee, R.; Spiro, T. G. *Journal of the American Chemical Society* **1999**, *121*, 7063.
(53) Dong, S. L.; Padmakumar, R.; Maiti, N.; Banerjee, R.; Spiro, T. G. *Journal of the American Chemical Society* **1998**, *120*, 9947.
(54) Mancia, F.; Evans, P. R. *Struct Fold Des* **1998**, *6*, 711.
(55) Mancia, F.; Keep, N. H.; Nakagawa, A.; Leadlay, P. F.; McSweeney, S.; Rasmussen, B.; Bosecke, P.; Diat, O.; Evans, P. R. *Structure* **1996**, *4*, 339.

(56) Shibata, N.; Masuda, J.; Tobimatsu, T.; Toraya, T.; Suto, K.; Morimoto, Y.; Yasuoka, N. *Structure* **1999**, *7*, 997.

(57) Hammes-Schiffer, S.; Benkovic, S. J. *Annu. Rev. Biochem.* **2006**, *75*, 519.

(58) Benkovic, S. J.; Hammes, G. G.; Hammes-Schiffer, S. *Biochemistry-Us* **2008**, *47*, 3317.

(59) Hammes, G. G. *Biochemistry* **2002**, *41*, 8221.

(60) Eisenmesser, E. Z.; Millet, O.; Labeikovsky, W.; Korzhnev, D. M.; Wolf-Watz, M.; Bosco, D. A.; Skalicky, J. J.; Kay, L. E.; Kern, D. *Nature* **2005**, *438*, 117.

(61) Henzler-Wildman, K. A.; Thai, V.; Lei, M.; Ott, M.; Wolf-Watz, M.; Fenn, T.; Pozharski, E.; Wilson, M. A.; Petsko, G. A.; Karplus, M.; Hubner, C. G.; Kern, D. *Nature* **2007**, *450*, 838.

(62) Hay, S.; Pudney, C. R.; McGrory, T. A.; Pang, J.; Sutcliffe, M. J.; Scrutton, N. S. *Angew. Chem. Int. Ed.* **2009**, *48*, 1452.

(63) Nagel, Z. D.; Klinman, J. P. *Nature Chem. Biol.* **2009**, *5*, 543.

(64) Watt, E. D.; Shimada, H.; Kovrigin, E. L.; Loria, J. P. *J Biol Chem* **2007**, *104*, 11981.

(65) Schwartz, S. D.; Schramm, V. L. *Nature Chem. Biol.* **2009**, *5*, 551.

(66) Zhang, Z. Q.; Rajagopalan, P. T. R.; Selzer, T.; Benkovic, S. J.; Hammes, G. G. *P Natl Acad Sci USA* **2004**, *101*, 2764.

(67) Antikainen, N. M.; Smiley, R. D.; Benkovic, S. J.; Hammes, G. G. *Biochemistry* **2005**, *44*, 16835.

(68) Hill, J. A.; Williams, R. J. P.; Pratt, J. M. *Journal of the Chemical Society* **1964**, 5149.

(69) Walker, L. A.; Jarrett, J. T.; Anderson, N. A.; Pullen, S. H.; Matthews, R. G.; Sension, R. J. *Journal of the American Chemical Society* **1998**, *120*, 3597.

(70) Shiang, J. J.; Walker, L. A.; Anderson, N. A.; Cole, A. G.; Sension, R. J. *Journal of Physical Chemistry B* **1999**, *103*, 10532.

(71) Chen, E. F.; Chance, M. R. *Abstracts of Papers of the American Chemical Society* **1990**, *200*, 196.

(72) Chen, E.; Chance, M. R. *Biochemistry* **1993**, *32*, 1480.

(73) Kruppa, A. I.; Taraban, M. B.; Leshina, T. V.; Natarajan, E.; Grissom, C. B. *Inorganic Chemistry* **1997**, *36*, 758.

(74) Walker, L. A.; Jarret, J. T.; Anderson, N. A.; Pullen, S. H.; Matthews, R. G.; Sension, R. J. *J. Am. Chem. Soc.* **1998**, *120*, 3597.

(75) Sension, R. J.; Cole, A. G.; Harris, A. D.; Fox, C. C.; Woodbury, N. W.; Lin, S.; Marsh, E. N. G. *Journal of the American Chemical Society* **2004**, *126*, 1598.

(76) Sension, R. J.; Harris, D. A.; Cole, A. G. *Journal of Physical Chemistry B* **2005**, *109*, 21954.

(77) Harkins, T. T.; Grissom, C. B. *Journal of the American Chemical Society* **1995**, *117*, 566.

(78) Lott, W. B.; Chagovetz, A. M.; Grissom, C. B. *J. Am. Chem. Soc.* **1995**, *117*, 12194.

(79) Yoder, L. M.; Cole, A. G.; Walker, L. A.; Sension, R. J. *Journal of Physical Chemistry B* **2001**, *105*, 12180.

(80) Cole, A. G.; Yoder, L. M.; Shiang, J. J.; Anderson, N. A.; Walker, L. A.; Holl, M. M. B.; Sension, R. J. *Journal of the American Chemical Society* **2002**, *124*, 434.

(81) Endicott, J. F.; Netzel, T. L. *Journal of the American Chemical Society* **1979**, *101*, 4000.

(82) Shiang, J. J.; Cole, A. G.; Sension, R. J.; Hang, K.; Weng, Y. X.; Trommel, J. S.; Marzilli, L. G.; Lian, T. Q. *Journal of the American Chemical Society* **2006**, *128*, 801.

(83) Shiang, J. J.; Cole, A. G.; Sension, R. J.; Hang, K.; Weng, Y.; Trommel, J.; Marzilli, L.; Lian, T. *J. Am. Chem. Soc.* **2006**, *128*, 801.

(84) Noyes, R. M. *Prog React Kinet Mec* **1961**, *1*, 129.

(85) Walker, L. A.; Shiang, J. J.; Anderson, N. A.; Pullen, S. H.; Sension, R. J. *Journal of the American Chemical Society* **1998**, *120*, 7286.

(86) Sension, R. J.; Walker, L. A.; Shiang, J. J. *Abstracts of Papers of the American Chemical Society* **1998**, *216*, U684.

(87) Cole, A. G.; Anderson, N.; Shiang, J. J.; Sension, R. J. *Abstracts of Papers of the American Chemical Society* **2000**, *220*, U223.

(88) Chen, E.; Chance, M. *Biophysical Journal* **1990**, *57*, A49.

(89) Brownawell, A. M.; Chen, E.; Chance, M. R. *Biophysical Journal* **1993**, *64*, A161.

(90) Hay, B. P.; Finke, R. G. *J. Am. Chem. Soc.* **1987**, *109*, 8012.

(91) Hay, B. P.; Finke, R. G. *Journal of the American Chemical Society* **1987**, *109*, 8012.

(92) Halpern, J. *Accounts of Chemical Research* **1982**, *15*, 238.

(93) Jaworska, M.; Lodowski, P.; Andruniow, T.; Kozlowski, P. M. *J. Chem. Phys. B* **2007**, *111*, 2419.

(94) Dölker, N.; Maseras, F.; Lledos, A. *J. Phys. Chem. B* **2001**, *105*, 7564.

(95) Dölker, N.; Maseras, F.; Siegbahn, P. E. M. *Chem. Phys. Lett.* **2004**, *386*, 174.

(96) Kwiecien, R. A.; Khavrutskii, I. V.; Musaev, D. G.; Morokuma, K.; Banerjee, R.; Paneth, P. *J. Am. Chem. Soc.* **2006**, *128*, 1287.

(97) Sension, R. J.; Harris, D. A.; Stickrath, A.; Cole, A. G.; Fox, C. C.; Marsh, E. N. G. *Journal of Physical Chemistry B* **2005**, *109*, 18146.

(98) Pett, V. B.; Liebman, M. N.; Murrayrust, P.; Prasad, K.; Glusker, J. P. *J Am Chem Soc* **1987**, *109*, 3207.

(99) Masuda, J.; Shibata, N.; Morimoto, Y.; Toraya, T.; Yasuoka, N. *Structure* **2000**, *8*, 775.

(100) Khoroshun, D. V.; Warncke, K.; Ke, S. C.; Musaev, D. G.; Morokuma, K. *Journal of the American Chemical Society* **2003**, *125*, 570.

(101) Padmakumar, R.; Padmakumar, R.; Banerjee, R. *Biochemistry-Us* **1997**, *36*, 3713.

(102) Marsh, E. N. G.; Ballou, D. P. *Biochemistry* **1998**, *37*, 11864.

(103) Licht, S. S.; Booker, S.; Stubbe, J. *Biochemistry-Us* **1999**, *38*, 1221.

(104) Bandarian, V.; Reed, G. H. *Biochemistry-Us* **2000**, *39*, 12069.

(105) Gani, D.; Wallis, C. O.; Young, D. W. *Eur. J. Biochem.* **1983**, *136*, 303.

(106) Yan, S.-J.; McKinnie, B. G.; Abacherii, C.; Hill, R. K.; Babior, B. M. *J. Am. Chem. Soc.* **1984**, *106*, 2961.

(107) Douzou, P. *Cryobiochemistry: An Introduction*; Academic Press: New York, 1977.

(108) Bergkamp, M. A.; Dalton, J.; Netzel, T. L. *Journal of the American Chemical Society* **1982**, *104*, 253.

(109) Harris, D. C. *Quantitative Analytical Chemistry*; 7 ed.; W. H. Freeman and Company: New York, 2007.

(110) Faust, L. R. P.; Connor, J. A.; Roof, D. M.; Hoch, J. A.; Babior, B. M. *Journal of Biological Chemistry* **1990**, *265*, 12462.

(111) Faust, L. P.; Babior, B. M. *Archives of Biochemistry and Biophysics* **1992**, *294*, 50.

(112) Kaplan, B. H.; Stadtman, E. R. *Journal of Biological Chemistry* **1968**, *243*, 1787.

(113) Giannotti, C. *Electronic Spectra of B12 and Related Systems*; John Wiley and Sons, New York, 1982; Vol. 1.

(114) Huhta, M. S.; Chen, H. P.; Hemann, C.; Hille, C. R.; Marsh, E. N. G. *Biochemical Journal* **2001**, *355*, 131.

(115) Huhta, M. S.; Chen, H.-P.; Hemann, C.; Hille, C. R.; Marsh, E. N. G. *Biochem. J.* **2001**, *355*, 131.

(116) Hogenkam.Hp *Biochemistry-Us* **1966**, *5*, 417.

(117) Jarrett, J. T.; Drennan, C. L.; Amaratunga, M.; Scholten, J. D.; Ludwig, M. L.; Matthews, R. G. *Bioorganic & Medicinal Chemistry* **1996**, *4*, 1237.

(118) Endicott, J. F.; Ferraudi, G. J. *J. Am. Chem. Soc.* **1977**, *99*, 243.

(119) Kunkely, H.; Vogler, A. *J. Organomet. Chem.* **1993**, *453*, 269.

(120) Taylor, R. T.; Smucker, L.; Hanna, M. L.; Gill, J. *Arch. Biochem. Biophys.* **1973**, 521.

(121) Babior, B. M. In *B12, Volume 2*; Dolphin, D., Ed.; Wiley: New York, 1982; Vol. 2, p 263.

(122) Moore, J. W.; Pearson, R. G. *Kinetics and Mechanism*; Wiley and Sons: New York, 1981.

(123) Retey, J. *Angew. Chem. Int. Ed. Engl.* **1990**, *29*, 355.

(124) Zavitsas, A. A.; Chatgilialoglu, C. *J. Am. Chem. Soc.* **1995**, *117*, 10645.

(125) Robertson, W. D.; Warncke, K. *Biochemistry-Us* **2009**, *48*, 140.

(126) Stickrath, A. B.; Carroll, E. C.; Dai, X.; Harris, A.; Rury, A.; Smith, B.; Tang, K.-C.; Wert, J.; Sension, R. J. *J. Phys. Chem. A* **2009**, *113*, 8513.

(127) Dong, S. L.; Padmakumar, R.; Banerjee, R.; Spiro, T. G. *J. Am. Chem. Soc.* **2004**, *121*, 7063.

(128) Mansoorabadi, S. O.; Magnusson, O. T.; Poyner, R. R.; Frey, P. A.; Reed, G. H. *Biochmistry* **Web 110906**, *ASAP*.

(129) Jones, A. R.; Hay, S.; Woodward, J. R.; Scrutton, N. S. *J. Am. Chem. Soc.* **2007**, *129*, 15718.

(130) Jones, A. R.; Woodward, J. R.; Scrutton, N. S. *J. Am. Chem. Soc.* **2009**, *131*, 17246.

(131) Sharma, P. K.; Chu, Z. T.; Olsson, M. H. M.; Warshel, A. *Proc. Natl. Acad. Sci.* **2007**, *104*, 9661.

(132) Olson, J. M. *Photosynth Res* **2006**, *88*, 109.

(133) Miyamoto, K. In *(FAO Agricultural Services Bulletin - 128). Food and Agriculture Organization of the United Nations* 2009.

(134) Garrett, R.; Grisham, C. M. *Biochemistry*; 3 ed.; Thomson Brooks/Cole, 2005.

(135) Edwards, C. H.; Golding, B. T.; Kroll, F.; Beatrix, B.; Broker, G.; Buckel, W. *Journal of the American Chemical Society* **1996**, *118*, 4192.

(136) Sofia, H. J.; Chen, G.; Hetzler, B. G.; Reyes-Spindola, J. F.; Miller, N. E. *Nucleic Acids Res* **2001**, *29*, 1097.

(137) Frey, P. A. *Annual Review of Biochemistry* **2001**, *70*, 121.

(138) Jarrett, J. T. *Current Opinion in Chemical Biology* **2003**, *7*, 174.

(139) Sterner, R.; Hocker, B. *Chemical Reviews* **2005**, *105*, 4038.

(140) Halmann, M. M.; Steinberg, M. *Greenhouse gas carbon dioxide mitigation science and technology*; Lewis Publishers: Boca Raton, FL, 1999.

(141) Sutin, N.; Creutz, C.; Fujita, E. *Comments on Inorganic Chemistry* **1997**, *19*, 67.

(142) Arakawa, H.; Aresta, M.; Armor, J. N.; Barteau, M. A.; Beckman, E. J.; Bell, A. T.; Bercaw, J. E.; Creutz, C.; Dinjus, E.; Dixon, D. A.; Domen, K.; DuBois, D. L.; Eckert, J.; Fujita, E.; Gibson, D. H.; Goddard, W. A.; Goodman, D. W.; Keller, J.; Kubas, G. J.; Kung, H. H.; Lyons, J. E.; Manzer, L. E.; Marks, T. J.; Morokuma, K.; Nicholas, K. M.; Periana, R.; Que, L.; Rostrup-Nielson, J.; Sachtler, W. M. H.; Schmidt, L. D.; Sen, A.; Somorjai, G. A.; Stair, P. C.; Stults, B. R.; Tumas, W. *Chemical Reviews* **2001**, *101*, 953.

(143) Behr, A. *Angewandte Chemie-International Edition in English* **1988**, *27*, 661.

(144) Gibson, D. H. *Chemical Reviews* **1996**, *96*, 2063.

(145) Meyer, T. J. *Accounts Chem Res* **1989**, *22*, 163.

(146) Grodkowski, J.; Behar, D.; Neta, P.; Hambright, P. *J Phys Chem A* **1997**, *101*, 248.

(147) Dhanasekaran, T.; Grodkowski, J.; Neta, P.; Hambright, P.; Fujita, E. *J Phys Chem A* **1999**, *103*, 7742.

(148) Fisher, B.; Eisenberg, R. *Journal of the American Chemical Society* **1980**, *102*, 7361.

(149) Ogata, T.; Yanagida, S.; Brunschwig, B. S.; Fujita, E. *Journal of the American Chemical Society* **1995**, *117*, 6708.

(150) Ogata, T.; Yamamoto, Y.; Wada, Y.; Murakoshi, K.; Kusaba, M.; Nakashima, N.; Ishida, A.; Takamuku, S.; Yanagida, S. *J Phys Chem-Us* **1995**, *99*, 11916.

(151) Yanagida, S.; Ogata, T.; Yamamoto, Y.; Wada, Y.; Murakoshi, K.; Kusaba, M.; Nakashima, N.; Ishida, A.; Takamuku, S. *Energ Convers Manage* **1995**, *36*, 601.

(152) Sagi, I.; Wirt, M. D.; Chen, E.; Frisbie, S.; Chance, M. R. *J. Am. Chem. Soc.* **1990**, *112*, 8639.

(153) Lexa, D.; Saveant, J. M. *Acc. Chem. Res.* **1983**, *16*, 235.

(154) Koga, O.; Hori, Y. *Electrochim Acta* **1993**, *38*, 1391.

(155) Szajna-Fuller, E., Bakac, Andreja *Eur. J. Inorg. Chem.* **2010**, 2488.

(156) Gibson, D. H. *Chemical Reviews* **1996**, *96*, 2063.

(157) Jessop, P. G.; Ikariya, T.; Noyori, R. *Chemical Reviews* **1995**, *95*, 259.

(158) Ogata, T.; Yanagida, S.; Brunschwig, B. S.; Fujita, E. *Energ Convers Manage* **1995**, *36*, 669.
(159) Pratt, D. A.; van der Donk, W. A. *Journal of the American Chemical Society* **2005**, *127*, 384.
(160) McCauley, K. M.; Pratt, D. A.; Wilson, S. R.; Shey, J.; Burkey, T. J.; van der Donk, W. A. *Journal of the American Chemical Society* **2005**, *127*, 1126.
(161) Arguello, J. E.; Costentin, C.; Griveau, S.; Saveant, J. M. *Journal of the American Chemical Society* **2005**, *127*, 5049.
(162) Costentin, C.; Robert, M.; Saveant, J. M. *Journal of the American Chemical Society* **2005**, *127*, 12154.
(163) Follett, A. D.; McNeill, K. *Inorganic Chemistry* **2006**, *45*, 2727.
(164) Follett, A. D.; McNeill, K. *Abstracts of Papers of the American Chemical Society* **2006**, *231*.
(165) Faust, L. R. P.; Connor, J. A.; Roof, D. M.; Hoch, J. A.; Babior, B. M. *J. Biol. Chem.* **1990**, *265*, 12463.
(166) Faust, L. R. P.; Babior, B. M. *Arch. Biochem. Biophys.* **1992**, *294*.
(167) Harkins, T. T.; Grissom, C. B. *J. Am. Chem. Soc.* **1995**, *117*, 566.
(168) Kaplan, B. H.; stadtman, E. R. *J. Biol. Chem.* **1968**, *243*, 1787.
(169) Zehnder, A.; Wuhrmann, K. *Science* **1976**, *194*, 1165.
(170) Zou, X.; Evans, D. R.; Brown, K. L. *Inorg. Chem.* **1995**, *34*, 1634.
(171) Brodie, J. D. *Proc. N. A. S.* **1969**, *62*, 461.
(172) Massey, V.; Hemmerich, P. *Biochemistry* **1978**, *17*, 9.
(173) Bhugun, I.; Lexa, D.; Saveant, J. M. *Anal. Chem.* **1994**, *66*, 3994.
(174) Butler, J. N. *Ionic Equilibrium*; Wiley: New York, 1998.
(175) Bryce-Smith, D.; Royal Society of Chemistry: London, 1986; Vol. 17.
(176) Ogata, T.; Yanagida, S.; Brunschwig, B. S.; Fujita, E. *J. Am. Chem. Soc.* **1995**, *117*, 6708.
(177) Dempsey, J.; Brunschwig, B. S.; Winkler, J. R.; Gray, H. B. *Acc. Chem. Res.* **2009**, *42*, 1995.
(178) Tackett, S. L.; Collat, J. W.; Abbott, J. C. *Biochemistry* **1963**, *2*, 919.